Investigating the Effect of Changing Ratios and Flowrates on Photovoltaic Thermal and

Evacuated Tube Collector Array Performance for Different Building Types

by

Hannah Weger

Bachelor of Science in Engineering, University of Saskatchewan, 2017

A major research project

presented to Ryerson University

in partial fulfillment of the

requirements for the degree of

Master of Building Science

In the Program of

Building Science

Toronto, Ontario, Canada, 2019

© Hannah Weger, 2019

AUTHOR'S DECLARATION FOR ELECTRONIC SUBMISSION OF A MAJOR RESEARCH PROJECT

I hereby declare that I am the sole author of this major research project. This is a true copy of the thesis, including any required final revisions.

I authorize Ryerson University to lend this thesis to other institutions or individuals for the purpose of scholarly research.

I further authorize Ryerson University to reproduce this major research project by photocopying or by other means, in total or in part, at the request of other institutions or individuals for the purpose of scholarly research.

I understand that my major research project may be made electronically available to the public.

Investigating the Effect of Changing Ratios and Flowrates on Photovoltaic Thermal and

Evacuated Tube Collector Array Performance for Different Building Types

Master of Building Science 2019, Hannah Weger

Building Science Program, Department of Architectural Science, Ryerson University

ABSTRACT

Photovoltaic thermal and/or evacuated tube collectors on building roofs can be effectively used to reduce fossil fuel use for heating and reliance on the electrical grid. To evaluate the potential of this reduction, a set of models were created for rooftop photovoltaic thermal and evacuated tube collector energy production, both thermal and electricity, and tested using a series of potential layouts. Five collector area ratios, two layout options, and three working fluid flowrates were investigated using five reference buildings as case studies. From these case studies it was determined that in Toronto's climate, the exclusive use of photovoltaic thermal collectors produces the most total energy, while using only evacuated tube collectors maximally offsets greenhouse gasses. The results suggest that district heating would be highly effective to reduce the carbon footprint of city cores like the Toronto 2030 District.

ACKNOWLEDGMENTS

CONTENTS

LIST OF TABLES

LIST OF FIGURES

1 Introduction

In many buildings, solar thermal water heating is the most effective way to collect usable energy. Photovoltaic thermal (PVT) collectors are one method of collecting both electrical and thermal energy at once. The heat that is absorbed by the panel is transferred to the working fluid, which in turn cools down the photovoltaic cells, making them more efficient. Evacuated tube (ET) collectors can only collect thermal energy, but they heat the working fluid to a much higher temperature than flat plate collectors and are typically considered to be more effective in cold climates. Due to the different properties of the two collectors, it is hypothesized that a combination of PVT and ET collectors would provide the most total energy collection. If this is the case, there is benefit to determining the optimal ratio for a given building or building cluster that would produce the greatest total energy, minimize buildingCO_2 emissions, and/or obtain the shortest payback period for their renewable energy system. This investigation will support a Community Energy Planning Tool funded by GreenON for use in the Toronto 2030 District that will serve as a model to Ontario municipalities to guide greenhouse gas (GHG) reductions at scale.

1.1 Research Objective

The objective of this project is to complete an investigation into the effect of changing the ratio of PVT and ET collectors on a rooftop, as well as how the flowrate through these collectors affects the energy output. This allows one to quickly estimate solar production for a given roof. Using the area allocated for solar collectors and information about the collectors, the optimum ratio of PVT to ET collectors for that roof can be determined. The outputs will be a) the area on the roof that should be used for PVT and for ET collectors to best meet the building loads, b) the estimated GHG savings associated with this strategy, and c) the estimated energy savings

associated with this strategy. This will support the development of medium and deep GHG emission reduction retrofits for developments as well as the 2030 district project.

1.2 Research Questions

This work will look to answer the following research questions:

1. Given a set of building loads and roof area, is there a standard approach to determine the optimum ratio of PVT to ET?

2. How does changing the ratio of the two collectors (on a fractional area basis) affect the environmental impact of the system?

3. If solar collectors on the roofs of buildings are implemented at a larger scale, what can be achieved in terms of energy savings and offsetting greenhouse gas emissions?

2   Background

The development of solar collectors has a long history. In 1941 a report on the heat absorption of various materials and colours was published [2], finding that black and other dark surfaces absorb more heat, and therefore become warmer in the sun. The applications and development of this knowledge are widespread; NASA published a paper [3] looking at solar heating within the context of space flight in 1963, and using the technology to heat buildings was noted as early as 1961 [4]. Solar collectors vary in types and application, therefore there is a variety of approaches to modeling their performance and energy generation. This project works to expand on past work by Dembeck-Kerekes [1] who created a model for a PVT collector that examined whether a constant or a variable flow rate was better for PVT panels in various situations. This work found that a variable flow rate is better, but only slightly. Therefore, for simplification, in this project only a constant flow rate is considered, though different flowrate conditions are examined, and, in addition to PVT collectors, ET collectors will also be examined.

This chapter summarizes the pertinent literature related to solar collectors. First, the structure and applications of PVT collectors are explained and approaches to modeling are examined. These approaches start with the work of Duffie and Beckman [5] and variations are created from there. Similarly, ET collectors and models are considered. Finally, the opportunity for using these technologies for buildings is examined to frame the research gap addressed in this Major Research Project.

2.1   Photovoltaic Thermal Models

PVT models are a combination of a flat-plate thermal panel and a photovoltaic laminate. An image and a cross-section diagram of a typical PVT collector can be seen in Figures 1 and 2.
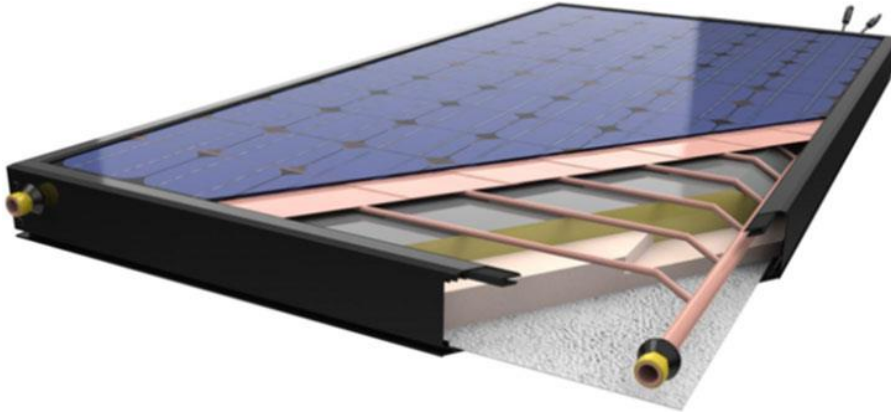
Figure 1: Image of a PVT collector [6].
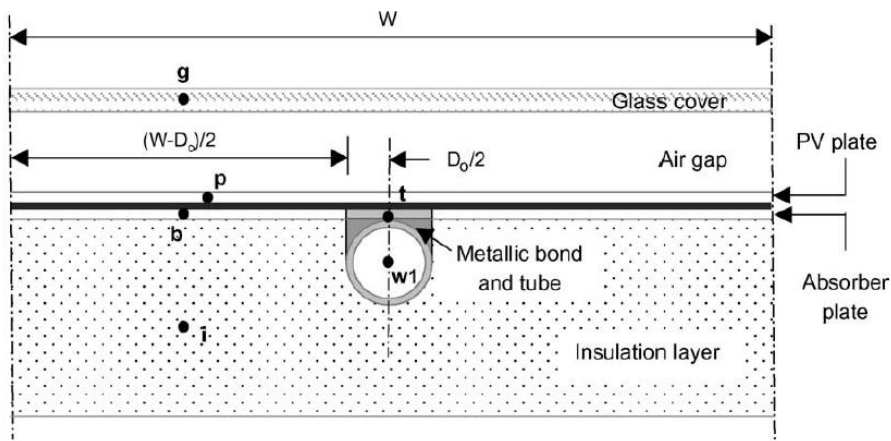
Figure 2: Diagram of a typical PVT collector cross-section [7].

A flat-plate thermal collector primarily consists of a working fluid, an absorbing surface that transfers energy from the solar energy to the working fluid, clear covers that reduce convection and radiation losses at the absorbing surface, and insulation behind and around the edges of the collector to reduce losses due to convection [5]. A PVT collector has the addition of a photovoltaic laminate above the absorber plate that produces electricity. This concept is introduced by Kern Jr. and Russell [8] as an alternative to traditional thermal panels and photovoltaic collectors. The efficiency of photovoltaic panels drops as their temperature increases, especially when solar insolation values are high, therefore when combined with a

4

thermal collector, the efficiency of the photovoltaics can be increased by removing the heat
(Figure 3) [9].
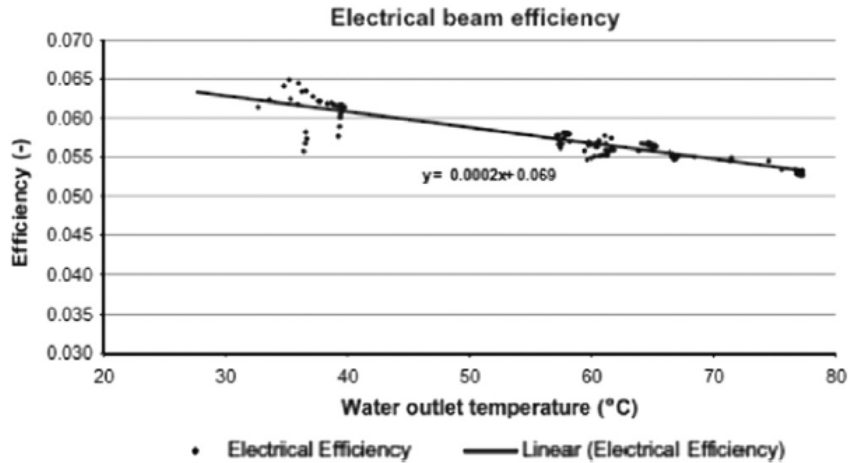
Figure 3: Electrical efficiency vs water outlet temperature [9].

According to a study by Vokas *et al.* [10], although the photovoltaic laminate decreases the
thermal performance of the collector, by using a portion of the solar insolation to produce
electricity, it only decreases the thermal performance by about 9%, while adding significant
electrical generation.

Duffie and Beckman [5] created a model of a flat-plate thermal collector that is widely used as a
base in other studies. Their model does not include the photovoltaic laminate that PVT collectors
have, but their basic equations for the thermal behaviour of the working fluid, absorber, and
other pieces are similar. A flowchart of the layout of the Duffie and Beckman [5] model for a
flat-plate collector can be seen in Figure 4.
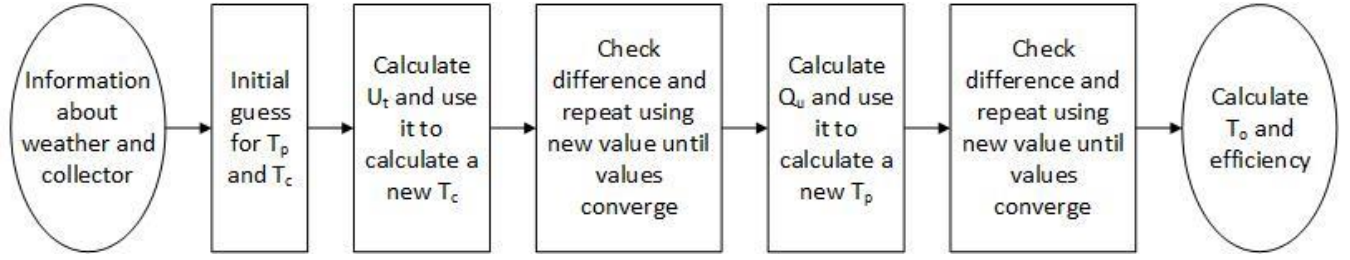
Figure 4:Layout of Duffie and Beckman [5] flat-plate collector model

Dubey and Tiwari [11] looked at the benefit of placing PVT collectors in series. Figure 5 from their article shows that although adding additional collectors in series adds additional thermal energy, it also decreases the instantaneous efficiency of the system.
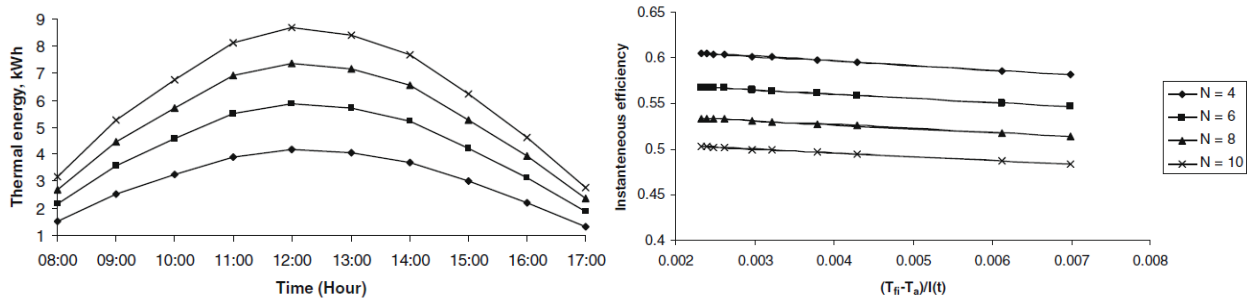
Figure 5: Thermal energy (left) and instantaneous efficiency (right) for different numbers of collectors in series [11].

The effect of changing the flowrate through PVT collectors was examined by Chow [7]. It was found that as the flowrate increases, both the thermal (η_t) and electrical efficiency (η_e) increase. But as can be seen in Figure 6 (different lines represent different collector conditions), the benefit plateaus as the flowrate increases.
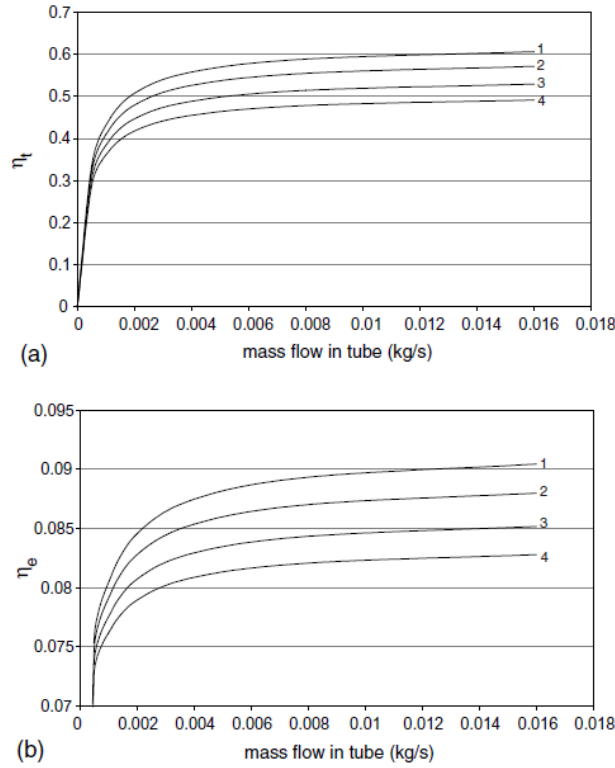
Figure 6: Effect of flowrate on efficiency [7].

Numerous models have been created to predict the performance of PVT collectors. Four numerical models were created by Zondag *et al.* [12]: 1-D, 2-D, and 3-D steady state models, as well as a 3-D dynamic model. The 1-D model was based on the Hottel-Whillier equations similar to the model outlined in Duffie and Beckman [5]. The 3-D dynamic model time-dependant and is actually quasi-3-D, as the absorber and photovoltaic plate are segmented in both parallel direction to the flow and the perpendicular direction, but the top of the collector is only segmented in the direction parallel to the flow. The 3-D steady state model is the same as the dynamic model, except that all equations that are derived with respect to time are set to zero, meaning that the model assumes that variables are not time-dependant. The 2-D model removed the time dependence entirely and instead does the calculations on a layer averaged basis. The model is 2-D because the collector is segmented only in the direction parallel to the flow, so the output of one segment becomes the input for the next segment. The 1-D model is based on

7

Hottel-Whiller and is similar to the model presented by Duffie and Beckman [5]. Comparing the outputs of the Zondag *et al.* [12] models, it was determined that the results were all within 5% accurate to the accompanying experimental results (Figure 7). The 1-D model had a substantially reduced run time (30 times faster than the 2-D model, which is 25 times faster than the 3-D steady state model), but the 2-D and 3-D models offered more flexibility in adapting to different designs [12].
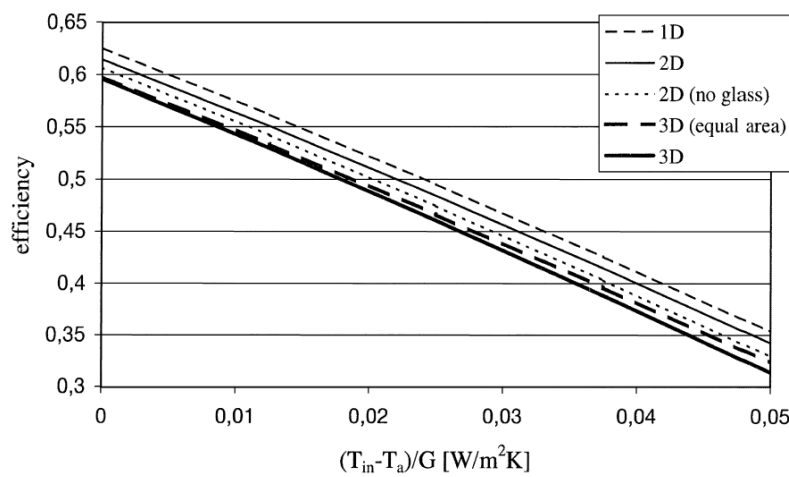
Figure 7: Comparison between the different models examined by Zondag et al. [12]

Dupeyrat *et al.* [13], as part of their study to make PVT collectors more efficient, created a 2-D model, similar to the Duffie and Beckman [5] model, but with the addition of the photovoltaic cells. The Dupeyrat *et al.* [13] model did this by modifying the thermal efficiency term to include the subtraction of the electrical efficiency.

A numerical model proposed by Ben cheikh el hocine *et al.* [14] in Algeria was based on 1-D energy balance equations and described a PVT collector with a photovoltaic module made of three layers: tempered glass, photovoltaic cells, and tedlar. A diagram of this collector can be seen in Figure 8.

Tsky Ta

h_{rad} RAD CONV h_c

COND λ_g/δ_g

Glass T_g

COND $\lambda_{cel}/\delta_{cel}$

PV cell T_{si}

COND $\lambda_{ted}/\delta_{ted}$

Tedlar T_{ted}

COND $\lambda_{abs}/\delta_{abs}$

Plat_h T_{absh}

$h_{rad(absh\_absl)}$ RAD CONV h1 CONV h2

Plat_1 T_{absl}

U_b

Ta

Symbols
T – temperature
h – heat transfer coefficient
λ – conductivity
δ – thickness
U_b – back loss coefficient

Subscripts
sky – sky
a – ambient
rad – radiation
c – convection
g – glass
cel – solar cell
si – silicon solar cell
ted – tedlar
abs – absorber
absh – higher absorber
absl – lower absorber

Figure 8: Diagram of Ben cheikh el hocine et al. PVT model [14].

The Ben cheikh el hocine *et al.* [14] model had an electrical efficiency of 11.12% and thermal efficiency of 16.24% when using air as the working fluid, and an electrical efficiency of 11.13% and thermal efficiency of 54.51% when using water as the working fluid. Therefore, the article concluded that natural air circulation is the easiest and cheapest way to cool the photovoltaic module but using a fluid offers a better performance. This fluid is often water, but in climates where freezing may become an issue, a glycol solution is often used for year-round operation. The model was validated in another paper by Touafek *et al.* [15]. The graph comparing the results can be seen in Figure 9, however no numerical description of the validation was offered.
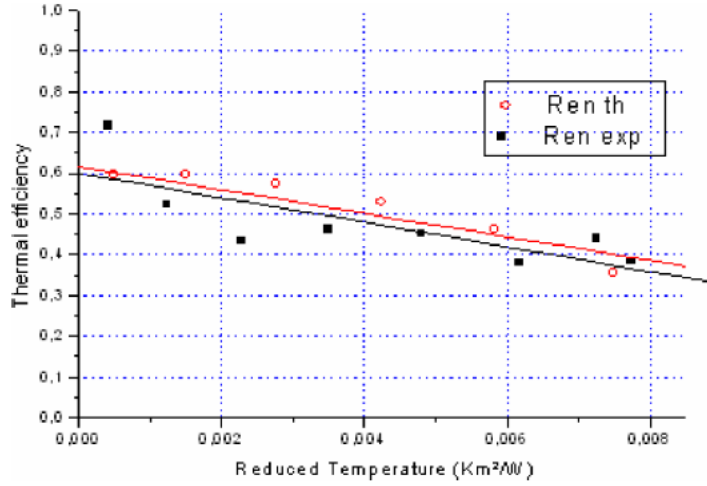
Figure 9: Validation of Ben cheikh el hocine et al. model to experimental results [15].

A model by Dubey and Tiwari [16] created an analytical model based on energy balance equations. The model was quasi-steady state and used 1-D heat conduction and looked at the effect of covering only a portion of the thermal collector in photovoltaics (Figure 10). Changing the photovoltaic covered area meant that the model effective absorptivity-transmissivity product and overall heat transfer coefficient was calculated differently for each case.
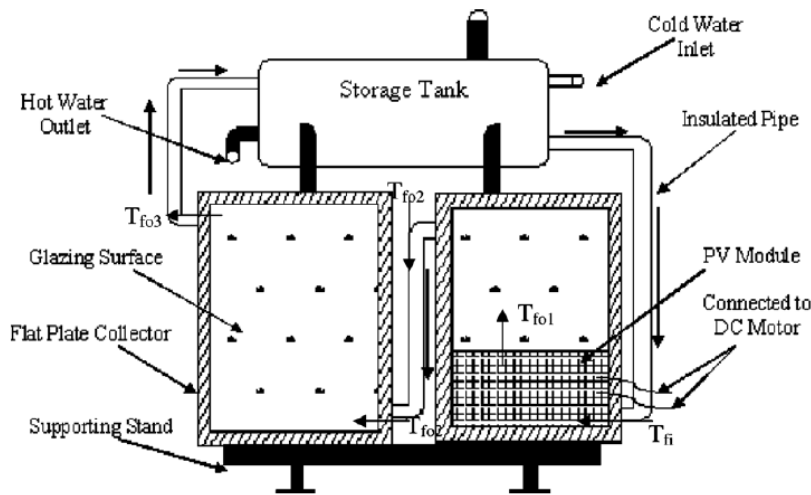
Figure 10: Dubey and Tiwari collector diagram [16].

The model was validated using experimental data from 2007 and the correlation coefficient, r, for the hourly variation of outlet temperature ranged from 0.9997 in March to 0.9996 in February and April and the instantaneous efficiency correlation coefficient ranged from 0.993 in February to 0.972 in March. The root mean square percent deviation, e, ranged from 0.843 to 1.37 for the hourly variation of outlet temperatures and from 16.81 to 22.35 for the instantaneous efficiency. The validation graphs for February 2007 can be seen in Figure 11.
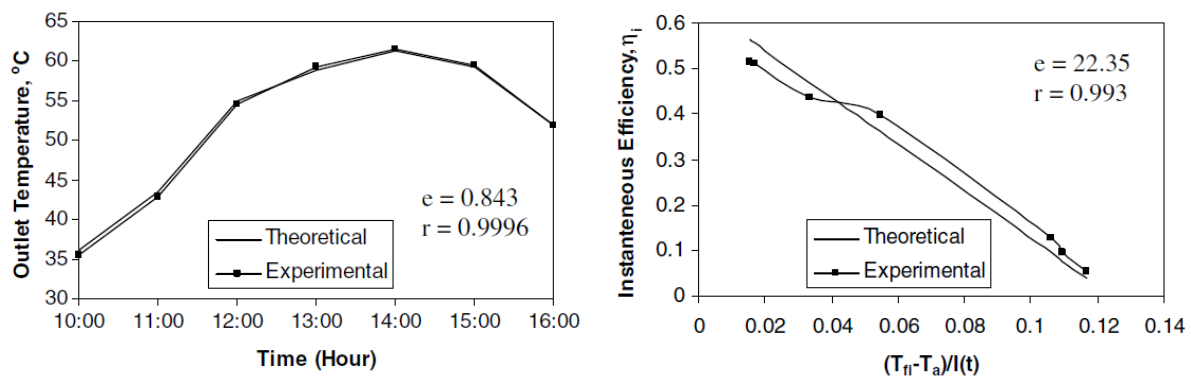
Figure 11: Validation of Dubey and Tiwari PVT model hourly variation of outlet temperature (left) and instantaneous efficiency (right) [16].

2.2 Evacuated Tube Models

Evacuated tube collectors are a type of concentrating solar collector. A concentrating collector has a concentration ratio, defined as the ratio of the aperture area to the receiver area. ET collectors are a type of concentrating collector that consist of an inner and outer tube with a vacuum between them. The outer tube is clear to allow the sun's rays to pass through, while the inner tube has an absorbing coating and is heated by the solar radiation. The working fluid runs through this inner tube to transfer the heat from the collector to its application. The vacuum between the inner and outer tubes reduces heat losses from convection. A diagram of an ET collector can be seen in Figure 12.
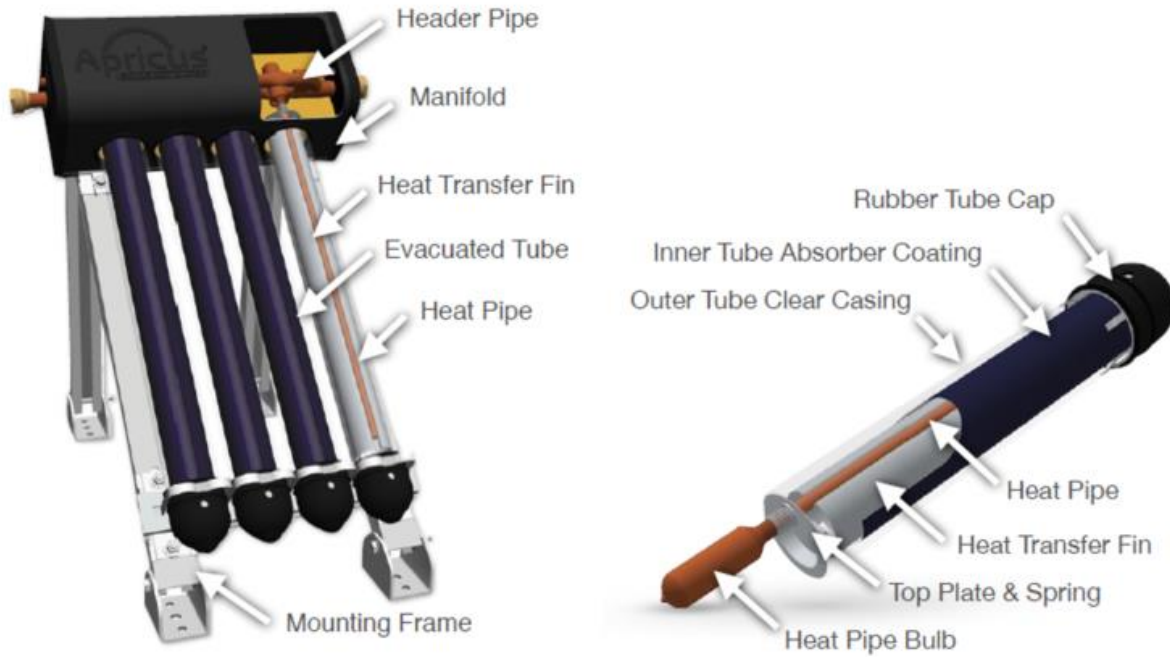
Figure 12: Diagram of an ET collector (left) and close-up of a single evacuated tube (right) [17].

A paper by Wang *et al.* [18] compared the performance of ET collectors to different PVT collectors (Figure 13).
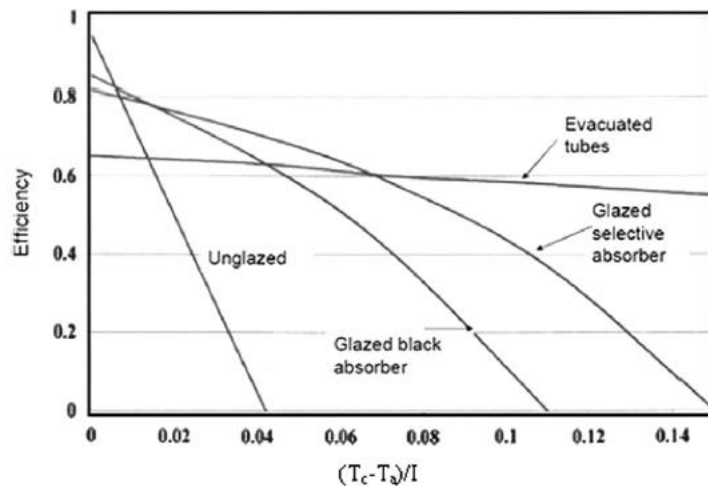
Symbols
Ta – ambient temperature
Tc – collector temperature

Figure 13: Comparison of PVT and ET performance [18].

The comparison shows that while the PVT collectors may perform better at lower temperature differences, the ET collector has a more constant performance across the range of temperature differences.

The most commonly used analytical model of a concentrating collector is the one created by Duffie and Beckman [5]. This steady state model is based on energy balance equations. The model is primarily made up of two large iteration loops: one for the temperature of the receiver, one for the temperature of the cover. These loops must be solved concurrently, as the two temperatures rely on each other. A flowchart of the structure of this model can be seen in Figure 14.
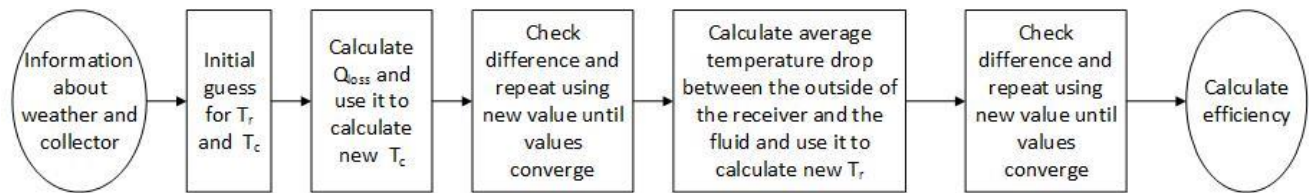
Figure 14:Layout of Duffie and Beckman [5] concentrating collector model

Duffie and Beckman's model [5] is often used as a starting point for other models that have been created. In their journal article, Yu *et al.* [19] created a steady-state model for a simple straight-through ET collector (Figure 15) with air as the working fluid and used thermal network equations (Figure 16), starting with the model suggested by Duffie and Beckman [5].

Yu *et al.* [19] included an additional iteration loop which was needed because, unlike Duffie and Beckman's [5] model, the flow rate through Yu *et al.*'s [19] collector was treated as an unknown. The flow through their collector did not have a fan but was instead driven by the thermal pressure difference between the air in the tube and the air in the room being heated. The extra iteration loop means that the model has an additional unknown value, and also creates an additional level of complexity in the calculations.

(b)
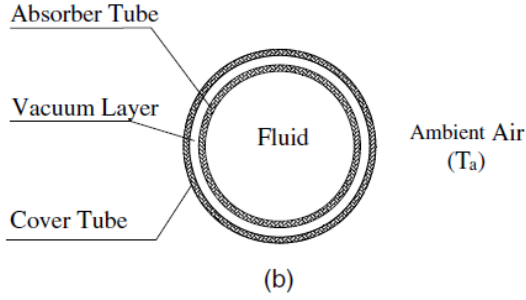
Figure 15: Cross-section of a straight-through ET collector [19].
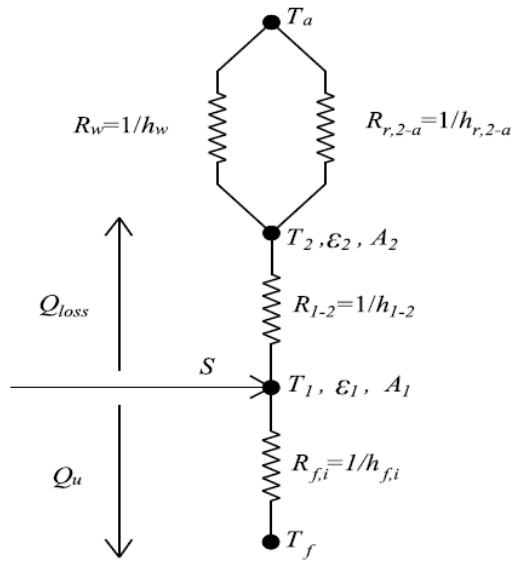
Symbols
T – temperature
R – thermal resistance
h – heat transfer coefficient
ε – emissivity
A – area
Q_{loss} – thermal loss
Q_u – useful heat gain

Subscripts
a – ambient
r – radiative
w - convective
1 – absorber tube
2 – cover tube
f – airflow
i – absorber tube

Figure 16: Thermal network diagram for a straight-through ET collector [19].

Paradis *et al.* [20] created a model of a similar straight-through collector with air as the working fluid to the one created by Yu *et al.* [19], but is a steady state model where ambient air temperature, unsteady solar radiation, and wind speed are used to calculate data using energy conservation equations. To be able to analyze the change in temperature of the working fluid as it travels along the length of the collector, the evacuated tube is cut into theoretical slices as displayed in Figure 17.

Figure 17: Representation of the theoretical slices (top) and thermal network diagram (bottom) of Paradis et al. model [20].

This modeling process means that there are two iteration loops: the loop that advances the

timestep, and the loop inside the timestep loop that calculates the temperature for each

theoretical slice along the length of the tube. When compared to experimental results, the Paradis

et al. [20] model resulted in a root mean square error of 0.05 K and a mean bias difference equal

to 0.15 K in the outlet air temperature.

A model created by Kabeel *et al.* [21] modeled an evacuated tube by integrating the absorbed

solar radiation, as calculated by Duffie and Beckman [5], over the circumference of the tube and

then dividing the tube into theoretical slices and modeling each slice as if it were a flat-plate

collector; this was done earlier by Pyrko [22] and allows the use of flat-plate collector modelling

strategies to be applied to the curved surface of ET collectors. The model by Kabeel *et al*. [21]

also had the addition of a detailed calculation for the effect of the shading of one tube by another.

This was accomplished by taking the other tubes into account when determining the part of the

tube that has a direct line of sight to the sun and integrating to calculate the radiation of the

circumference of the tube. The starting and ending points for the integration change according to

the section that has access to sunlight and are shown in Figure 18. The advanced shading

calculation of this model increases the accuracy but adds a lot of complexity to that portion of

the model.
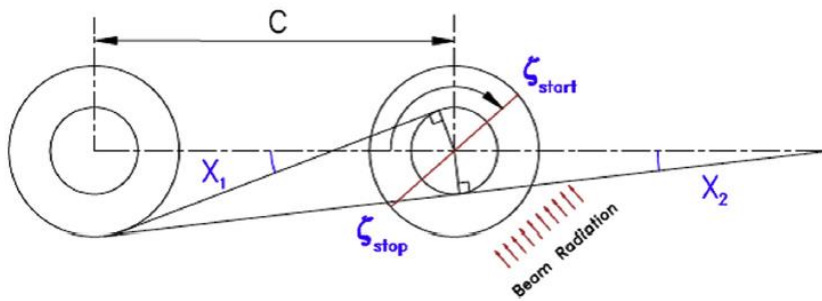
Figure 18: Shading calculation integration start and end points [21].

Gao *et al.* [23] modeled a U-pipe evacuated tube collector. Their model included a detailed

mathematical description of the interaction between the fin and the U-tube. The U-tube was

simplified into an equivalent single tube collector to simplify the model. This also means that the

location of the fin was changed to an equivalent position. These simplifications allow the model

to be easily analysed and reduces computation time. The simplifications are summarized in

Figures 19 and 20.
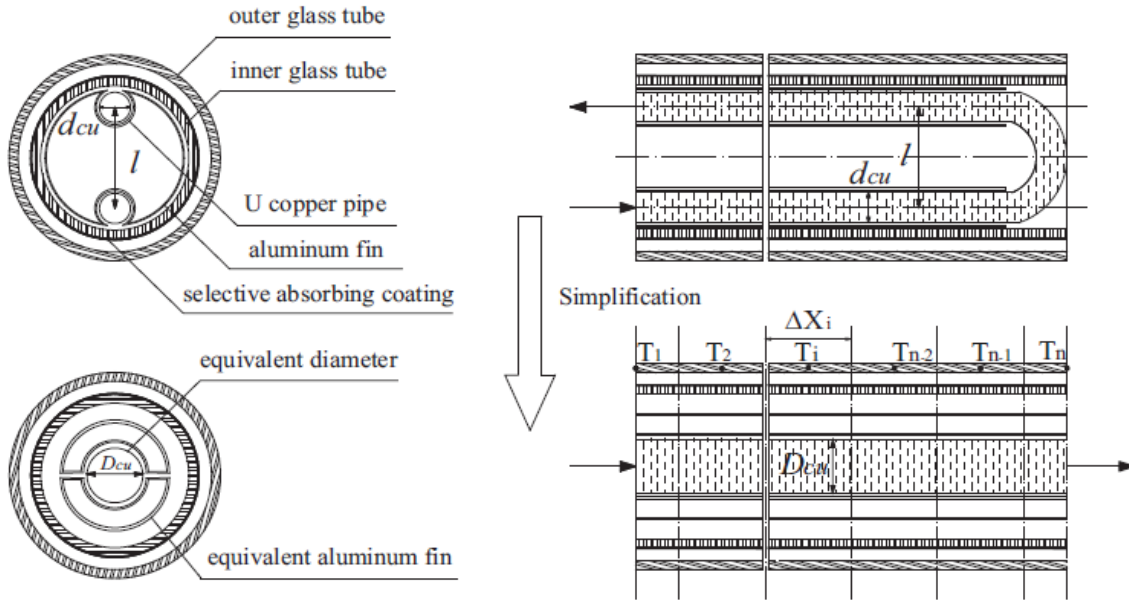
Figure 19: Simplification of U-pipe to single pipe [23].
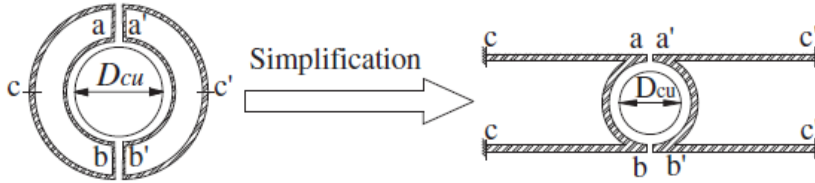
Figure 20: Diagram of simplification of the fin [23].

The detailed fin interaction model was constructed to be able to consider that the temperature around the circumference is not constant. When compared to an experimental set-up, the model by Gao *et al.* [23] produced a maximum error in the outlet temperatures of 0.35°C and 0.49°C for two different tests, and an average error in outlet temperatures for those same tests of 0.14°C and 0.16°C.

2.3   Feasibility Studies

Solar energy at the building scale works best on buildings with large footprints and minimal shading such as large box stores. Buildings like these exist all over the world and present an

important opportunity for the implementation of solar energy. Companies that own big box stores have already started to use their large roof spaces for this purpose; in the United States, the top 10 big box store solar producers are (in order of highest to lowest production): Target, Walmart, Prologis, Apple, Kohl's, Costco Wholesale, General Growth Properties, IKEA, Macy's, and Amazon [24]. Target alone has 203.5 MW of solar electricity production in the United States. The top 10 companies together added a total of 325 MW of solar production in 2017 [24].

Walmart has an overall goal of being supplied by 100% renewable energy in the future [25] with a more specific goal of being supplied by 50% renewable energy by 2025 [26]. In Illinois, Walmart and SunPower are adding 23 MW of solar power over 21 sites, increasing the solar capacity of Illinois by 25% [26].

A study by Dubey and Tiwari [11], mentioned earlier, concluded that if 10% of the houses in Delhi, India were covered in PVT collectors, then the carbon offsets would be worth USD $144.5 million per annum for thermal energy, and USD $14.3 million per annum for electricity.

From the research on solar collectors examined, there remains the question of which collector type or ratio of multiple types would perform the best for a building or district, from both an energy and a greenhouse gas perspective. Further, the best way to determine this ratio for building clusters is unclear and if these collectors were implemented on a larger scale what would be possible. These issues led to the development of the research objective and specific research questions and this investigation addresses these questions by presenting a methodology to test varying collector ratios, layouts, and flowrates to determine the preferred implementation for a given building or building cluster given the desire to minimize energy use or GHG emissions.

3 Methodology

To determine the best ratio and layout of, and flowrate through the PVT and ET collectors for a given building, as well as the potential benefits of implementation of these collectors on a district scale, it was determined that the following methodology would be used to develop, test, and use the tool for a few case studies (Figure 21).
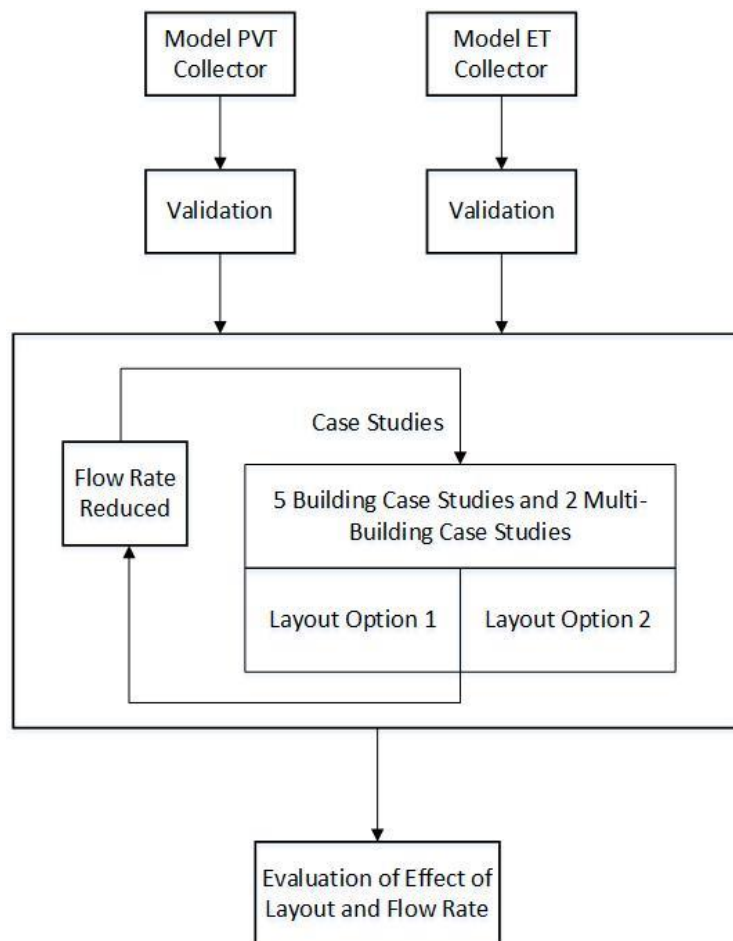
Figure 21: Overview of methodology.

The thesis by Dembeck-Kerekes [1] followed a somewhat similar methodology; he also created a model of a PVT collector and used it to test various cases. That study helped to inform the methodology of this project. The project began with a review of existing models to understand

what the current research in the area have been completed. Once the basis for the models for the required collectors created for this investigation were decided on, they were programmed using Maple 2016 [27]. Maple was chosen for three reasons. First, it shows the mathematical equations as formulae rather than computer code, rendering it human readable. Second, it incorporates programming elements to permit coding of the iterative loops, allowing a full year to be run and iterated at each step within a single simulation. Finally, this works builds on previous modeling of PVT collectors done by Dembeck-Kerekes [1] that was completed in Maple. To verify that the created models were accurate, they were validated using published collector performance values from a solarkeymark certified manufacturer's tests and a published study. The models were combined into one tool, with different layout, ratio, and flowrate options, using Excel, then the completed tool was used to examine five case studies.

3.1 Model Selection, Development, and Validation

Existing models were reviewed in order to understand the current research in the area, as well as to examine different approaches for modeling photovoltaic thermal (PVT) collectors and evacuated tube (ET) collectors. These existing models informed alterations and simplifications made when creating the models for the two types of collectors. Both the PVT and ET collector models were based heavily on the approach developed by Duffie and Beckman [5], with some alterations which will be discussed later in more detail. The PVT model was altered from the flat plate collector model in their textbook Solar Engineering of Thermal Processes [5] to include the addition of the photovoltaic laminate. Coding of the models was done using Maple 2016. The inputs that must change with each timestep were imported from an Excel spreadsheet. Once the code has been run, the output values from the Maple code were transferred to another Excel spreadsheet for ease of analysis.

The PVT and ET models were validated using performance data from existing academic studies and performance curves published by manufacturers. The PVT model was validated by comparing its outputted thermal and electrical energy collected to those from Vokas *et al.* [10] when the same input values were used. The ET model's thermal energy outputs were compared to the performance curve for the Apricus ETC-20 Solar Collector [17]. These validations were performed to confirm the accuracy of the models created.

3.2 Case Study Investigation

The case studies chosen were all from the Department of Energy (DOE) reference buildings [28]. The case studies chosen were: standalone retail building, midrise apartment, large hotel, medium office, and large office. The standalone retail building was chosen because it presents an important opportunity for solar energy production due to its large footprint, minimal shading and tendency to be single-storey. The other buildings were chosen because they make up a large proportion of the buildings in the Toronto 2030 District. For each building, it was assumed that they are connected to a ground-loop system that stores thermal energy, allowing it to be used year-round, and are connected to the electrical grip with a net-metering system. The geometry of the buildings was used to determine the roof area available for solar collectors, and heating and electrical loads for the building were used to compare with the energy production from the solar arrays.

This investigation considered two layout options for the combination of the two Maple models: one that split the flow between the collector arrays, and one which put all the flow through the PVT array, and then through the ET array. These two layouts were chosen to examine the effect that heating a large volume of working fluid just once vs heating a smaller total amount of

working fluid twice, first through a PVT collector and then an ET collector. These two layouts can be seen in Figures 22 and 23.
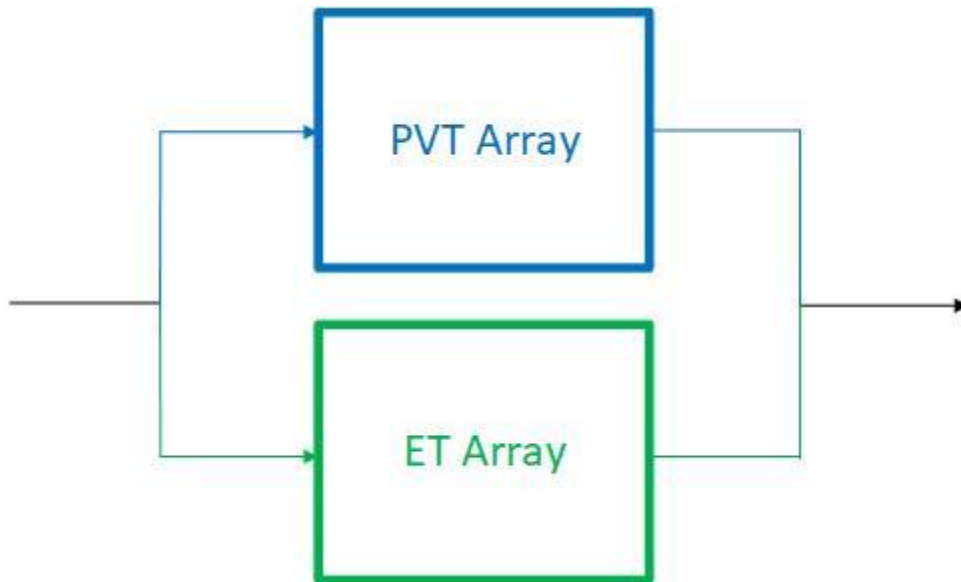
Figure 22: Parallel layout.
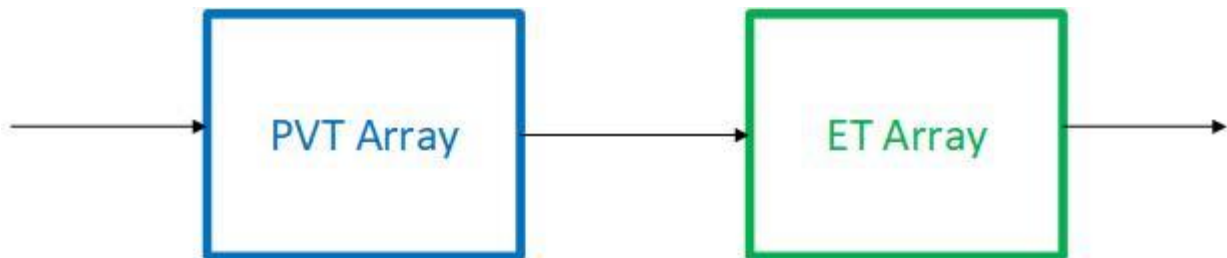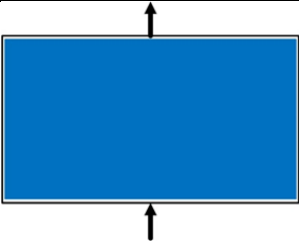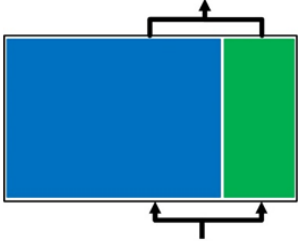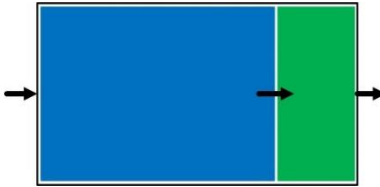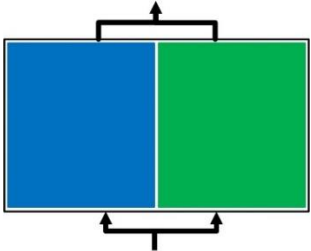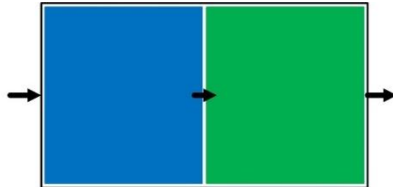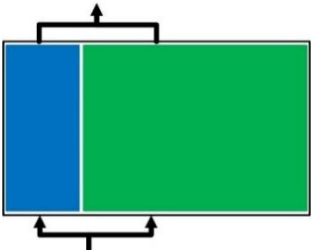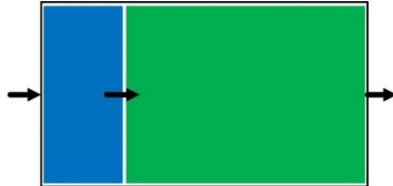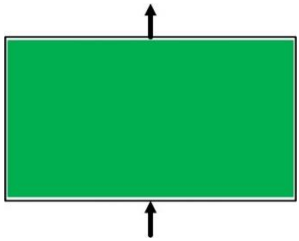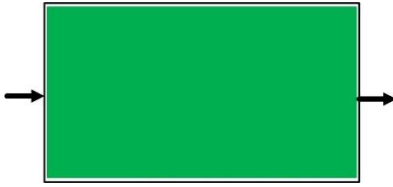
Figure 23: Series layout.

An Excel workbook where different ratios of collector could be compared and analyzed was created for each layout to combine the PVT and ET models. The investigation of the effect of different ratios was done by examining set ratios of 0:100, 25:75, 50:50, 75:25, and 100:0. The different ratios for each layout can be seen in Table 1.

Table 1: Ratios for each layout option.

Area Ratio (PVT:ET)	Parallel Layout	Series Layout
100:0		
75:25		
50:50		
25:75		
0:100		

The investigation also looked at the effect of reducing the flowrate through the collectors. Three different flowrates for each collector type were used: the flowrates recommended by the

manufacturers and journal articles used in the validation process, 50% of the recommended

flowrates, and 10% of the recommended flowrates.

3.3   Comparative Evaluation

The results of each ratio, layout, and flowrate were compared. The thermal, electrical, and total

energy produced were compared to see which options performed better. The greenhouse gas

(GHG) that was offset by the collectors in each case was also calculated so that they could be

compared alongside the energy production. The energy production and GHG offsets are both

being investigated because the optimal solution may vary depending on the motivation behind

installing the system. From these findings, the most productive combination of ratio, layout, and

flowrate was found for Toronto's climate for each case study examined. These findings were

used to determine the best strategy for each building, and what is possible for the Toronto 2030

District.

4   Model Creation

Two models were required to create the tool: one for a PVT collector, and one for an ET collector. After deciding on the basic geometry and layout of the collectors, Maple 2016 [27] was used to create both models. Both models are based on Duffie and Beckman [5], and then altered as needed for changes to the collectors and for different assumptions made based on other existing literature. Both the PVT and ET models contain simplifications:

1. The models overestimate the energy produced in the morning because the inlet temperature of the working fluid that has been stagnant in the pipes overnight is lower than the assumed inlet temperature for the models.

2. The models underestimate the energy produced in the evening because they do not consider that the thermal mass of the collectors will retain heat and therefore still heat the working fluid for a period of time after the sun has set.

3. The seasonal variation in ground loop temperature due to heat addition and removal from the system is ignored as this is intended to quantify the energy storage potential of the system rather than provide a detailed model of geo-exchange heat transfer mechanisms.

These simplifying assumptions were incorporated to prevent the model from becoming unnecessarily complex and to allow the models to run in a shorter amount of time.

4.1   PVT Model

The model of the PVT collector was based on the Duffie and Beckman flat-plate collector model [5] with a few alterations, the most notable of which was the addition of the photovoltaic laminate. The PVT collector used to create the model has one glass cover, which reduces the heat

25

loss, and then an air gap before the photovoltaic laminate and absorber plate. Behind the absorber plate is insulation with metal tubes running through it, touching the absorber plate.

The model contains two iteration loops: one for converging T_p, the temperature of the absorber plate, and one for converging T_c, the temperature of the cover. A flowchart that lays out the overall structure of the model is shown in Figure 24.

After an initial estimate was made for T_p and T_c, the loss coefficient U_l, was calculated [5]:

$$U_l = U_t + U_b + U_e \tag{1}$$

Where U_t is the top loss coefficient, U_b is the bottom loss coefficient, and U_e is the edge loss coefficient. U_b and U_e are functions of the collector geometry and insulation conductivity, while U_t is based on heat transfer coefficients [5]:

$$U_t = \cfrac{1}{\cfrac{1}{h_{r,p-c} + h_{c,p-c}} + \cfrac{1}{h_{r,c-a} + h_{c,c-a}}} \tag{2}$$

where $h_{r,p-c}$ and $h_{c,p-c}$ are the radiative heat transfer coefficient and the conductive heat transfer coefficient respectively between the plate and the cover, and $h_{r,c-a}$ and $h_{c,c-a}$ are the coefficients between the cover and the air. There is a slight difference here from the Duffie and Beckman method: the convective heat transfer coefficient between the cover and the air, $h_{c,c-a}$, was calculated based on the simpler correlation as cited by Khoukhi and Maruyama [29] rather than using the wind heat transfer coefficient used by Duffie and Beckman [5] because the coefficient used by Duffie and Beckman requires information that is not always available, so this simplification makes the model more usable. The equation cited by Khoukhi and Maruyama [29] is seen in Eq. 3.

Input matrix is imported from Excel file

Initial guess for T_p

Initial guess for T_c based on T_p value

Value of $newT_c$ calculated

Set value of T_c to the calculated value or $newT_c$

Check if T_c and $newT_c$ match within set tolerance

Calculate U_l, F', Fr, Q_u, and $newT_p$

Set value of T_p to the calculated value of $newT_p$

Adjust Q_u for value of $newT_p$ and recalculate both

Check if T_p and $newT_p$ match within set tolerance

Calculate η_c, T_o, Q_e, and η_e

Export output matrix to Excel

Symbols
T – temperature
newT – new value for temperature
U_l – loss coefficient
F' – collector efficiency factor
Fr – heat removal factor
Q_u – useful thermal energy
Q_e – useful electrical energy
η – efficiency

Subscripts
p – plate
c – cover
o – outlet
c – thermal
e – electrical

Figure 24: Flowchart showing the structure of the PVT model.

27

$$h_{c,c-a} = 2.8 + 3v \tag{3}$$

The other coefficients are defined as follows:

$$h_{r,p-c} = \frac{\sigma * (T_p + T_c) * (T_p^2 + T_c^2)}{\frac{1}{\varepsilon_p} + \frac{1}{\varepsilon_c} - 1} \tag{4}$$

$$h_{c,p-c} = \frac{Nu * k_{air}}{L} \tag{5}$$

$$h_{r,c-a} = \sigma * \varepsilon_c * (T_c + T_s) * (T_c^2 + T_s^2) \tag{6}$$

where σ is the Stefan-Boltzmann constant, ε_p is the emissivity of the plate, ε_c is the emissivity of the cover, Nu is the Nusselt number, k_{air} is the thermal conductivity of the air, L is the length of the collector, and T_s is the temperature of the sky, which was assumed to be 6°C colder than the ambient air.

There are properties of air that must be known to calculate other variables. These include k_{air}, as well as the density, ρ_{air}, and the viscosity, v_{air}. The thermal conductivity and density were calculated using empirical equations proposed by Zografos *et al.* [30], while the viscosity was calculated using published data by Boueloup [31] for the given temperature and pressure. These empirical equations were used because in the Duffie and Beckman [5] model the properties are extracted from a table of values. The empirical equations allow the programmed model to find the values much faster. The empirical equations are seen in Eqs. 7 to 9.

$$k_{air} = 1.5797 * 10^{-17} * \left(\frac{T_c + T_p}{2}\right)^5 + 9.46 * 10^{-14} * \left(\frac{T_c + T_p}{2}\right)^4 + 2.2012 * 10^{-10}$$

$$* \left(\frac{T_c + T_p}{2}\right)^3 - 2.3758 * 10^{-7} * \left(\frac{T_c + T_p}{2}\right)^2 + \tag{7}$$

$$1.7082 * 10^{-4} * \left(\frac{T_c + T_p}{2}\right) - 7.488 * 10^{-3}$$

$$\rho_{air} = 345.57 * \left(\left(\frac{T_c + T_p}{2}\right) - 2.6884\right)^{-1} \tag{8}$$

$$\nu_{air} = -1.1555 * 10^{-14} * \left(\frac{T_c + T_p}{2}\right)^3 + 9.5728 * 10^{-11} * \left(\frac{T_c + T_p}{2}\right)^2 +$$

$$3.7604 * 10^{-8} * \left(\frac{T_c + T_p}{2}\right) - 3.4484 * 10^{-6} \tag{9}$$

These properties allow for the calculation of the Rayleigh number, Ra and the Nusselt number, Nu, which were required for equations above. The thermal diffusivity, α_{th} [5] was calculated as follows:

$$\alpha_{th} = \frac{k_{air}}{\rho_{air} * C_{pa}} \tag{10}$$

where C_{pa} is the heat capacity of air. Once U_l is calculated, a new cover temperature, $newT_c$, is calculated [5]:

$$newT_c = T_p - \frac{U_l * (T_p - T_a)}{h_{r,p-c} + h_{c,p-c}} \tag{11}$$

where T_a is the ambient air temperature. This value was then compared to the initial assumption for T_c, creating a loop where if the difference between the two values for cover temperature are more than a set tolerance, T_c was set to the value of $newT_c$ and the process to calculate U_l and $newT_c$ repeats until the values for cover temperature converged. Once the values converged, the fin efficiency factor, F, collector efficiency factor, F', and heat removal factor, Fr, were calculated [5]. The variable m was used in the calculation of F to simplify the equation. The

calculation of m varies from Duffie and Beckman [5] as it must account for the addition of the photovoltaic laminate in the calculation in addition to the absorber plate. The equations are as follows:

$$m = \sqrt{\left| \frac{U_l}{k_{ab} * \delta_{ab} + k_{pv} * \delta_{pv}} \right|} \tag{12}$$

$$F = \frac{\tanh\left(\frac{m * (W - d)}{2}\right)}{\frac{m * (W - d)}{2}} \tag{13}$$

$$F' = \frac{\frac{1}{U_l}}{W * \left(\frac{1}{U_l * (d + (W - d) * F)} + \frac{1}{\pi * d * h_{fi}}\right)} \tag{14}$$

$$Fr = \frac{mfr * cpf}{A_c * U_l} * \left(1 - e^{\left(-\frac{A_c * U_l * F'}{mfr * cpf}\right)}\right) \tag{15}$$

where k_{ab} and k_{pv} are the conductivities of the absorber plate and the photovoltaic laminate respectively, δ_{ab} and δ_{pv} are the thickness of the absorber plate and the photovoltaic laminate, W is the distance between the pipes containing the working fluid, d is the pipe diameter, h_{fi} is the heat transfer coefficient between the pipe and the working fluid, mfr is the mass flow rate through the pipes, cpf is the heat capacity of the working fluid, and A_c is the area of the collector.

The solar energy that is turned into electricity by the photovoltaic laminate is no longer available (due to conservation of energy) to heat the working fluid; therefore, the Hottel-Whillier-Bliss equation used in Duffie and Beckman's method [5] was altered to subtract the energy that is turned into electricity from the energy that heats the working fluid. Once the useful thermal

energy, Qu, was calculated using this altered equation, the temperature of the plate can be

calculated [1]:

$$Q_u = A_c * Fr * \left((S * \alpha_p * \tau_c - S * 0.12) - U_l * (T_i - T_a) \right) \qquad (16)$$

$$newT_p = T_i + \frac{\frac{Q_u}{A_c}}{Fr * U_l} * (1 - Fr) \qquad (17)$$

where S is the solar irradiance on the surface of the collector and T_i is the temperature of the

fluid at the inlet of the collector. In this model T_i is assumed to be constant at 283 K. This is

because the working fluid is assumed to have passed through a ground loop before entering the

collector, and the ground is at a constant temperature of 283 K year-round [32].

The calculation of Q_u and $newT_p$ is then repeated, with one difference; the second calculation of

Q_u considers that photovoltaics' performance is altered by their operating temperature [1].

Therefore, the second Q_u equation uses the plate temperature that has just been calculated to

adjust the efficiency of the photovoltaics accordingly. The value for $newT_p$ is then repeated using

the updated Q_u value. This process could be repeated until the values no longer change, but after

the first iteration the value remained within a reasonable threshold (0.01°C) and thus two

iterations were deemed a reasonable balance between model accuracy and computational cost.

$$Q_u = A_c * Fr * \left(\left(S * \alpha_p * \tau_c - S * \left(0.12 * \left(1 - 0.0045 * (newT_p - 298) \right) \right) \right) - U_l * (T_i - T_a) \right) (18)$$

The calculated value for $newT_p$ is compared to the initial assumption for T_p, made at the start of

the calculations. If the values do not match, then the value calculated using Eq. 17 is used to

repeat Eqs. 1 to 18 again, creating the second, larger iterative loop. This continued until the

values converge. After both loops converged, the thermal efficiency of the collector, η_c, and the

outlet temperature, T_o, can be calculated [5]:

$$\eta_c = \frac{Q_u}{S * A_c} \tag{19}$$

$$T_o = T_i + \frac{Q_u}{mfr * cpf} \tag{20}$$

Once the electrical energy, Q_e, is calculated, the electrical efficiency, η_e, can also be calculated

[1]:

$$Q_e = S * \left(0.12 * \left(1 - 0.0045 * \left(newT_p - 298\right)\right)\right) * A_c \tag{21}$$

$$\eta_e = \frac{Q_e}{S * A_c} \tag{22}$$

The energy that is not converted into electrical energy by the photovoltaic laminate is available

to be absorbed into thermal energy. Therefore, the sum of Q_u and Q_e allows the calculation of the

total energy produced by the PVT collector.

4.2 ET Model

The ET model was based on Duffie and Beckman's concentrating collector model [5]. The ET

model, like the PVT model, contains two iteration loops. The loops in this model are for

converging T_{r_ET}, the temperature of the receiver, and one for converging Q_{loss_ET}, the energy

losses in the collector. A flowchart that lays out the overall structure of the model is shown in

Figure 25.
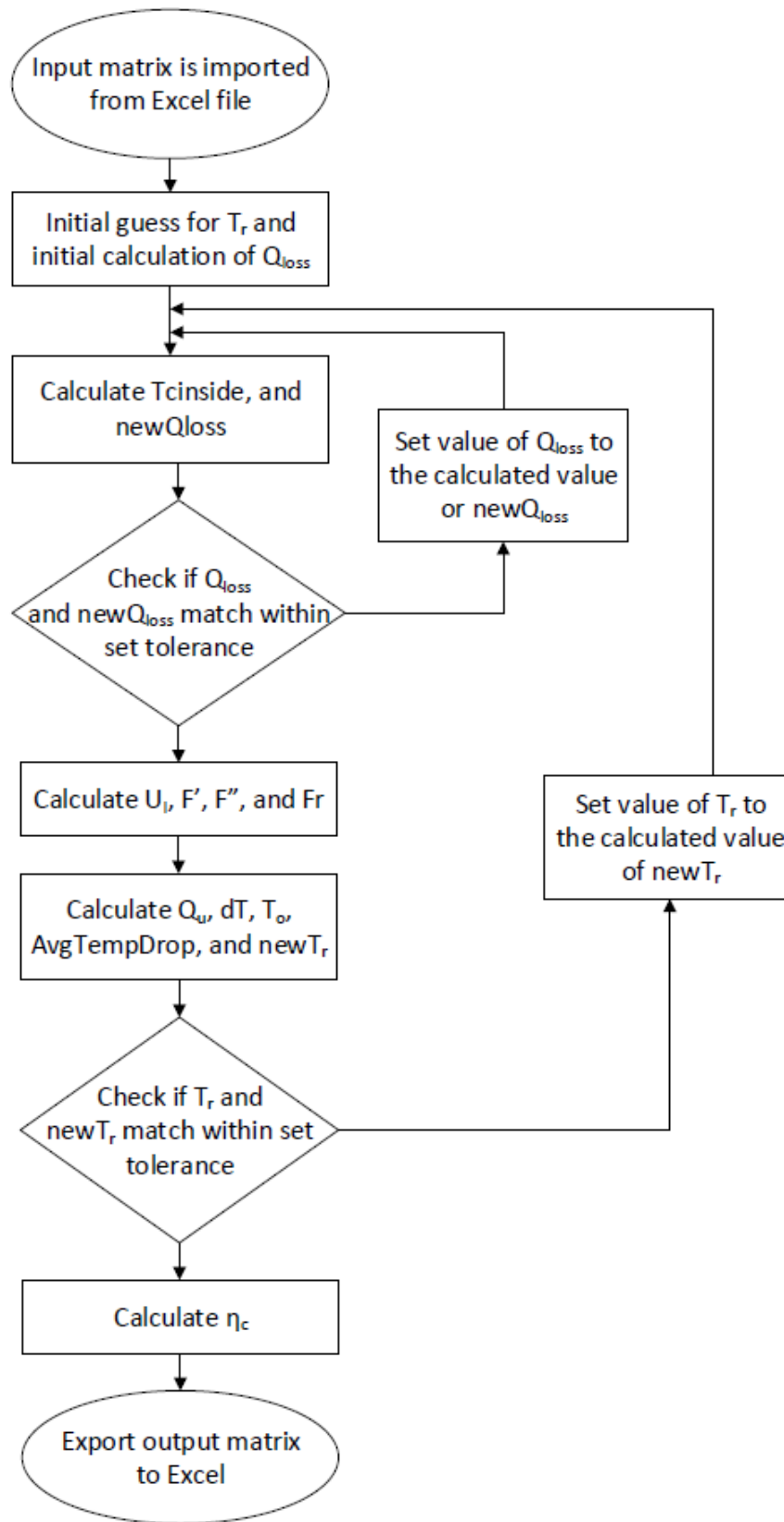
Symbols
T – temperature
newT – new value for temperature
Qloss – energy losses
newQloss – new value for energy losses
U_l – loss coefficient
F' – collector efficiency factor
F" – collector flow factor
Fr – heat removal factor
Q_u – useful thermal energy
dT – change in temperature of the working fluid
AvgTempDrop – average temperature drop
η_c – thermal efficiency

Subscripts
r – receiver
cinside – inside of the cover
o – outlet

Figure 25: Flowchart showing the structure of the ET model.

33

The model begins by assuming a value for the temperature of the receiver, T_{r_ET}, and calculating

an initial value for Q_{loss_ET}. The calculation of Q_{loss_ET} is from the Duffie and Beckman model

[5], but is altered based an assumption made about the behaviour of the evacuated tubes. It is

assumed that, since the evacuated space is a very good insulator, the temperature of the outside

of the glass cover is the same temperature as the ambient air. The validity of this assumption was

verified by cross-checking the outputs of the Duffie and Beckman [5] model including and not

including this assumption. These outputs were within 1.5% of one another, confirming that this

simplification did not introduce noticeable simulation error. The equation to calculate Q_{loss_ET} is

as follows:

$$Q_{loss\_ET} = \varepsilon_{g\_ET} * \sigma * \left(T_{a\_ET}^4 - T_{s\_ET}^4 \right) \tag{23}$$

where ε_{g_ET} is the emissivity of the glass cover, T_{a_ET} is the ambient temperature, and T_{s_ET} is the

temperature of the sky. As in the PVT model, T_{s_ET} is assumed to be 6 °C colder than T_{a_ET}. The

temperature of the inside of the cover, T_{ci_ET}, was calculated as follows [5]:

$$T_{ci\_ET} = T_{a\_ET} + \frac{Q_{loss\_ET} * \ln\left(\dfrac{D_{co\_ET}}{D_{ci\_ET}} \right)}{2\pi * k_{g\_ET}} \tag{24}$$

where D_{co_ET} and D_{ci_ET} are the diameter of the outside of the cover and the inside of the cover

respectively, and k_{g_ET} is the thermal conductivity of the glass cover. The second calculation of

the energy loss, $newQ_{loss\_ET}$, was then calculated to compare to the initial calculation [5]:

$$newQ_{loss\_ET} = \frac{\pi * D_{ro\_ET} * \sigma * \left(T_{r\_ET}^4 - T_{ci\_ET}^4 \right)}{\dfrac{1}{\varepsilon_{r\_ET}} + \dfrac{1 - \varepsilon_{g\_ET}}{\varepsilon_{g\_ET}} * \dfrac{D_{ro\_ET}}{D_{co\_ET} - t_{g\_ET}}} \tag{25}$$

where D_{ro_ET} is the outer diameter of the receiver, D_{co_ET} is the outer diameter of the cover, T_{ci_ET} is the temperature of the inside of the cover, ε_{r_ET} is the emissivity of the receiver, and t_{g_ET} is the thickness of the glass cover. The two energy loss values calculated were then compared and if they did not fall in a set tolerance then Eqs. 24 and 25 are repeated after setting the value of Q_{loss_ET} to the calculated value of newQ_{loss_ET}. Once the values converge the loss coefficient, U_{l_ET}, is calculated [5]:

$$U_{l\_ET} = \frac{Q_{loss\_ET}}{\pi * D_{ro\_ET} * \left(T_{r\_ET} - T_{a\_ET}\right)} \tag{26}$$

The values for collector efficiency factor, $F'_{\_ET}$, collector flow factor, $F''_{\_ET}$, and heat removal factor, $Fr_{\_ET}$, were calculated based on the loss coefficient [5]:

$$F'_{\_ET} = \frac{\dfrac{1}{U_{l\_ET}}}{\dfrac{1}{U_{l\_ET}} + \dfrac{D_{ro\_ET}}{h_{f\_ET} * D_{ri\_ET}} + \left(\dfrac{D_{ro\_ET}}{2 * k_{r\_ET}} * \ln\left(\dfrac{D_{ro\_ET}}{D_{ri\_ET}}\right)\right)} \tag{27}$$

$$F''_{\_ET} = \frac{mfr_{ET} * C_{p\_ET}}{A_{r\_ET} * U_{l\_ET} * F'_{\_ET}} * \left(1 - e^{-\frac{A_{r\_ET} * U_{l\_ET} * F'_{\_ET}}{mfr\_ET * C_{p\_ET}}}\right) \tag{28}$$

$$Fr_{\_} = F'_{\_} * F''_{\_} \tag{29}$$

where h_{f_ET} is the heat transfer coefficient inside the receiver tubes, D_{ri_ET} is the diameter of the inside of the receiver, k_{r_ET} is the thermal conductivity of the receiver, C_{p_ET} is the specific heat of the working fluid, $mfr_{\_ET}$ is the mass flow rate through the collector, and A_{r_ET} is the area of the receiver. The useful thermal energy that the collector produces, Q_{u_ET}, could then be calculated [5]:

$$Q_{u\_ET} = A_{c\_ET} * Fr_{\_ET} * \left(S_{\_ET} - \frac{A_{r\_ET}}{A_{a\_ET}} * U_{l\_ET} * \left(T_{r\_ET} - T_{a\_ET} \right) \right) \tag{30}$$

where S$_{\_ET}$ is the solar irradiance on the surface of the collector, and A$_{a\_ET}$ is the area of the aperture. The change in the temperature of the working fluid from the inlet to the outlet of the collector, d$_{t\_ET}$, was calculated to then calculate the outlet temperature, T$_{o\_ET}$ [5]:

$$d_{t\_ET} = \frac{Q_{u\_ET}}{mfr_{\_ET} * C_{p\_ET}} \tag{31}$$

$$T_{o\_ET} = T_{inlet\_ET} + d_{t\_ET} \tag{32}$$

where T$_{inlet\_ET}$ is the inlet temperature of the working fluid. Like the PVT model, the working fluid was assumed to have come from a ground loop with a constant temperature of 10°C [32]. To calculate the temperature of the receiver, T$_{r\_ET}$, the average temperature drop from the outside of the receiver to the fluid, AvgTempDrop$_{\_ET}$, was calculated [5]:

$$AvgTempDrop_{\_ET} = Q_{u\_ET} * \left(\frac{1}{\pi * D_{ri\_ET} * L_{r\_ET} * h_{f\_ET}} + \frac{\ln\left(\frac{D_{ro\_ET}}{D_{ri\_ET}}\right)}{2\pi * k_{r\_ET} * L_{r\_ET}} \right) \tag{33}$$

$$newT_{r\_ET} = \frac{T_{inlet\_ET} + T_{o\_ET}}{2} + \left(T_{ro\_ET} - T_{f\_ET} \right) \tag{34}$$

The two values for the temperature of the receiver were then compared using a set tolerance. If the difference did not fall within the tolerance, the value of Tr$_{\_ET}$ is set to the calculated value of newTr$_{\_ET}$ and Eqs. 23 to 34 were repeated until the two converged. The thermal efficiency of the collector, η$_{c\_ET}$ was then calculated as follows [5]:

$$\eta_{c\_ET} = \frac{Q_{u\_ET}}{S_{\_ET} * A_{c\_ET}}$$
(35)

4.3   Combination into One Tool

The two models created, PVT and ET, were combined into one tool, using Microsoft Excel as an in-between step. The process used to go between Microsoft Excel and Maple 2016 [27] is presented in Figures 26 and 27.
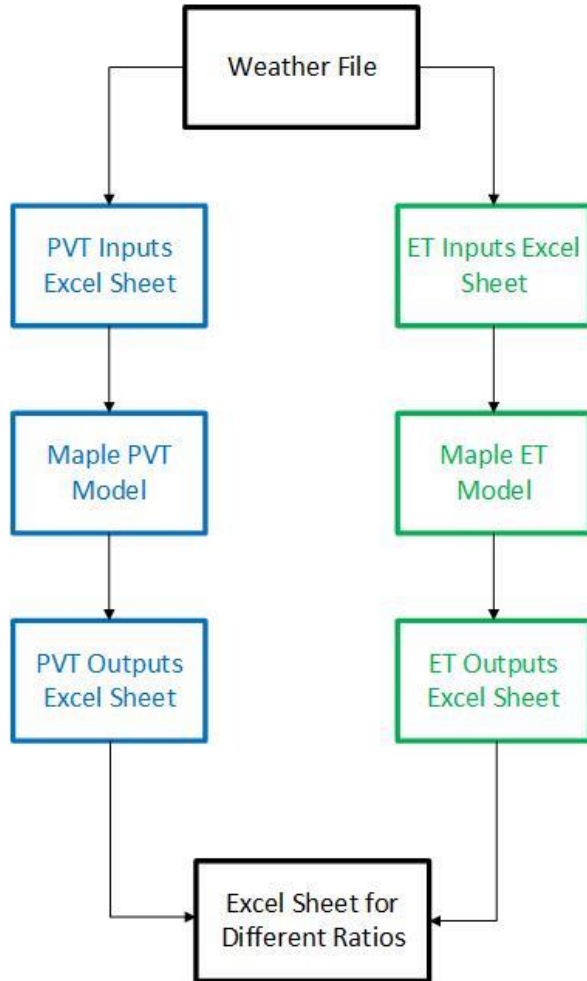
Figure 26: Maple and Excel process for parallel layout.
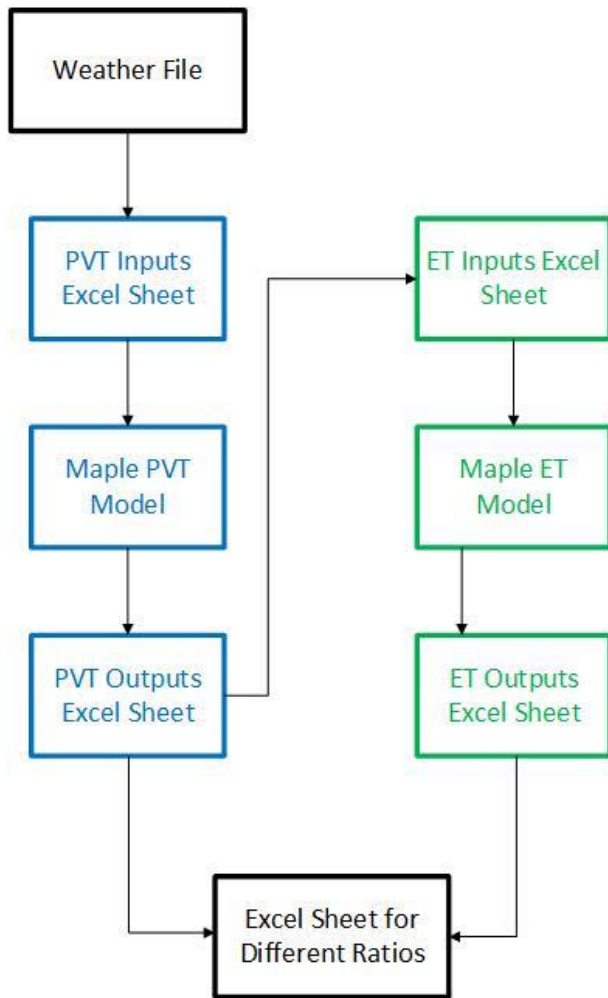
Figure 27: Maple and Excel process for series layout.

There are two options for the layout of the collector types. The parallel layout has the two arrays in parallel; it splits the flow of the working fluid and part goes into the PVT array while the rest enters the ET array (Figure 28). The series layout has the arrays in series; the whole flow goes first through the PVT array, and then the ET array (Figure 29).
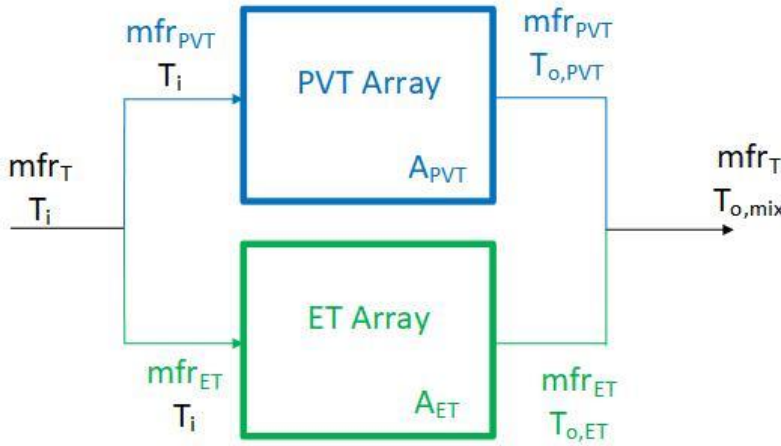
Figure 28: Parallel layout for solar collector arrays.
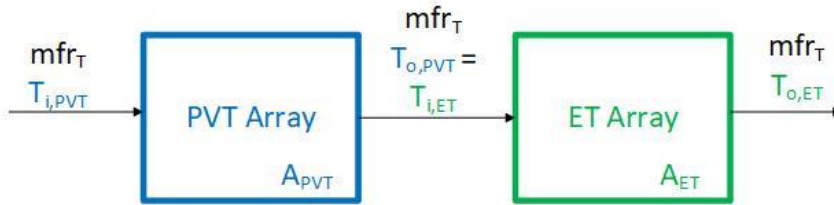
Figure 29: Series layout for solar collector arrays.

In the first layout, an input matrix was imported to both Maple models from Excel, one for the PVT model and one for the ET model. This matrix contains the variables that change with each timestep: ambient temperature, wind speed, and solar insolation. Once the models have been run, the output matrix created were exported back to Excel to be combined into the different ratios considered. These calculations were used to compare the thermal and electrical energy produced and the corresponding GHG offsets associated with each ratio option.

The series layout, like the first, used an input matrix containing ambient temperature, wind speed, and solar insolation, which is input to the PVT Maple model. Once the PVT model had been run, its outputs were exported back to Excel and the outlet temperature from the matrix replaced the inlet temperature for the ET model. Once the ET model had been run, the output matrix was exported to Excel to be combined into the ratios considered. This process is similar to

that of the parallel layout but is complicated slightly because only a portion of the working fluid from the PVT array enters the ET array because the ET collectors require a much lower flowrate than the PVT collectors. The flow that passes through the PVT array but not the ET array is combined with the flow that has gone through both arrays at the end.

These two layouts were created to be able to optimize the array area fractions of each collector type for the given roof. In addition, the two layouts allow a comparison of the outputs to determine which performs better in the Toronto climate, and if there is a seasonal advantage of one layout over another.

5 Model Validation

To verify accuracy, each model was individually validated using results from previously published work.

5.1 PVT Panel Model

The PVT collector was validated by comparing its outputs to those of a model created by Vokas *et al.* [10]. The model used in this paper is also based on the one created by Duffie and Beckman [5], and uses an iterative process similar to the proposed model. Table 2 shows the input values used for the comparison.

Figure 30 shows the thermal efficiency versus the reduced temperature for the two models. The efficiency difference at a reduced temperature difference of 0 Km^2/W is 1.5%, and the largest difference is 2.81% at a reduced temperature difference of 0.05625 Km^2/W. The line showing the Vokas *et al.* [10] model is straight because of the assumed linear relationship between radiative heat loss and the difference between the plate and ambient temperatures. The proposed model generates a curve because the model recalculates the heat loss for each timestep, resulting in non-linear behaviour.

Table 2: Input parameters for the Vokas et al. [10] validation.

Variable	Value	Units
Ambient air temperature, T_a	283	K
Sky temperature, T_s	277	K
Wind speed, v	1	m/s
Emissivity of cover, ε_c	0.88	
Emissivity of absorber plate, ε_p	0.95	
Length of air gap, L (assumed)	0.025	m
Collector angle, β	45	degrees
Heat capacity of air, C_{pa}	1005	J/kgK
Heat capacity of working fluid, c_{pf}	3600	J/kgK
Width between pipes, W	0.095	m
Pipe diameter, d	0.01	m
Pipe-fluid heat transfer coefficient, h_{fi}	300	W/m^{2}K
Absorber thickness, $\delta_{\_ab}$	0.002	m
Absorber conductivity, k_{ab}	390	W/mK
Photovoltaic laminate thickness, δ_{pv}	0.04	m
Photovoltaic laminate conductivity, $k_{\_pv}$	84	W/mK
Area of collector, A_c (adjusted*)	1	m^2
Working fluid flow rate, mfr	0.5016	kg/s
Solar irradiance, S	800	W/m^2
Transmittance-absorptance product, $(\tau\alpha)$	0.74	
Insulation conductivity, K_b	0.045	W/mK
Thickness of back insulation, L_{bi}	0.05	m
Thickness of edge insulation, L_{ei}	0.025	m
Perimeter of collector, perimeter (adjusted*)	4	m

*Note that the actual area of the panel is 1.32 m^2; this area and corresponding geometry was scaled to a 1 m^2 basis for ease of calculation
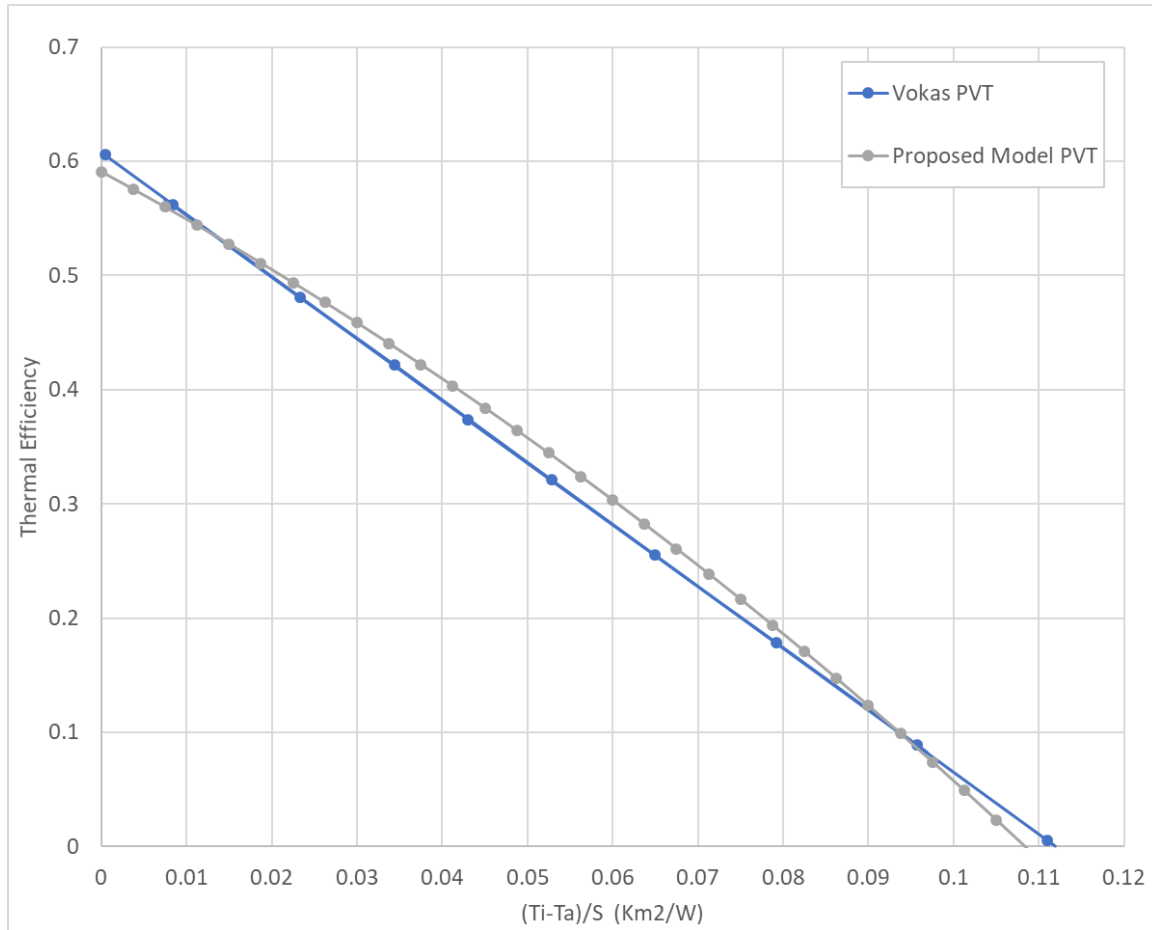
Figure 30: Thermal efficiency vs temperature for Vokas et al. [10] model and proposed model.

5.2   Evacuated Tube Model

The ET collector was validated by comparing the outputs of the Maple model to the published performance data for the Apricus ETC-20 Solar Collector [17]. Table 3 shows the input values taken from the Apricus document and used in the Maple model:

Variable	Value	Units
Area of collector, A_{c_ET} (adjusted[*])	1	m^2
Solar irradiance, $S_{\_ET}$	800	W/m^2
Receiver emissivity, ε_{r_ET}	0.93	
Outside diameter of receiver, D_{ro_ET}	0.047	m
Thickness of receiver tube, $t_{\_ET}$ (assumed)	0.0018	m
Inside diameter of receiver, D_{ri_ET}	0.0434	m
Length of receiver, L_{r_ET} (adjusted[*])	1	m
Thermal conductivity of receiver, k_{r_ET}	401	W/mK
Receiver area, A_{r_ET} (adjusted[*])	0.638242	m^2
Aperture area, A_{a_ET} (adjusted[*])	0.727273	m^2
Outside diameter of cover, D_{co_ET}	0.058	m
Thickness of glass cover, t_{g_ET}	0.0018	m
Inside diameter of cover, D_{ci_ET}	0.0544	m
Glass emissivity, ε_{g_ET}	0.8	
Thermal conductivity of cover, k_{g_ET}	1.2	W/mK
Working fluid flow rate, $mfr_{\_ET}$	0.0078	kg/s
Heat transfer coefficient inside tube, h_{f_ET}	300	W/m^2K
Specific heat capacity of working fluid, C_{p_ET}	3600	J/kgK
Ambient air temperature, T_{a_ET}	293	K
Sky temperature, T_{s_ET}	287	K

[*]Note that the actual area of the panel is $3m^2$; this area and corresponding geometry was scaled to a 1 m^2 basis for ease of calculation.

At the y-axis intercept, where the difference between the ambient and mean collector temperature is 0 K, the Maple model is within 0.4% of the published data. After this point, the Apricus performance curve (Figure 31) decreases less than the proposed Maple model, likely because the Apricus model makes assumptions about heat losses while the proposed Maple model presented calculates these losses for each time step.
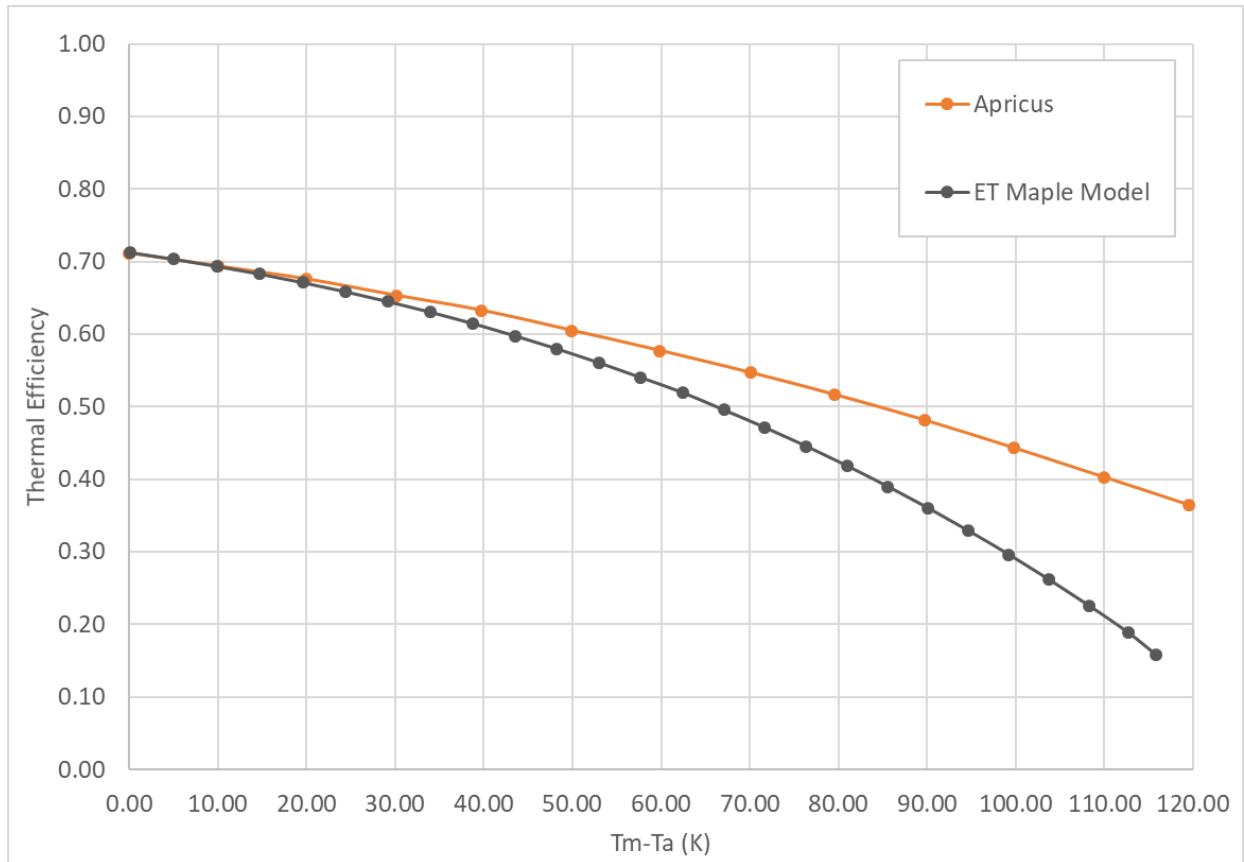
Figure 31: Thermal efficiency vs temperature difference for Apricus collector [17] and proposed model.

6   Case Study Investigations

A series of case studies were based on prototypical building models produced by the Department of Energy [33]. To best represent the diversity of buildings in Toronto, as well as provide insights on potential suburban interventions, the following building typologies were considered: standalone retail, midrise apartment, highrise apartment, medium office, and large office. All case study buildings have been assumed to be tied to a ground-loop to store the thermal energy produced and are connected to the electric grid using a net-metering system.

6.1   Standalone Retail

The standalone retail building is one storey, with a large geographic footprint. An image of the building can be seen in Figure 32 [33].
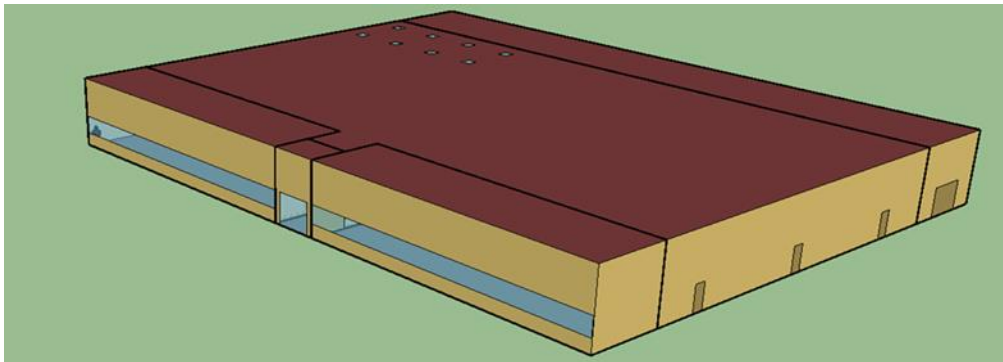
Figure 32: DOE standalone retail reference building.

It was assumed that 50% of the roof area (2,294 m^2) could host solar collectors, allowing for approximately 1,147 m^2 of collector area. The collectors are tilted 45° from horizontal, but to decrease shading each square metre of collector is still assumed to be placed to take up one square metre of space on the roof. The weather file selected for the case study was a Canadian Weather for Energy Calculations (CWEC) file for Toronto City Centre made up of twelve typical meteorological months selected from 30 years of data [34]. The characteristics of the collectors

46

used in the investigation can be found in Tables 2 and 3. They are the same collectors that were

used in the model validation; the Vokas *et al.* [10] collector was used for the PVT, and the

Apricus ETC-20 Solar Collector [17] was used for the ET. The only change was that the

flowrates were changed for some simulations. This was done to see what affect lowering the

flowrate had on energy production and outlet temperature. The table showing the flowrates per

collector can be seen in Table 4.

Table 4: Flowrates per Collector used in Simulations

Simulation	PVT Flowrate (kg/s/m^2)	ET Flowrate (kg/s/m^2)
Manufacturer Recommended Flowrate	0.38	0.0078
50% of Recommended Flowrate	0.19	0.0039
10% of Recommended Flowrate	0.038	0.00078

First, the parallel layout was used for simulations using each of the three flowrates. The resulting

graph of the thermal energy produced can be seen in Figure 33.

For all the ratios of PVT to ET, the recommended flowrate (100%) produced the most thermal

energy, however, for the case where there are only ET collectors the difference in flowrates

makes the most difference. As the ratio includes more PVT collectors, the amount of thermal

energy produced by the three flowrates starts to converge. This is because the change in flowrate

has a larger effect on the ET collectors than the PVT collectors. As the percent PVT increases,

thermal energy decreases for both the 100% and 50% recommended flowrates. In contrast, the

10% recommended flowrate exhibits the opposite trend. This is because 10% of the

recommended flowrate is very low for the ET collectors, creating the drastic change from the

10% flowrate to the 50% flowrate line. This suggests that there is a flowrate that would produce

the same amount of thermal energy for all the ratios.
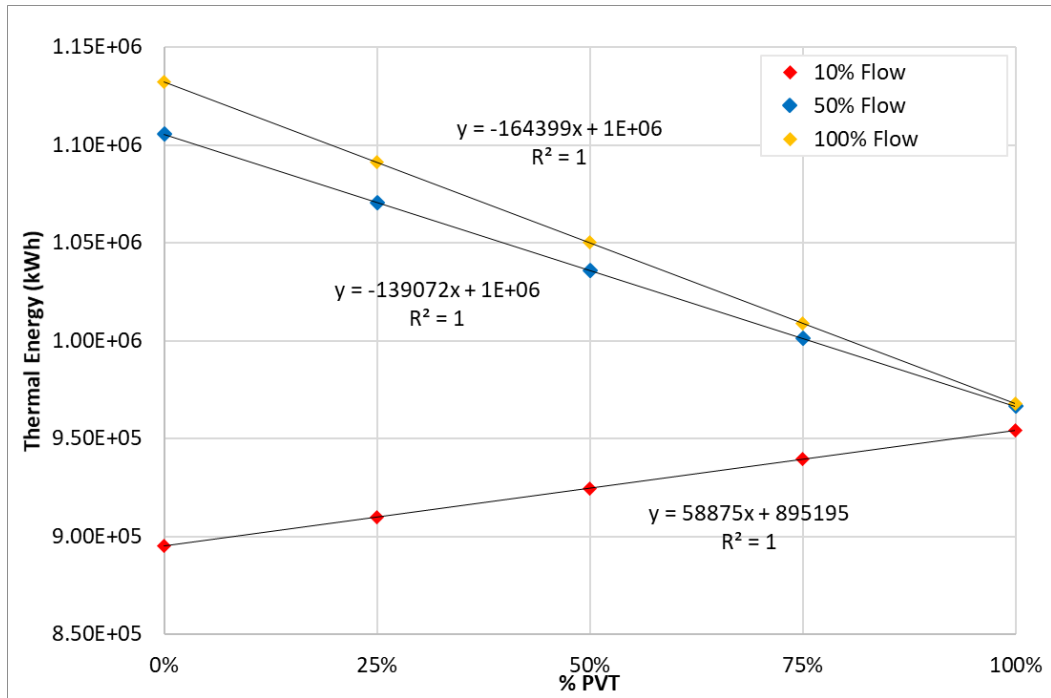
Figure 33: Parallel layout thermal energy production.

The electrical energy production from the same layout is displayed in Table 5.

Table 5: Parallel layout electrical energy production.

% PVT	0%	25%	50%	75%	100%
10% Recommended Flowrate	0 kWh	50,793 kWh	101,586 kWh	152,379 kWh	203,172 kWh
50% Recommended Flowrate	0 kWh	50,990 kWh	101,980 kWh	152,970 kWh	203,960 kWh
100% Recommended Flowrate	0 kWh	51,015 kWh	102,030 kWh	153,044 kWh	204,059 kWh

As expected, with increasing proportion of PVT collectors there is more electrical generation. Each flowrate displays a linear trend from 0 to 100% PVT collectors, and these lines are almost identical. The highest flowrate provides slightly more electrical energy than the lower flowrates. This is because the higher flowrate takes away more heat from the photovoltaic film, reducing de-rating due to excess heat and thus increasing its efficiency.

48

The total energy is the sum of the thermal and electrical energy produced by the arrays. Figure 34 shows the total energy, and Figure 35 shows the annual average outlet temperature of the system.
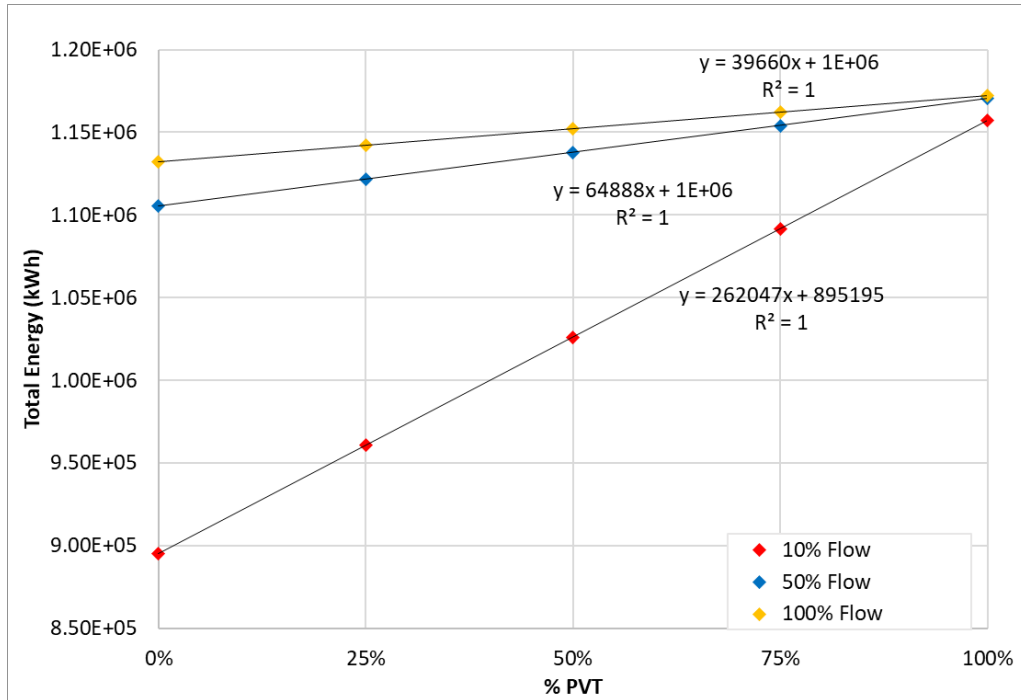
Figure 34: Parallel layout total energy.
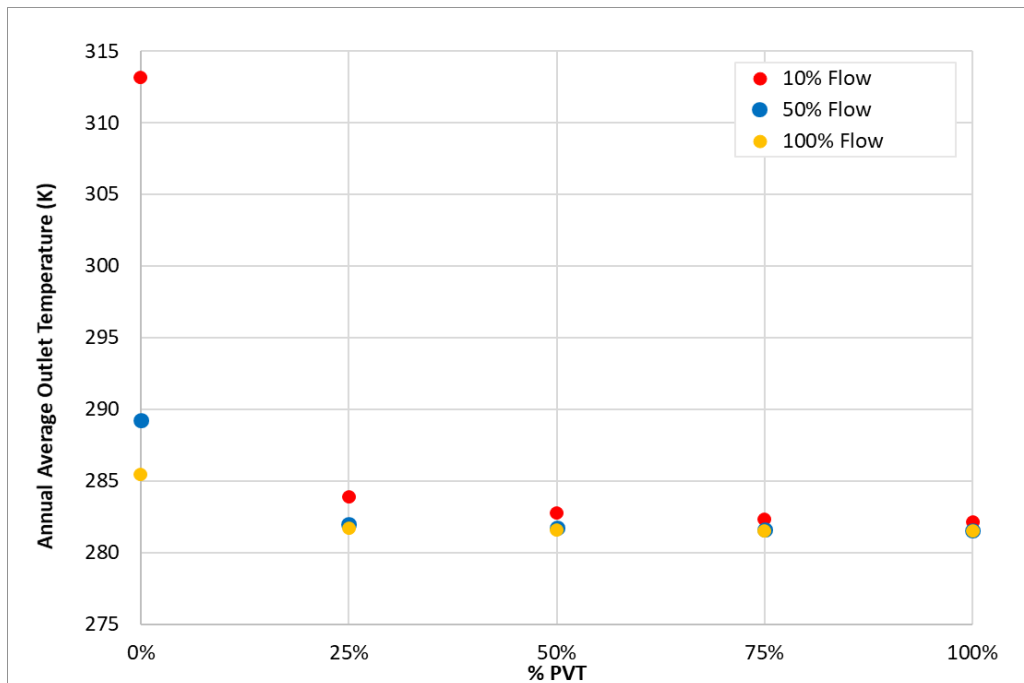
Figure 35: Parallel layout annual average outlet temperature.

49

Both the thermal and electrical energy production were highest when using 100% recommended flowrate, therefore total energy production is maximized at the highest flowrate. This raises the question: why would a lower flowrate be desirable? In some applications, such as when there is a counter-flow heat exchanger instead of a ground loop, the temperature at the outlet of the system must be above a minimum temperature to transfer heat to the building system. In this investigation, for the recommended flowrate, the output temperatures produced were only marginally higher than the input temperature, which is appropriate for thermal storage applications such as geoexchange. The temperature points follow the opposite rule as the total energy; the lower flowrate produces the highest temperatures, and 100% ET collectors also produce higher temperatures.

Another aspect that was examined as part of this investigation is the GHG that can be offset by installing the solar collector arrays. Figure 36 shows the GHG offsets for the parallel layout.
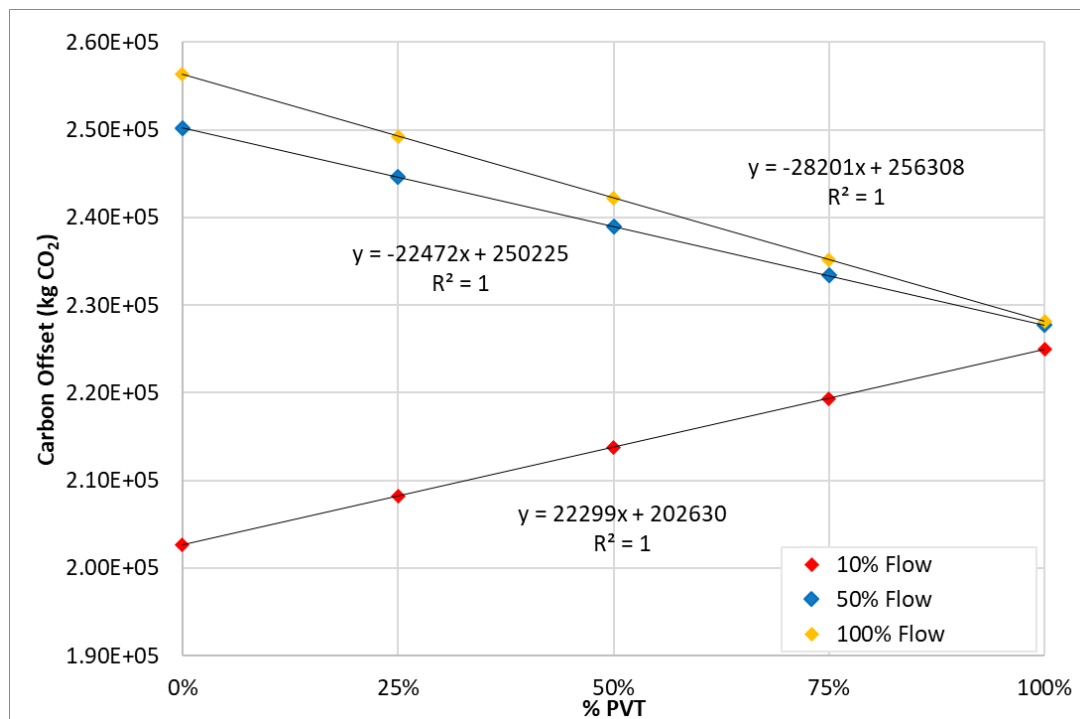
Figure 36: Parallel layout carbon offsets.

The above graph was created using the following values: electricity at 44.16 g CO_2/kWh [35]; and natural gas at 181 g CO_2/ekWh [36]. In addition, it assumed that the natural gas boiler in use has an efficiency of 80%. This graph nearly matches the one for thermal energy production. In Ontario the electrical grid contains a lot of low carbon sources of energy such as hydropower and nuclear power, therefore the natural gas that is offset has a much larger graph on the total GHG offset.

The simulations were repeated with the series layout. The thermal energy production of this layout can be seen in Figure 37
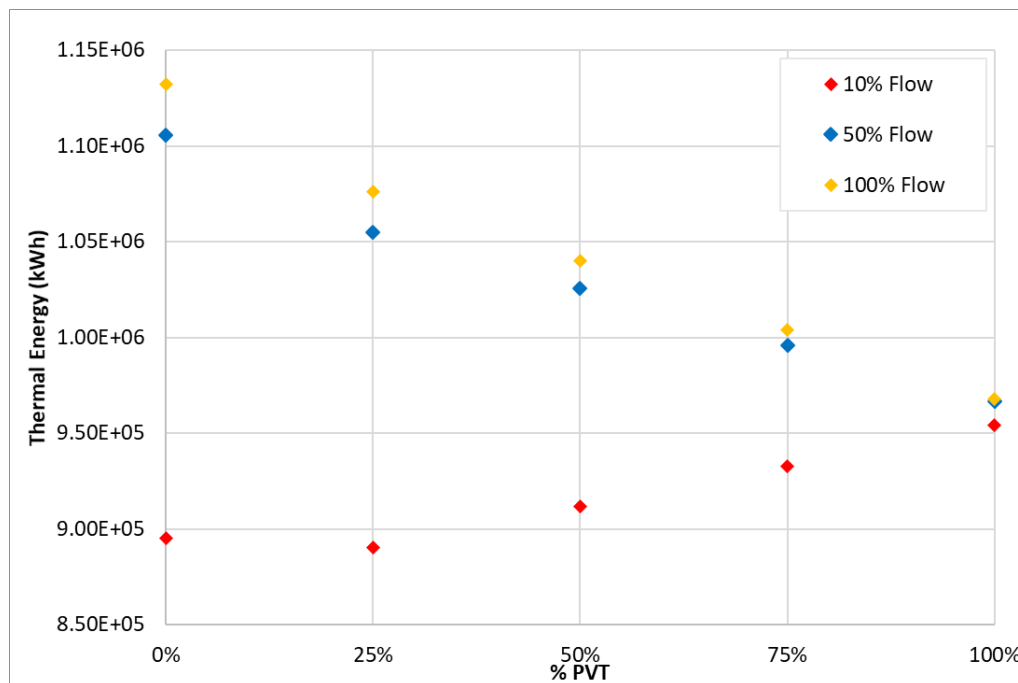
Figure 37: Series layout thermal energy production.

This graph shows a similar trend graph to Figure 33, but the trendlines are no longer perfectly linear. This is because the fluid that travels through the PVT array and the ET array is warmer than the fluid that only travels through the PVT array, and the amount of fluid that goes through both varies with the ratio changes.

51

The results for electrical energy production are identical to those presented in Table 5 because the PVT array is before the ET array in the series set-up, thus the thermal conditions for the PVT array do not change between layouts. The total energy produced is shown in Figure 38 and the average outlet temperature graph is seen in Figure 39. Both of these graphs are similar to those in the parallel layout.
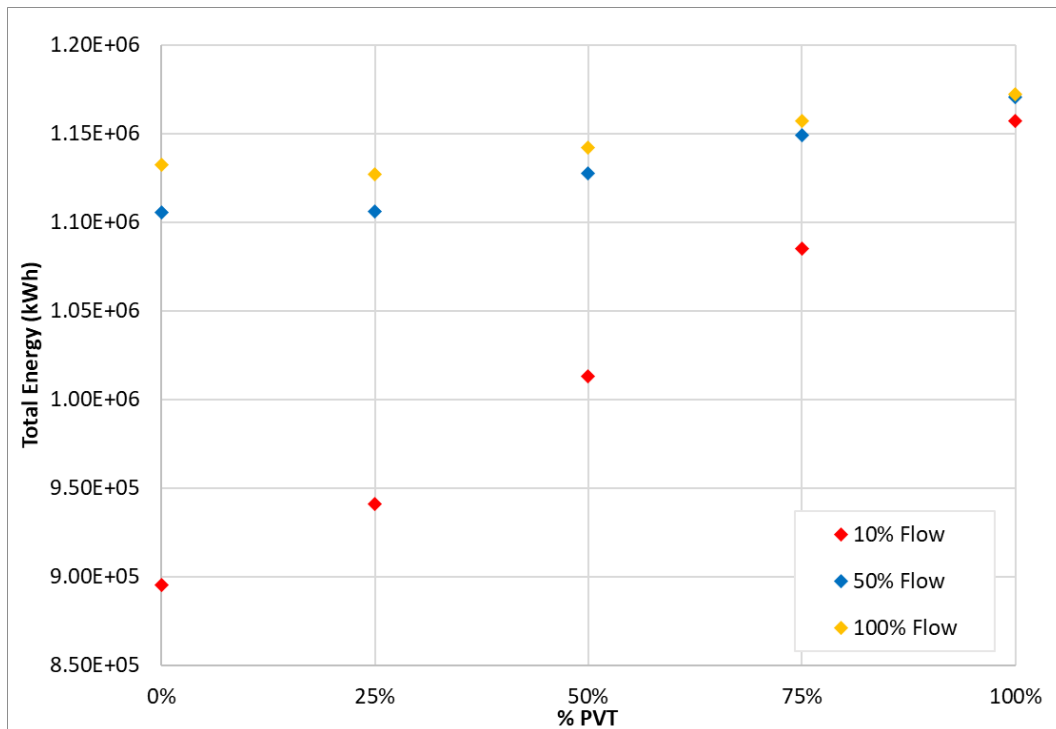
Figure 38: Series layout total energy.

For the same reasons as the thermal energy graph in Figure 37, the total energy trendlines are not quite linear.
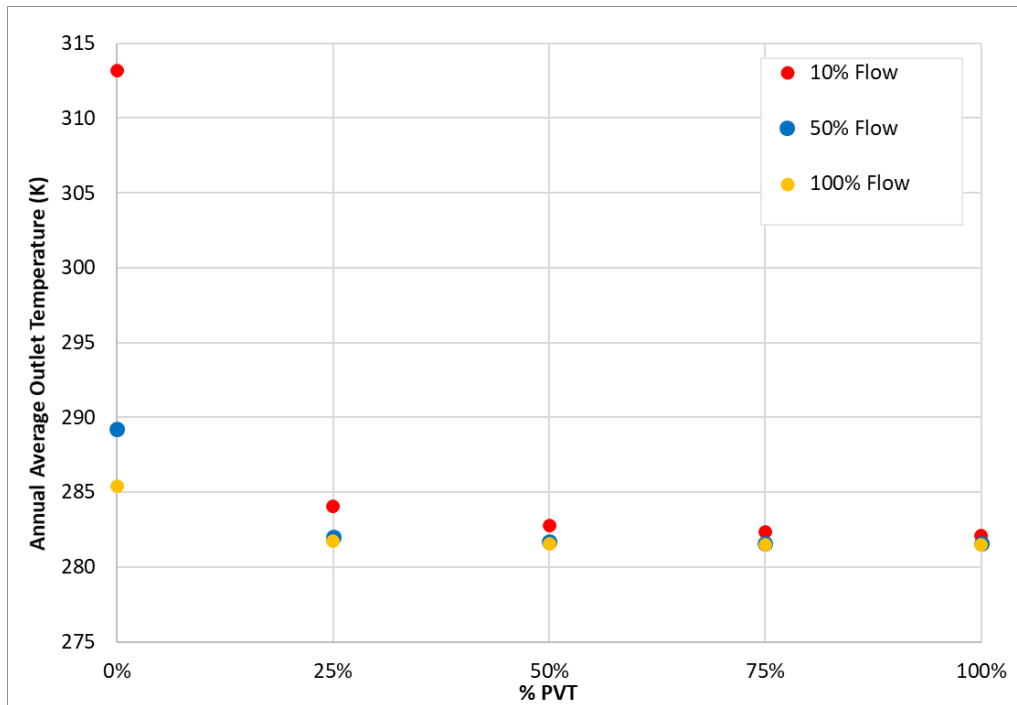
Figure 39: Series layout annual average outlet temperature.

The CO_2 offsets using the series layout can be seen in Figure 40 and are close to linear for the same reasons as the thermal energy and total energy production graphs.
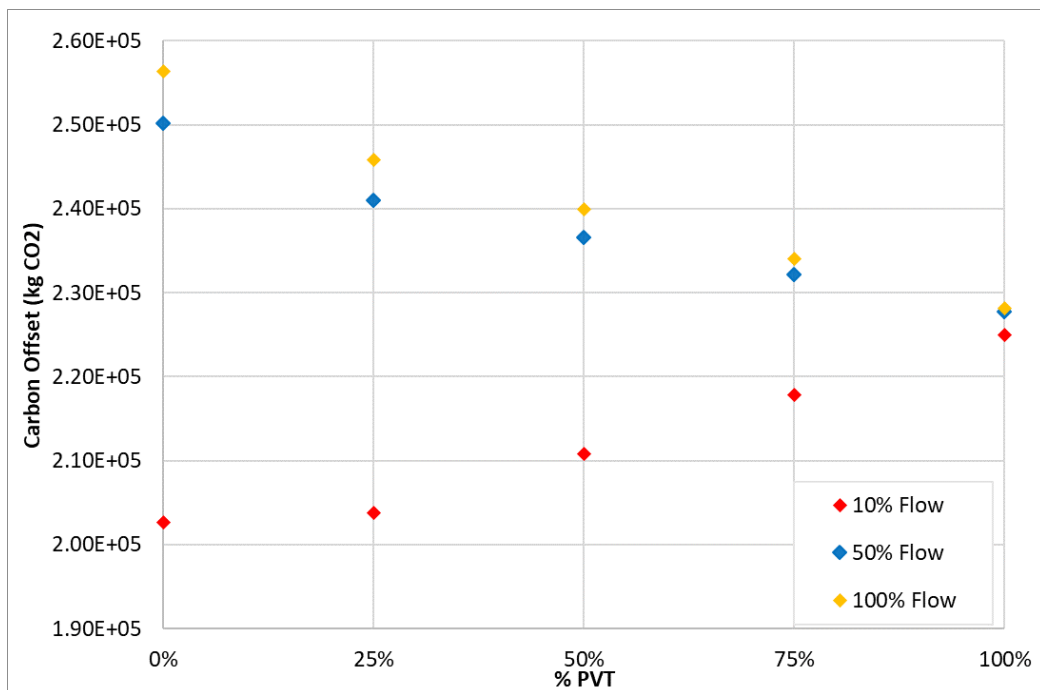
Figure 40: Series layout carbon offsets.

The two layout options can also be compared directly. Figure 41 shows different traits all using the 50% recommended flow rate.
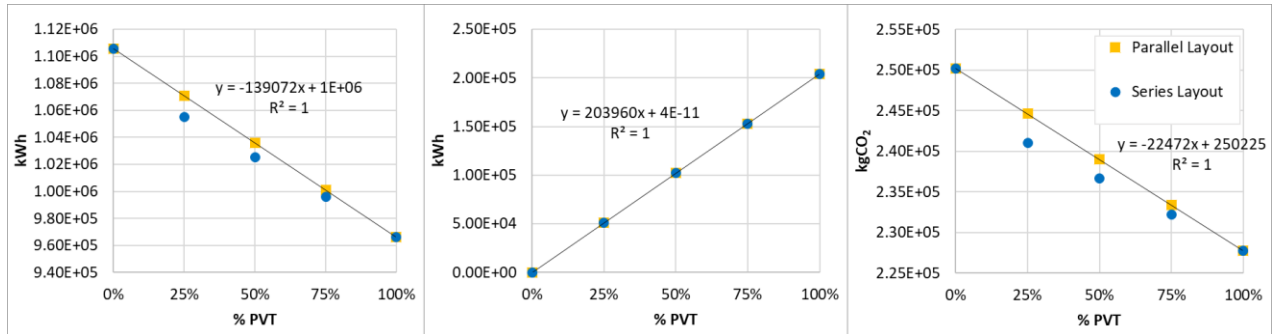
Figure 41 Thermal energy production (left), electrical energy production (middle), and GHG offsets (right) for both layouts.

These graphs show that the parallel layout performs better than the series layout for the PVT to ET ratios where the layouts differ (25%, 50%, and 75% PVT). 0% and 100% PVT ratios are the same for both layouts because there is only one array, either PVT or ET, so they cannot be in series or parallel. Note that there is no difference in electrical production; as noted before, this is because the PVT array is before the ET array in the series set-up, making the conditions for the PVT array the same in the parallel layout and the series layout. The average outlet temperatures from both layouts at 50% recommended flowrate are compared in Table 6.

Table 6: Standalone retail average outlet temperature for both layouts.

% PVT	Parallel Layout Average Outlet Temperature (K)	Series Layout Average Outlet Temperature (K)
0%	289.252	289.252
25%	282.003	282.039
50%	281.711	281.717
75%	281.609	281.610
100%	281.557	281.557

From this table it is clear that there is a barely discernable difference in the outlet temperature between the two layout options (0.01% difference), which may be due to rounding in calculations. Therefore, the parallel layout is better for the stand alone retail building.

The standalone retail building has a total heating load of 183,775 kWh and a total electrical load of 246,950 kWh [28]. Tables 7 to 9 show the percent of the total loads that are covered by the PVT and ET collectors.

Table 7: Standalone retail 10% recommended flowrate energy generation.

%PVT	10% Recommended Flowrate Parallel Layout		10% Recommended Flowrate Series Layout	
	Percent of Heating Load Covered (%)	Percent of Electrical Load Covered (%)	Percent of Heating Load Covered (%)	Percent of Electrical Load Covered (%)
0	487	0	487	0
25	495	21	485	21
50	503	41	496	41
75	511	62	508	62
100	519	82	519	82

Table 8: Standalone retail 50% recommended flowrate energy generation.

%PVT	50% Recommended Flowrate Parallel Layout		50% Recommended Flowrate Series Layout	
	Percent of Heating Load Covered (%)	Percent of Electrical Load Covered (%)	Percent of Heating Load Covered (%)	Percent of Electrical Load Covered (%)
0	602	0	602	0
25	583	21	574	21
50	564	41	558	41
75	545	62	542	62
100	526	83	526	83

%PVT	100% Recommended Flowrate Parallel Layout		100% Recommended Flowrate Series Layout	
	Percent of Heating Load Covered (%)	Percent of Electrical Load Covered (%)	Percent of Heating Load Covered (%)	Percent of Electrical Load Covered (%)
0	616	0	616	0
25	594	21	585	21
50	571	41	566	41
75	549	62	546	62
100	527	83	527	83

These tables show that in all cases the arrays on the roof of the standalone retail building produce a lot more thermal energy than the building requires. Also, when 100% PVT collectors are used, most of the electrical load can be covered.

The potential GHG offsets per square metre of floor area ($kgCO_2/m^2$) of this building typology are found in Table 10.

Table 10: Potential annual GHG offsets per square metre of floor area of standalone retail for all flowrates.

%PVT	Annual GHG offsets per square metre of floor area ($kgCO_2/m^2/year$)					
	10% Recommended Flowrate		50% Recommended Flowrate		100% Recommended Flowrate	
	Parallel Layout	Series Layout	Parallel Layout	Series Layout	Parallel Layout	Series Layout
0	88	88	109	109	112	112
25	91	89	107	105	109	107
50	93	92	104	103	106	105
75	96	95	102	101	103	102
100	98	98	99	99	99	99

Assuming that all thermal energy produced offsets natural gas and all electricity produced offsets electricity from the Ontario electrical grid, from a GHG reduction perspective, 100% ET

collectors using the recommended flowrate provides the best outcome and would offset 489% of the annual CO_2 emissions for this building type. However, if the electricity produced using the PVT collectors is used for heating as well, then 100% PVT collectors becomes the best option for GHG reductions. If the electricity produced when using 100% PVT collectors is used to power a heat pump with a coefficient of performance of 3.0, then 60 $kgCO_2/m^2/yr$ of gross floor area could be offset by the electricity, for a total of 156 $kgCO_2/m^2/yr$ when combined with 96 $kgCO_2/m^2/yr$ from thermal energy.

Overall, for the standalone retail building, there are different top-performing options depending on the priorities for the system. To achieve the most total energy, the best option is 100% PVT collectors with 100% of the recommended flowrate through them, which generates 511 $kWh/m^2/yr$ of gross floor area. However, if offsetting the largest amount of CO_2 is more important, then 100% PVT collectors is the best option only if the electricity generated is used for heating. This case offsets 156 $kgCO_2/m^2/yr$. If not, then 100% ET collectors with 100% of the recommended flowrate is the best option as it offsets 112 kg $CO_2/m^2/year$ of gross floor area. The parallel layout always outperforms the series layout.

6.2 Midrise Apartment

The midrise apartment reference building (Figure 42) has four storeys and a total roof area of

783 m^2 [33]. As before, the assumption that 50% of the roof area (391m^2) is available for solar

collectors has been applied.
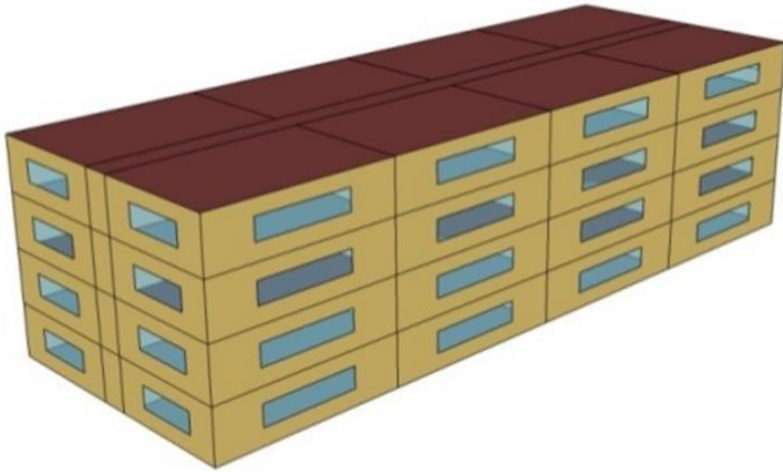
Figure 42: DOE midrise apartment reference building.

The total annual heating load for the midrise apartment is 211,311 kWh and the total electrical

load is 204,285 kWh [28]. Tables 11 to 13 summarize the potential energy generation as a

percentage of the total building load and the total energy produced.

Table 11: Midrise apartment 10% recommended flowrate energy generation.

%PVT	10% Recommended Flowrate Parallel Layout			10% Recommended Flowrate Series Layout		
	Percent of Heating Load Covered (%)	Percent of Electrical Load Covered (%)	Total Energy Produced (kWh)	Percent of Heating Load Covered (%)	Percent of Electrical Load Covered (%)	Total Energy Produced (kWh)
0	144	0	305,162	144	0	305,162
25	147	8	327,495	144	8	320,842
50	149	17	349,827	147	17	345,392
75	152	25	372,159	150	25	369,942
100	154	34	394,491	154	34	394,491

Table 12: Midrise apartment 50% recommended flowrate energy generation.

%PVT	50% Recommended Flowrate Parallel Layout			50% Recommended Flowrate Series Layout		
	Percent of Heating Load Covered (%)	Percent of Electrical Load Covered (%)	Total Energy Produced (kWh)	Percent of Heating Load Covered (%)	Percent of Electrical Load Covered (%)	Total Energy Produced (kWh)
0	178	0	376,841	178	0	376,841
25	173	9	382,370	170	9	377,030
50	167	17	387,900	165	17	384,340
75	162	26	393,430	161	26	391,650
100	156	34	398,960	156	34	398,960

Table 13: Midrise apartment 100% recommended flowrate energy generation.

%PVT	100% Recommended Flowrate Parallel Layout			100% Recommended Flowrate Series Layout		
	Percent of Heating Load Covered (%)	Percent of Electrical Load Covered (%)	Total Energy Produced (kWh)	Percent of Heating Load Covered (%)	Percent of Electrical Load Covered (%)	Total Energy Produced (kWh)
0	183	0	386,002	183	0	386,002
25	176	9	389,382	174	9	384,176
50	169	17	392,762	168	17	389,291
75	163	26	396,142	162	26	394,407
100	156	34	399,522	156	34	399,522

Compared to the standalone retail building, the midrise apartment has a smaller roof and a higher heating load. Still, the collector arrays can always cover the entire annual heating load (building heat and domestic hot water). The midrise apartment has a slightly lower electrical load than the standalone retail. Therefore, less of the electrical load can be covered, even with 100% PVT collectors.

The midrise apartment has a total floor area of 3,131 m^2. Table 14 summarizes the potential GHG offsets per square metre of floor area (kgCO$_2$/m^2/year) for this building typology.

Table 14: Potential annual GHG offsets per square metre of midrise apartment floor area for all flowrates.

%PVT	Annual GHG offsets per square metre of floor area (kgCO$_2$/m^2/year)					
	10% Recommended Flowrate		50% Recommended Flowrate		100% Recommended Flowrate	
	Parallel Layout	Series Layout	Parallel Layout	Series Layout	Parallel Layout	Series Layout
0	22	22	27	27	28	28
25	23	22	27	26	27	27
50	23	23	26	26	26	26
75	24	24	25	25	26	25
100	24	24	25	25	25	25

From a GHG reduction perspective, 100% ET collectors using the recommended flowrate is the best solution, which would offset 154% of the annual CO$_2$ emissions of this building type, unless the electricity from the PVT collectors is used for heating. As in the first case study, if a heat pump with a coefficient of performance of 3.0 was run using the electricity produced then 100% PVT collectors offsets the most CO$_2$. For the midrise apartment, using 100% PVT collectors 39 kgCO$_2$/m^2/yr could be offset.

The offsets per area of for the midrise apartment are significantly smaller than those from the standalone retail building. This is due to the smaller roof area compared to the total floor area of the midrise apartment, meaning that there are fewer collectors for a larger total floor area. The more storeys that a building has, the smaller the ratio of available roof area to total floor area becomes.

For the midrise apartment, like the standalone retail building, the parallel layout is better than the series layout. There are different options for ratio that perform the best depending on the

priorities for the system. To achieve the most total energy, the best option is 100% PVT collectors with 100% of the recommended flowrate through them, which generates 128 kWh/m^2/year of gross floor area. If offsetting CO_2 is more important, then 100% ET collectors with 100% of the recommended flowrate is the best option as it offsets 28 kg CO_2/m^2/year of gross floor area unless the electricity from the PVT collectors is used for heating as well.

6.3   Large Hotel

The large hotal (Figure 43) is a six storey building with a total roof area of 1,478 m^2 [33]. The half of the roof area available for solar collectors is 739 m^2.
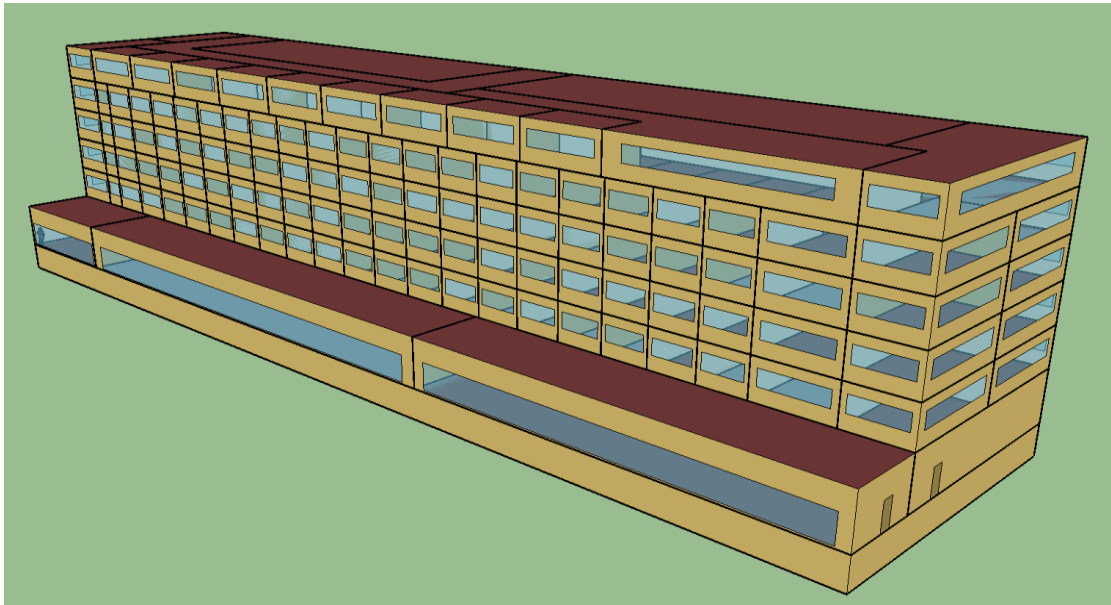
Figure 43: DOE large hotel reference building.

The total annual heating load for the large hotel reference building is 1,660,704 kWh and the total electrical load is 1,032,939 kWh [28]. Tables 15 to 17 summarize the potential energy generation as a percentage of the total building load.

Table 15: Large hotel 10% recommended flowrate energy generation.

%PVT	10% Recommended Flowrate Parallel Layout			10% Recommended Flowrate Series Layout		
	Percent of Heating Load Covered (%)	Percent of Electrical Load Covered (%)	Total Energy Produced (kWh)	Percent of Heating Load Covered (%)	Percent of Electrical Load Covered (%)	Total Energy Produced (kWh)
0	35	0	576,765	35	0	576,765
25	35	3	618,973	35	3	606,400
50	36	6	661,182	35	6	652,799
75	36	10	703,390	36	10	699,199
100	37	13	745,599	37	13	745,599

Table 16: Large hotel 50% recommended flowrate energy generation.

%PVT	50% Recommended Flowrate Parallel Layout			50% Recommended Flowrate Series Layout		
	Percent of Heating Load Covered (%)	Percent of Electrical Load Covered (%)	Total Energy Produced (kWh)	Percent of Heating Load Covered (%)	Percent of Electrical Load Covered (%)	Total Energy Produced (kWh)
0	43	0	712,238	43	0	712,238
25	42	3	722,690	41	3	712,596
50	40	6	733,142	40	6	726,413
75	39	10	743,593	39	10	740,229
100	37	13	754,045	37	13	754,045

%PVT	100% Recommended Flowrate Parallel Layout			100% Recommended Flowrate Series Layout		
	Percent of Heating Load Covered (%)	Percent of Electrical Load Covered (%)	Total Energy Produced (kWh)	Percent of Heating Load Covered (%)	Percent of Electrical Load Covered (%)	Total Energy Produced (kWh)
0	44	0	729,553	44	0	729,553
25	42	3	735,942	42	3	726,103
50	41	6	742,330	40	6	735,771
75	39	10	748,718	39	10	745,438
100	38	13	755,106	38	13	755,106

The large hotel has much higher heating and electrical loads than the standalone retail building while only having 64% of the available roof area. Because of the scale of the loads, the arrays cannot cover the whole annual heating or electrical loads.

The large hotel has a total floor area of 11,346 m^2. Table 18 summarizes the potential GHG offsets per square metre of floor area (kgCO$_2$/m^2) of this building typology.

Table 18: Potential annual GHG offsets per square metre of large hotel floor area for all flowrates.

%PVT	Annual GHG offsets per square metre of floor area (kgCO$_2$/m^2/year)					
	10% Recommended Flowrate		50% Recommended Flowrate		100% Recommended Flowrate	
	Parallel Layout	Series Layout	Parallel Layout	Series Layout	Parallel Layout	Series Layout
0	12	12	14	14	15	15
25	12	12	14	14	14	14
50	12	12	14	13	14	14
75	12	12	13	13	13	13
100	13	13	13	13	13	13

From a GHG reduction perspective, 100% ET collectors using the recommended flowrate is the best solution, which would offset 40% of the annual CO_2 emissions of this building type unless the PVT electricity went to heating, in which case 20 $kgCO_2/m^2/yr$ of gross floor area could be offset. The GHG offsets for the large hotel are even slimmer than those for the midrise apartment. This is because the large hotel has many floors, and therefore a large total floor area, but a comparatively small available roof area for the solar arrays.

The large hotel has different options that perform best depending on priorities. To achieve the most total energy, the best option is the parallel layout with 100% PVT collectors and 100% of the recommended flowrate through them, which generates 67 $kWh/m^2/year$ of gross floor area. If offsetting CO_2 is more important, then 100% PVT collectors using the electricity for heating is the best option, or if the electricity is used for offsetting electricity from the grid, then the parallel layout with 100% ET collectors and 100% of the recommended flowrate is the best option as it offsets 15 kg $CO_2/m^2/year$ of gross floor area.

6.4   Medium Office

The medium office reference building (Figure 44) has a total roof area of 1,660 m^2 [33], making the available area 830 m^2.
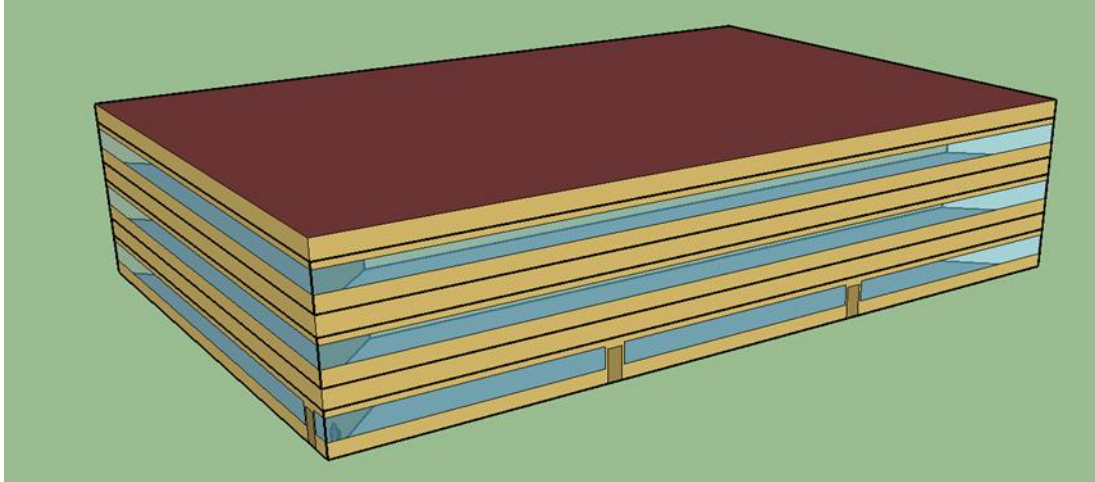
Figure 44: DOE medium office reference building.

The total annual heating load for the medium office is 153,819 kWh and the total electrical load is 363,873 kWh [28]. Tables 19 to 21 summarize the potential energy generation as a percentage of the total building load.

Table 19: Medium office 10% recommended flowrate energy generation.

%PVT	10% Recommended Flowrate Parallel Layout			10% Recommended Flowrate Series Layout		
	Percent of Heating Load Covered (%)	Percent of Electrical Load Covered (%)	Total Energy Produced (kWh)	Percent of Heating Load Covered (%)	Percent of Electrical Load Covered (%)	Total Energy Produced (kWh)
0	421	0	647,787	421	0	647,787
25	428	10	695,193	419	10	681,072
50	435	20	742,599	429	20	733,185
75	442	30	790,005	439	30	785,298
100	449	40	837,411	449	40	837,411

Table 20: Medium office 50% recommended flowrate energy generation.

%PVT	50% Recommended Flowrate Parallel Layout			50% Recommended Flowrate Series Layout		
	Percent of Heating Load Covered (%)	Percent of Electrical Load Covered (%)	Total Energy Produced (kWh)	Percent of Heating Load Covered (%)	Percent of Electrical Load Covered (%)	Total Energy Produced (kWh)
0	520	0	799,943	520	0	799,943
25	504	10	811,682	496	10	800,345
50	487	20	823,420	482	20	815,863
75	471	30	835,159	469	30	831,380
100	455	41	846,898	455	41	846,898

Table 21: Medium office 100% recommended flowrate energy generation.

%PVT	100% Recommended Flowrate Parallel Layout			100% Recommended Flowrate Series Layout		
	Percent of Heating Load Covered (%)	Percent of Electrical Load Covered (%)	Total Energy Produced (kWh)	Percent of Heating Load Covered (%)	Percent of Electrical Load Covered (%)	Total Energy Produced (kWh)
0	533	0	819,390	533	0	819,390
25	513	10	826,565	506	10	815,515
50	494	20	833,740	489	20	826,373
75	475	30	840,915	472	30	837,231
100	455	41	848,089	455	41	848,089

The medium office solar arrays can produce much more heat than is required by the building. When 100% of the collectors are PVT collectors, they can also cover a large portion of the electrical load.

The medium office has a total floor area of 4,980 m^2. Table 22 summarizes the potential GHG offsets per square metre of floor area ($kgCO_2/m^2$) of this building typology.

| %PVT | Annual GHG offsets per square metre of floor area (kgCO$_2$/m^2/year) | | | | | |
| | 10% Recommended Flowrate | | 50% Recommended Flowrate | | 100% Recommended Flowrate | |
	Parallel Layout	Series Layout	Parallel Layout	Series Layout	Parallel Layout	Series Layout
0	29	29	36	36	37	37
25	30	30	36	35	36	36
50	31	31	35	34	35	35
75	32	32	34	34	34	34
100	33	33	33	33	33	33

From a GHG reduction perspective, 100% ET collectors using the recommended flowrate is the best solution, offsetting 144% of the annual CO$_2$ emissions of this building type, unless the electricity from the PVT collectors is used for heating. If a heat pump with a coefficient of performance of 3.0 was used, then the electricity and thermal energy from the PVT collectors could offset 52 kgCO$_2$/m^2/yr. The GHG offset values for the medium office are similar to the midrise apartment, which is unsurprising considering that the buildings have a similar available roof area to total floor area ratio.

The medium office has different options that perform best depending on priorities. The parallel layout is always better than the series layout. To achieve the most total energy, the best option is 100% PVT collectors with 100% of the recommended flowrate through them which generates 170 kWh/m^2/year of gross floor area. 100% PVT collectors is also the best option for offsetting CO$_2$ if the electricity is used for heating and therefore also offsetting natural gas. If the electricity is not offsetting natural gas, then 100% ET collectors with 100% of the recommended flowrate is the best option as it offsets 37 kg CO$_2$/m^2/year of gross floor area.

6.5 Large Office

The large office (Figure 45) is a 13 storey building with a total roof area of 3,563 m^2 [33], allowing an area of 1,782 m^2 for solar collectors.
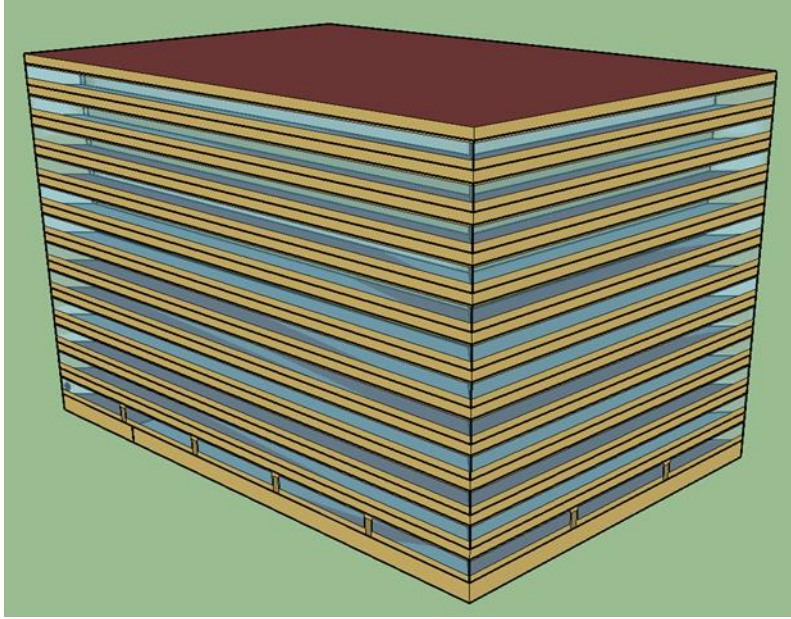

Figure 45: DOE large office reference building.

The total annual heating load for the large office reference building is 1,167,205 kWh and the total electrical load is 5,745,751 kWh [28]. Tables 23 to 25 summarize the potential energy generation as a percentage of the total building load.

Table 23: Large office 10% recommended flowrate energy generation.

%PVT	10% Recommended Flowrate Parallel Layout			10% Recommended Flowrate Series Layout		
	Percent of Heating Load Covered (%)	Percent of Electrical Load Covered (%)	Total Energy Produced (kWh)	Percent of Heating Load Covered (%)	Percent of Electrical Load Covered (%)	Total Energy Produced (kWh)
0	119	0	1,390,792	119	0	1,390,792
25	121	1	1,492,572	119	1	1,462,252
50	123	3	1,594,352	121	3	1,574,139
75	125	4	1,696,132	124	4	1,686,025
100	127	5	1,797,912	127	5	1,797,912

68

%PVT	50% Recommended Flowrate Parallel Layout			50% Recommended Flowrate Series Layout		
	Percent of Heating Load Covered (%)	Percent of Electrical Load Covered (%)	Total Energy Produced (kWh)	Percent of Heating Load Covered (%)	Percent of Electrical Load Covered (%)	Total Energy Produced (kWh)
0	147	0	1,717,468	147	0	1,717,468
25	143	1	1,742,671	140	1	1,718,331
50	138	3	1,767,873	136	3	1,751,647
75	133	4	1,793,076	133	4	1,784,963
100	129	6	1,818,279	129	6	1,818,279

Table 25: Large office 100% recommended flowrate energy generation.

%PVT	100% Recommended Flowrate Parallel Layout			100% Recommended Flowrate Series Layout		
	Percent of Heating Load Covered (%)	Percent of Electrical Load Covered (%)	Total Energy Produced (kWh)	Percent of Heating Load Covered (%)	Percent of Electrical Load Covered (%)	Total Energy Produced (kWh)
0	151	0	1,759,221	151	0	1,759,221
25	145	1	1,774,625	143	1	1,750,901
50	140	3	1,790,029	138	3	1,774,213
75	134	4	1,805,433	134	4	1,797,525
100	129	6	1,820,838	129	6	1,820,838

The large office has by far the highest total electrical load, so it is unsurprising that only a small portion can be covered by the solar collectors, even when 100% PVT collectors are used.

The large office has a total floor area of 46,321 m^2. Table 26 summarizes the potential GHG offsets per square metre of floor area (kgCO$_2$/m^2) of this building typology.

Table 26: Potential annual GHG offsets per square metre of large office floor area for all flowrates.

%PVT	Annual GHG offsets per square metre of floor area (kgCO$_2$/m^2/year)					
	10% Recommended Flowrate		50% Recommended Flowrate		100% Recommended Flowrate	
	Parallel Layout	Series Layout	Parallel Layout	Series Layout	Parallel Layout	Series Layout
0	7	7	8	8	9	9
25	7	7	8	8	8	8
50	7	7	8	8	8	8
75	7	7	8	8	8	8
100	8	8	8	8	8	8

As with the previous case studies, from a GHG reduction perspective, 100% ET collectors using the recommended flowrate is the best solution, offsetting 80% of the annual CO$_2$ emissions of the building, unless the electricity was also used for heating. In this case, using a heat pump with a coefficient of performance of 3.0, the 100% PVT option could offset 12 kgCO$_2$/m^2/yr of gross floor area. These are the smallest GHG offset per square metre of all the case studies examined. This is again due to the very large total floor area when compared to the smaller roof area available for the solar arrays.

The large office, like all the previous case studies, has different options that perform best depending on priorities. To achieve the most total energy, the best option is the parallel layout with 100% PVT collectors and 100% of the recommended flowrate, which generates 39 kWh/m^2/year of gross floor area. Similar to the other case studies, if offsetting CO$_2$ is more important, then the parallel layout with 100% PVT collectors using the electricity for heating is the best option, but if the electricity is not offsetting natural gas, then 100% ET collectors and 100% of the recommended flowrate is the best option as it offsets 9 kg CO$_2$/m^2/year of gross floor area.

6.6   Multi-Building Case Study #1: Toronto 2030 District

From the case studies examined, an estimated potential GHG offset for the entire Toronto 2030

District (Figure 46) can be calculated. The Toronto 2030 Platform [37] was used to find the total

floor area of each building type, which can be seen in Table 27.
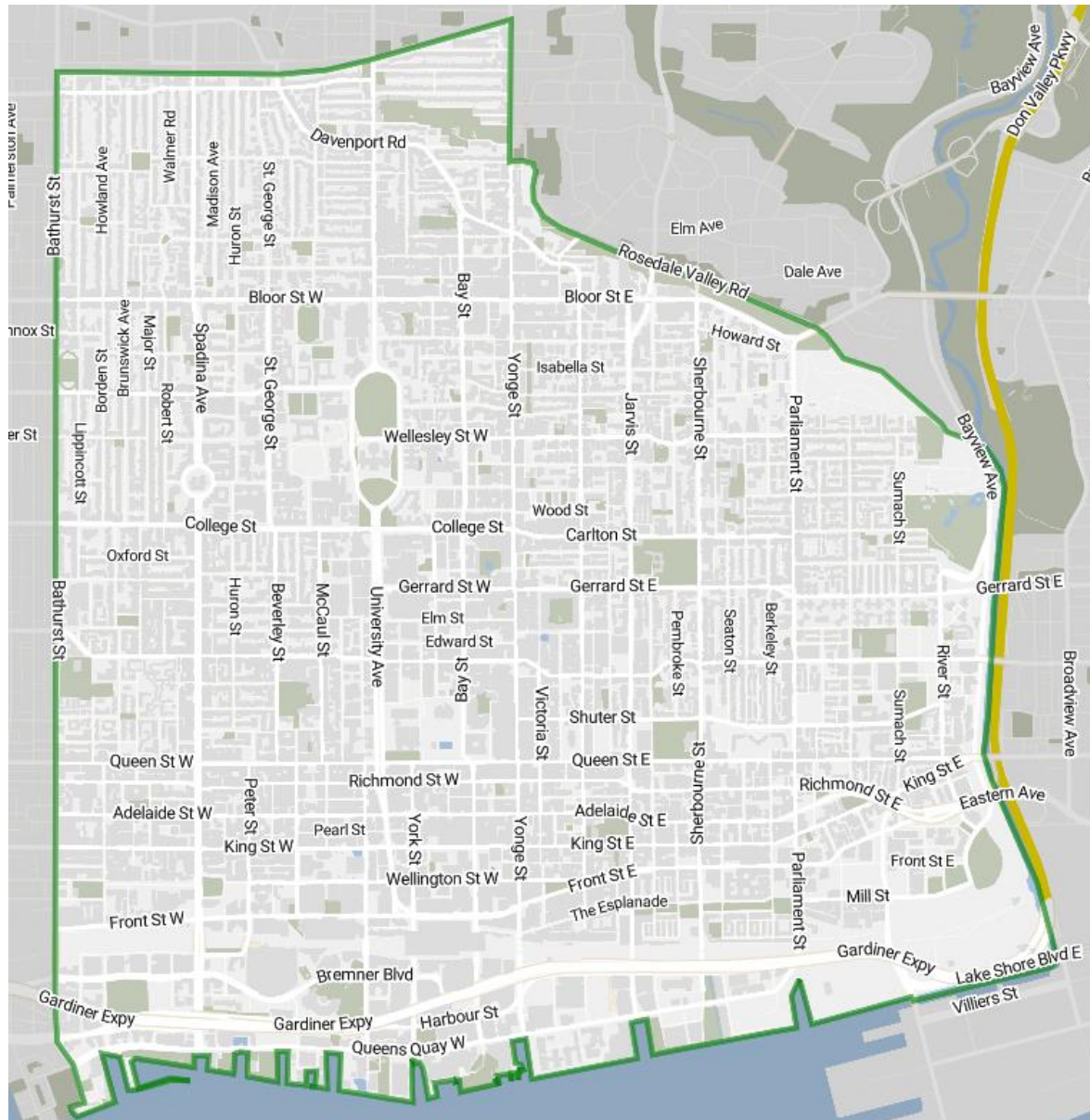
Figure 46: Toronto 2030 District [37].

Building Type	Gross Floor Area (m^2)	Percent of Total
Office	8,671,000	27.7%
Retail/Hospitality	5,544,000	17.7%
Multi-unit Residential	10,711,000	34.2%
Residential	2,848,000	9.1%
Institutional	3,495,000	11.2%
Industrial	61,000	0.2%

The following assumptions were made about the breakdown of each of these categories using the building types from the case studies that were completed:

(1) 100% of the offices in the district are large offices;

(2) 100% of the retail/hospitality buildings are large hotels;

(3) Multi-unit residential buildings are made up of 80% high-rise apartments (approximated by large hotels) and 20% are mid-rise residential; and

(4) Residential, institutional, and industrial buildings have no solar collectors.

Using these assumptions, it was found that if 100% ET collectors with 100% of the recommended flowrate are used, then approximately 350,000 tonnes of CO_2 per year can be offset in the 2030 District. If 100% PVT collectors are used, because the most total energy was desired, then approximately 306,000 tonnes of CO_2 per year can be offset, assuming that the electricity is not used for heating. If the electricity is used for heating using a heat pump with an annual average coefficient of performance of 3.0, then 470,000 tonnes of CO2 per year can be offset. The annual emissions from the 2030 district total 1,190,000 tonnes [37], so these options can offset approximately 29%, 26%, and 39% of the emissions respectively.

A similar study was run comparing the available roof area compared to total heating and electricity loads for the district. The same assumption as the single building case studies about 50% of the roof area being available is used. This assumption is used to take into account the roof area needed for mechanical equipment, as well as shading from adjacent buildings. Further, because all buildings are assumed on average to be the "large" typology, the presence of low- and medium-rise office and residential buildings within the district renders this a reasonably conservative assumption. The total electrical load of the 2030 district is 3,680 GWh, and the total natural gas load is 4,840 GWh [37]. If 100% PVT collectors are installed and the same assumptions about the breakdown of the building types from before are used, 455 GWh of electricity, and 2,090 GWh of heat can be produced. This is approximately 12% of the electrical load and 43% of the heating load.

6.7   Multi-Building Case Study #2: Suburban Retail & Residential Micro-grid

A second real-life scenario was examined to look at the feasibility of using district heating to use the energy generated from solar arrays on the roof of a big box store to heat nearby high-rise residential buildings. In Richmond Hill, Ontario, there are three high-rise apartment buildings across from a Home Depot and two other large box stores (Figure 47).

The online application Daft Logic [39] was used to find the approximate roof areas of the buildings involved, and this was multiplied by the number of floors to find the gross floor area. The case studies showed that using only PVT collectors produces the most total energy in this climate and is therefore used in this scenario. It also assumes that the electricity produced is used by the box stores themselves, so only the thermal energy produced by the PVT collectors is used for heating. Using the results from the standalone retail and large hotel reference buildings case studies and assuming that 50% of the roof is available for solar collectors, the Home Depot can

produce enough thermal energy to heat itself and apartment building 1 completely, as well as almost 50% of the second apartment. If one other box store (box store 1 in Figure 47) is included, then together they can provide enough thermal energy for themselves, all of apartment building 1, and about 85% of apartment 2. If box store 2 is also included, then the three stores combined can heat apartment buildings 1 and 2 completely, as well as 70% of the third apartment building. Note that these calculations do not include transmission losses, which are assumed to be small for the short distances involved.

Figure 47: Diagram of placement of box stores and apartment buildings [background image from Google Maps [38]].

7   Reflection on Findings

From examining the case studies, four trends were consistent across all the reference buildings for flowrate and panel area variations: (1) the total energy produced always increased with increasing PVT percentage; (2) the lowest flowrate always produced the highest annual average outlet temperature; (3) the 100% recommended flowrate always produced the highest total energy and the largest GHG offsets; and (4) GHG offsets increased with increasing ET percentage except at the lowest flowrate. Generally, ET collectors are thought to be more efficient in cold climates because of their ability to efficiently heat the working fluid and their increased outlet temperature. Therefore, in Toronto's cold climate, it is surprising that the ratio that produced the most total energy was 100% PVT collectors. This finding implies that more focus should be placed on PVT collectors when designing renewable energy systems that include ground loops in Toronto. The lowest flowrate produces the highest annual average outlet temperature because the working fluid has more time to heat up while travelling through the collector. Though high outlet temperatures might be desirable in some situations, very low flowrates produce less total thermal energy than higher flowrates, as well as a smaller GHG offset. Having higher temperatures in the PVT collectors also negatively affect the performance of the photovoltaic laminate. GHG offsets generally increase with increasing ET percentage because of the fuel that they offset. The electrical grid in Ontario includes many low carbon energy sources, making the carbon offsets produced by the photovoltaic laminate on the PVT collectors lower than those produced by offsetting natural gas use.

Comparing the two layout options, the parallel layout always produced more thermal energy and higher GHG offsets than the series, while also producing the same amount of electrical energy. The annual average output temperature was only slightly (<1%) higher for the series layout. The

series layout requires slightly less total flow through the system, as some of the working fluid passes through both the PVT collectors and the ET collectors. That the parallel layout performed better than the series suggests that the thermal benefit of two-stage heating of a smaller volume of working fluid does not outweigh the thermal energy produced by having a slightly larger total flowrate and passing through the collector arrays in parallel.

An interesting similarity between the standalone retail and medium office case studies is that they have a similar percent of their heating loads covered by the collectors. This similarity is because both buildings, although very different in size and loads, have a similar heating load to roof area ratio. The standalone retail building has a ratio of 160:1 and the medium office has a ratio of 185:1. This means that for any building where the heating load and roof area are known, the percentage of the heating load that can be covered can be easily estimated.

These findings have implications for the Toronto 2030 District and other multi-building contexts. Some of the building types examined were able to produce more thermal energy than they could use (standalone retail, midrise apartment, medium office, and large office), while others could only produce part of their heating requirements (large hotel; which previous research [40] has determined is very similar to high-rise residential towers). This makes the idea of district energy systems very attractive. If a standalone retail building can produce up to 600% of its annual heating load, then on a district heating system it can provide heat to many other buildings in the vicinity, allowing all of those surrounding buildings to be off the heating grid. If a standalone building was put onto a district heating system, and 20% system losses are assumed, each 1000 m^2 of standalone retail could provide heating to about 2,800 m^2 of large hotel floor area, which could be similar to high rise residential.

8   Conclusions

The objective of this project was to investigate the effect of changing array layout, ratio, and flowrate of PVT and ET collectors on the performance of the overall system. This investigation included modeling both a PVT and an ET collector using Maple, combining these models in different ratios and layouts using Excel, and using the data to look at various case studies.

The first research question asked was whether there was a standard approach to determine the optimum ratio of PVT to ET, given a set of building loads and the roof area. Using the models and excel sheets provided in this project, the optimum ratio of collectors could be determined. This project looked widely at five ratios, and the best ratio for all the case studies examined was 100% PVT collectors, but if this was not the case for a different building or location, using the method provided the ratios could be easily broken down further into more specific ratios by altering only the Excel sheets.

The second research question was how changing the ratio of the collectors affects the environmental impact of the system. A system on a standalone retail building that is made up of 100% PVT collectors can produce 1,171,998 kWh of combined thermal energy and electricity. If the electricity produced by the PVT collectors is used to offset electricity from the electrical grid, using 100% ET collectors offsets the most GHG because the fuel the energy is offsetting is natural gas. However, if the electricity produced by the PVT collectors is used for heating, especially if the heating involves a heat pump with a coefficient of performance greater than one, then 100% PVT collectors offset the most GHG. This is because 100% PVT collectors produces the most total energy.

The final research question asked was what could be achieved in terms of energy savings and GHG emissions if installing solar collectors on rooftops were implemented on a larger scale. Two multi-building case studies were examined as part of this investigation. The first looked at potential GHG offsets in the Toronto 2030 District. It was found that if 100% ET collectors with 100% of the recommended flowrate were used, then approximately 350,000 tonnes of CO_2 per year could be offset in the 2030 District. If 100% PVT collectors were used, because the most total energy was desired, then approximately 306,000 tonnes of CO_2 per year could be offset, assuming that the electricity is not used for heating. If the electricity was used for heating with a heat pump with a coefficient of performance of 3.0, then 470,000 tonnes of CO_2 per year could be offset. These amounts account for 29%, 26%, and 39% respectively of the total emissions from the district. The second multi-building case study looked at the potential for district heating involving standalone retail buildings. It was found that, for example in Richmond Hill, Ontario, three big box stores could heat themselves as well as two full apartment buildings as most of a third using the thermal energy produced by arrays composed of 100% PVT collectors.

In addition to the best ratio, this study also examined the effect of having the collector arrays in parallel or series. The parallel layout always out-performed the series layout, suggesting that two-stage heating of a smaller total volume of working fluid does not outweigh the benefit produced by having a larger total flow passing through the collector arrays in parallel.

Another aspect that was investigate as part of this project was the effect of lowering the flowrate through the collectors on energy production and outlet temperature. The flowrate recommended by the manufacturers of the collectors were used, as well as 50% and 10% of the recommended flowrate. When using a system with a ground-loop, the best performing flowrate is 100% of the recommended flowrate because it produces the most total energy, but this is not necessarily the

case for other systems that require higher outlet temperatures. For cases where the outlet temperature must be above a certain threshold to be useful, a lower flowrate may be required. For those cases, the 50% recommended flowrate is a good compromise between energy production and outlet temperature.

8.1   Limitations

There are three key limitations to this research. First, this investigation only considers combinations of PVT and ET collectors, while there are other solar-thermal collectors such as flat-plate collectors and other concentrating collectors. Second, this investigation only considered one type of ET collector, the Apricus ETC-20 Solar Collector, and one type of PVT collector, described by Vokas *et al.* [10]. To get a larger picture of the solar generation potential in the 2030 district, other collector types and collector models should be considered. Finally, the results are specific to the Toronto climate as it was the only one considered in this investigation.

8.2   Future Research

The following areas have been identified for future research. First, if a balance of energy production and outlet temperature is required, then a lower flowrate than recommended may be beneficial and additional simulations would be required to determine the optimal flowrate for a given application. Based on this study, 50% of the recommended flowrate appears to provide a good compromise, but it would be helpful to other points to determine the optimal flowrate. This could also include determining at what flowrate the thermal energy production changes from a decreasing to an increasing trend with increasing PVT percentage. Further investigation could also be undertaken concerning how changing the flowrates affects monthly outlet temperatures. Another area where further research is required is modeling real-time energy uses for the energy produced, rather than charging a ground-loop system and net-metering the electricity to the

electrical grid. Finally, though this investigation was done with the Toronto 2030 District in mind, it would be interesting to do similar investigations in other climates and see what effects this may have on the ratio and layout options.

References

[1] T. Dembeck-Kerekes, Variable versus Constant Flow Performance Investigations for Photovoltaic-Thermal Panels, Toronto, Ontario: Ryerson University, 2018.

[2] H. V. Cottony and R. S. Dill, Building Materials and Structures - Solar Heating of Various Surfaces, Washington: National Bureau of Standards, 1941, pp. 1-5.

[3] A. Heath Jr. and P. Maxwell, "Solar collector development," *Astronautics and Aerospace Engineering,* vol. May, pp. 58-61, 1963.

[4] D. Shceegoley, "Heating buildings by solar radiation," *Solar Energy,* vol. 5, no. 2, p. 73, 1961.

[5] J. A. Duffie and W. A. Beckman, Solar Engineering of Thermal Processes, Hoboken, New Jersey: John Wiley & Sons Inc., 2013.

[6] Newform Energy, "Photovoltaic Thermal PVT," 2014. [Online]. Available: http://products.newformenergy.ie/photovoltaic-thermal-pvt.php. [Accessed 11 12 2018].

[7] T. Chow, "Performance analysis of photovoltaic-thermal collector by explicit dynamic model," *Solar Energy,* vol. 75, pp. 143-152, 2003.

[8] E. Kern Jr. and M. Russell, "Combined photovoltaic and thermal hybrid collector systems," Washington, D.C., USA, 1978.

[9] A. Kumar, P. Baredar and U. Qureshi, "Historical and recent development of photovoltaic thermal (PVT) technologies," *Renewable and Sustainable Energy Reviews,* vol. 42, pp. 1428-1436, 2015.

[10] G. Vokas, N. Christandonis and F. Skittides, "Hybrid photovoltaic-thermal systems for domestic heating and cooling - A theoretical approach," *Solar Energy,* no. 80, pp. 607-615, 2006.

[11] S. Dubey and G. Tiwari, "Analysis of PV/T flat plate water collectors connected in series," *Solar Energy,* vol. 83, pp. 1485-1489, 2009.

[12] H. Zondag, D. De Vries, W. Van Helden, R. Van Zolingen and A. Van Steenhoven, "THE THERMAL AND ELECTRICAL YIELD OF A PV-THERMAL," *Solar Energy,* pp. 113-128, 2002.

[13] P. Dupeyrat, C. Ménézo, M. Rommel and H.-M. Henning, "Efficient single glazed flat plate photovoltaic–thermal hybrid collector for domestic hot water system," *Solar Energy,* vol. 85, pp. 1457-1468, 2011.

[14] H. Ben cheikh el hocine, K. Touafek, F. Kerrour, H. Haloui and A. Khelifa, "Model Validation of an Empirical Photovoltaic Thermal (PV/T) Collector," *Energy Procedia,* vol. 74, pp. 1090-1099, 2015.

[15] K. Touafek, M. Haddadi and A. Malek, "Modeling and Experimental Validation of a New Hybrid Photovoltaic Thermal Collector," *IEEE TRANSACTIONS ON ENERGY CONVERSION,* vol. 26, no. 1, pp. 176-183, 2011.

[16] S. Dubey and G. Tiwari, "Thermal modeling of a combined system of photovoltaic thermal (PV/T) solar water heater," *Solar Energy,* vol. 82, pp. 602-612, 2008.

[17] Apricus Solar Co., "ETC Solar Collector Product Overview," 2016. [Online]. Available: http://www.apricus.com/upload/userfiles/downloads/ETC_Collector_Overview_Int.pdf. [Accessed 5 10 2018].

[18] Z. Wang, W. Yang, F. Qiu, X. Zhang and X. Zhao, "Solar water heating: From theory, application, marketing and research," *RenewableandSustainableEnergyReviews,* vol. 41, pp. 68-84, 2015.

[19] G. Yu, W. Guo, H. Chen, C. Du, L. Xiong and H. Wang, "Modeling and Experimental Verification of a Straight-Through Evacuated Tube INstalled on a Facade for Solar Heating," *J. Energy Eng.,* vol. 144, 2018.

[20] P.-L. Paradis, D. R. Rousse, S. Hallé, L. Lamarche and G. Quesada, "Thermal Modeling of evacuated tube solar air collectors," *Solar Energy,* vol. 115, pp. 708-721, 2015.

[21] A. E. Kabeel, A. Khalil, S. S. Elsayed and A. M. Alatyar, "Modified mathmatical model for evaluating the performance of water-in-glass evacuated tube solar collector considering tube shading effect," *Energy,* vol. 89, pp. 24-34, 2015.

[22] Pyrko, "A Model of the Average Solar Radiation for the Tubular Collector," *Int J Solar Energy,* pp. 563-565, 1984.

[23] Y. Gao, R. Fan, X. Y. Zhang, Y. J. AN, M. X. Wang, Y. K. Gao and Y. Yu, "Thermal performance and parameter analysis of a U-pipe evacuated solar tube collector," *Solar Energy,* vol. 107, pp. 714-727, 2014.

[24] A. Frangoul, "10 massive corporations going big on solar power," 28 5 2018. [Online]. Available: https://www.cnbc.com/2018/05/28/10-massive-corporations-going-big-on-solar-power.html. [Accessed 11 12 2018].

[25] Walmart Inc., "Walmart's Approach to Renewable Energy," [Online]. Available: https://cdn.corporate.walmart.com/eb/80/4c32210b44ccbae634ddedd18a27/walmarts-approach-to-renewable-energy.pdf. [Accessed 11 12 2018].

[26] Walmart Inc., "Walmart, SunPower Announce 23-Megawatt Solar Agreement," 2018. [Online]. Available: https://news.walmart.com/2018/10/23/walmart-sunpower-announce-23-megawatt-solar-agreement. [Accessed 11 12 2018].

[27] Maplesoft, *Maple 2016,* Waterloo, Ontario: Waterloo Maple Inc., 2016.

[28] U.S. Department of Energy, "Commercial Prototype Building Models," 24 10 2018. [Online]. Available: https://www.energycodes.gov/development/commercial/prototype_models. [Accessed 15 10 2018].

[29] M. Khoukhi and S. Maruyama, "Theoretical approach of a flat plate solar collector with clear and low-iron glass covers taking into account the spectral absorption and emission within glass covers layer," *Renewable Energy,* vol. 30, pp. 1177-1194, 2005.

[30] A. I. Zografos, W. A. Martin and E. Sunderland, "Equations of Properties as a Function of Temperature for Seven Fluids," *Computer Methods in Applied Mechanics and Engineering,* vol. 61, pp. 177-187, 1987.

[31] P. Boueloup, "Viscosity of Air," 2007.

[32] G. Reysa, "Ground Temperatures as a Function of Location, Season, and Depth," Build It Solar, 2005. [Online]. Available: https://www.builditsolar.com/Projects/Cooling/EarthTemperatures.htm. [Accessed 22 6 2018].

[33] U.S. Department of Energy, "PNNL Scorecard Prototypes Retail Standalone," 18 10 2018. [Online]. Available: https://www.energycodes.gov/development/commercial/prototype_models. [Accessed 22 10 2018].

[34] Government of Canada, "Engineering Climate Datasets," 20 07 2018. [Online]. Available: http://climate.weather.gc.ca/prods_servs/engineering_e.html. [Accessed 28 10 2018].

[35] Canadian Energy Issues, "Ontario power stats," 2018. [Online]. Available: http://canadianenergyissues.com/ontario-power-stats/. [Accessed 22 11 2018].

[36] U.S. Energy Information Administration, "How much carbon dioxide is produced when different fuels are burned?," 2018. [Online]. Available: https://www.eia.gov/tools/faqs/faq.php?id=73&t=11. [Accessed 21 11 2018].

[37] Canadian Urban Institute, "Toronto 2030 Platform," 2018. [Online]. Available: https://www.toronto2030platform.ca/. [Accessed 28 11 2018].

[38] Google, "Google Maps," 2018. [Online]. Available: maps.google.ca. [Accessed 29 11 2018].

[39] Daft Logic, "Google Maps Area Calculator Tool," 11 8 2018. [Online]. Available: https://www.daftlogic.com/projects-google-maps-area-calculator-tool.htm. [Accessed 29 11 2018].

[40] C. X. Mendieta, A comparison of bottom-up methods for estimating institutional building energy use to inform resource and emission reduction strategies, Toronto: Ryerson University, 2018.

[41] R. Daghigh and A. Shafieian, "Theoretical and experimental analysis of thermal performance of a solar water heating system with evacuated tube heat pipe collector," *Applied Thermal Engineering,* vol. 103, pp. 1219-1227, 2016.

[42] B. K. Naik, A. Varshney, P. Muthukumar and C. Somayaji, "Modelling and Performance Analysis of U Type Evacuated Tube Solar Collector Using Different Working Fluids," *Energy Procedia,* vol. 90, pp. 227-237, 2016.

[43] N. Sharma and G. Diaz, "Performance model of a novel evacuated-tube solar collector based on minichannels," *Solar Energy,* vol. 85, pp. 881-890, 2011.

[44] P. Dupeyrat, C. Ménézo, H. Wirth and M. Rommel, "Improvement of PV module optical properties for PV-thermal hybrid collector application," *Solar Energy Materials & Solar Cells,* vol. 95, pp. 2028-2036, 2011.

[45] R. Liang, J. Zhang, L. Ma and Y. Li, "Performance evaluation of new type hybrid photovoltaic/thermal solar collector by experimental study," *Applied Thermal Engineering,* vol. 75, pp. 487-492, 2015.

[46] A. H. Al-Waeli, K. Sopian, H. A. Kazem and M. T. Chaichan, "Photovoltaic/Thermal (PV/T) systems: Status and future prospects," *Renewable and Sustainable Energy Reviews,* vol. 77, pp. 109-130, 2017.

[47] N. Amrizal, D. Chemisana and J. I. Rosell, "Hybrid photovoltaic-thermal solar collectors dynamic modeling," *Applied Energy,* vol. 101, pp. 797-807, 2013.

[48] V. K. Agarwal and D. C. Larson, "Calculation of the top loss coefficient of a flat-plate collector," *Solar Energy,* vol. 27, no. 1, pp. 69-71, 1981.

[49] F. Shan, F. Tang, L. Cao and G. Fang, "Performance evaluations and applications o fphotovoltaic–thermal colletors and systems," *Renewable and Sustainable Energy Reviews,* vol. 33, pp. 467-483, 2014.

Appendix A: Maple Code

This appendix contains the code for the PVT and ET collectors. The numbers shown are for the

100% recommended flowrate, but the same code was used for the other flowrates.

Stefan-Boltzmann Constant (Wm^{-2}K^{-4})
$\sigma := 5.67 \cdot 10^{-8}$

$$5.670000000\ 10^{-8} \tag{1}$$

Temperature of ambient air (K)
$Ta := 283.3$

$$283.3 \tag{2}$$

Sky temperature (K)
$Ts := Ta - 6$

$$277.3 \tag{3}$$

Wind Velocity (m/s)
$v := 3.61$

$$3.61 \tag{4}$$

Emissivity of cover
$\epsilon c := 0.88$

$$0.88 \tag{5}$$

Emissivity of plate
$\epsilon p := 0.95$

$$0.95 \tag{6}$$

Length of air gap (m)
$L := 0.025$

$$0.025 \tag{7}$$

Tilt of collector (° from horizontal)
$\beta := 45$

$$45 \tag{8}$$

$o := \cos\left(\dfrac{45 \cdot Pi}{180} \right)$

$$\frac{1}{2}\sqrt{2} \tag{9}$$

$evalf((9))$

$$0.7071067810 \tag{10}$$

$o := (10)$

$$0.7071067810 \tag{11}$$

Heat Capacity of air (J/kgK)
$Cpa := 1005$

$$1005 \tag{12}$$

Heat capacity of fluid (J/kgK)
$cpf := 3600$

$$3600 \tag{13}$$

Width between pipes (m) APRICUS
$W := 0.095$

$$0.095 \tag{14}$$

Pipe Diameter (m) APRICUS
$d := 0.01$

$$0.01 \tag{15}$$

Pipe-Fluid heat transfer coefficient (W/m^{2}K) APRICUS
$hfi := 300$

$$300 \qquad (16)$$

Plate thickness (m) APRICUS
$\delta\_ab := 0.002$

$$0.002 \qquad (17)$$

Plate conductivity (W/mK) APRICUS
$kab := 390$

$$390 \qquad (18)$$

PV laminate thickness (m)
$\delta pv := 0.04$

$$0.04 \qquad (19)$$

PV laminate conductivity (W/mK)
$k\_pv := 84$

$$84 \qquad (20)$$

Area of collector (m^2) APRICUS
$Ac := 1$

$$1 \qquad (21)$$

Mass flow rate per area of collector (kg/sm^2) APRICUS
$mfrperareacollector := 0.38$

$$0.38 \qquad (22)$$

Mass flow rate through collector (kg/s)
$mfr := mfrperareacollector \cdot Ac$

$$0.38 \qquad (23)$$

Solar irradience on collector surface (W/m^2)
$S := 680$

$$680 \qquad (24)$$

Inlet water temperature (K)
$Ti := 293$

$$293 \qquad (25)$$

Absorptivity APRICUS
$\alpha p := 0.87$

$$0.87 \qquad (26)$$

Cover Transmittance APRICUS
$\tau c := 0.85$

$$0.85 \qquad (27)$$

Insulation Conductivity (W/mK)
$Kb := 0.045$

$$0.045 \qquad (28)$$

Back Insulation Thickness (m)
$Lbi := 0.05$

$$0.05 \qquad (29)$$

Edge Insulation Thickness (m)
$Lei := 0.025$

$$0.025 \qquad (30)$$

Collector Perimeter Length (m)
$perimeter := 4$

$$4 \tag{31}$$

Collector Thickness (m)
$thickness := 0.0526$

$$0.0526 \tag{32}$$

Back Losses
$Ub := \dfrac{Kb}{Lbi}$

$$0.9000000000 \tag{33}$$

Side Losses
$Ue := \dfrac{Kb}{Lei} \cdot \dfrac{perimeter \cdot thickness}{Ac}$

$$0.3787200000 \tag{34}$$

Check for Us+Ub value
$Usbcheck := Ub + Ue$

$$1.278720000 \tag{35}$$

$CoverTemp := \mathbf{proc}(Tp, Tc, v, Ts, L, o, Cpa, \epsilon c, \epsilon p, Ue, Ub)$
$\mathbf{local}\ \rho a, vair, kair, \alpha th, x1, x2, x3, x4, Ra, Nu\_, Nu\_1, Nu\_2, y1, y2, Ul, newTc;$

$$\rho a := 345.57 \cdot \left(\left(\frac{Tc + Tp}{2} \right) - 2.6884 \right)^{-1};$$

$$vair := -1.1555 \cdot 10^{-14} \cdot \left(\frac{(Tc + Tp)}{2} \right)^3 + 9.5728 \cdot 10^{-11} \cdot \left(\frac{(Tc + Tp)}{2} \right)^2 + 3.7604 \cdot 10^{-8}$$
$$\cdot \frac{(Tc + Tp)}{2} - 3.4484 \cdot 10^{-6};$$

$$kair := 1.5797 \cdot 10^{-17} \cdot \left(\frac{Tc + Tp}{2} \right)^5 + 9.46 \cdot 10^{-14} \cdot \left(\frac{Tc + Tp}{2} \right)^4 + 2.2012 \cdot 10^{-10} \cdot \left(\frac{Tc + Tp}{2} \right)^3$$
$$- 2.3758 \cdot 10^{-7} \cdot \left(\frac{Tc + Tp}{2} \right)^2 + 1.7082 \cdot 10^{-4} \cdot \left(\frac{Tc + Tp}{2} \right) - 7.488 \cdot 10^{-3};$$

$$\alpha th := \frac{kair}{\rho a \cdot Cpa};$$

$$Ra := \frac{9.81 \cdot \left(\dfrac{1}{\dfrac{(Tc + Tp)}{2}} \right) \cdot \text{abs}(Tp - Tc) \cdot L^3}{vair \cdot \alpha th};$$

$\mathbf{if}\ 1 - \dfrac{1708}{Ra \cdot o} < 0\ \mathbf{then}\ Nu\_1 := 0\ \mathbf{else}\ Nu\_1 := 1 - \dfrac{1708}{Ra \cdot o}\ \mathbf{end\ if};$

$\mathbf{if}\ \left(\text{abs}\left(\dfrac{Ra \cdot o}{5830} \right) \right)^{0.3333} - 1 < 0\ \mathbf{then}\ Nu\_2 := 0\ \mathbf{else}\ Nu\_2 := \left(\text{abs}\left(\dfrac{Ra \cdot o}{5830} \right) \right)^{0.3333} - 1\ \mathbf{end\ if};$

$$Nu\_ := 1 + 1.44 \left(1 - \frac{1708 \cdot \left(abs\left(sin\left(1.8 \cdot \beta \cdot \left(\frac{Pi}{180} \right) \right) \right) \right)^{1.6}}{Ra \cdot o} \right) \cdot Nu\_1 + Nu\_2;$$

$$x1 := \frac{\sigma \cdot (Tp + Tc) \cdot \left(Tp^2 + Tc^2 \right)}{\frac{1}{\epsilon p} + \frac{1}{\epsilon c} - 1};$$

$$x2 := \frac{Nu\_ \cdot kair}{\sqrt{Ac}};$$

$$x3 := \sigma \cdot \epsilon c \cdot (Tc + Ts) \cdot \left(Tc^2 + Ts^2 \right);$$

$$x4 := 2.8 + 3 \cdot v;$$

$$y1 := \frac{1}{x3 + x4};$$

$$y2 := \frac{1}{x2 + x1};$$

$$Ul := \frac{1}{y1 + y2} + Ue + Ub;$$

$$newTc := Tp - \frac{(Ul - Ue - Ub) \cdot (Tp - Ta)}{x1 + x2};$$

return *newTc, Ul*;
end proc

proc(*Tp, Tc, v, Ts, L, o, Cpa, ϵc, ϵp, Ue, Ub*)   **(36)**

    local *ρa, vair, kair, αth, x1, x2, x3, x4, Ra, Nu_, Nu_1, Nu_2, y1, y2, Ul, newTc*;

    ρa := 345.57 / (1/2 * *Tc* + 1/2 * *Tp* − 2.6884);

    vair := (−1) * 1.1555 * (1/2 * *Tc* + 1/2 * *Tp*)^3 / 100000000000000 + 9.5728 * (1/2 * *Tc* + 1/2 * *Tp*)^2 / 100000000000 + 3.7604 * (1/2 * *Tc* + 1/2 * *Tp*) / 100000000 + (−1) * 3.4484 / 1000000;

    kair := 1.5797 * (1/2 * *Tc* + 1/2 * *Tp*)^5 / 100000000000000000 + 9.46 * (1/2 * *Tc* + 1/2 * *Tp*)^4 / 100000000000000 + 2.2012 * (1/2 * *Tc* + 1/2 * *Tp*)^3 / 10000000000 + (−1) * 2.3758 * (1/2 * *Tc* + 1/2 * *Tp*)^2 / 10000000 + 1.7082 * (1/2 * *Tc* + 1/2 * *Tp*) / 10000 + (−1) * 7.488 / 1000;

    αth := *kair* / (*ρa* * *Cpa*);

    Ra := 9.81 * 1 / (1/2 * *Tc* + 1/2 * *Tp*) * abs(*Tp* − *Tc*) * *L*^3 / (*vair* * *αth*);

    if −1708 / (*Ra* * *o*) < −1 **then** *Nu_1* := 0 **else** *Nu_1* := 1 − 1708 / (*Ra* * *o*) **end if**;

    if abs(1/5830 * *Ra* * *o*)^0.3333 < 1 **then**

        Nu_2 := 0

    else

        Nu_2 := abs(1/5830 * *Ra* * *o*)^0.3333 − 1

    end if;

    Nu_ := 1 + 1.44 * (1 − 1708 * abs(sin(1.8 * β * 1/180 * π))^1.6 / (*Ra* * *o*)) * *Nu_1* + *Nu_2*;

$x1 := \sigma * (Tc + Tp) * (Tp\text{^}2 + Tc\text{^}2) / (1 / \epsilon p + 1 / \epsilon c - 1);$

$x2 := Nu\_ * kair / \text{sqrt}(Ac);$

$x3 := \sigma * \epsilon c * (Tc + Ts) * (Tc\text{^}2 + Ts\text{^}2);$

$x4 := 2.8 + 3 * v;$

$y1 := 1 / (x3 + x4);$

$y2 := 1 / (x2 + x1);$

$Ul := 1 / (y1 + y2) + Ue + Ub;$

$newTc := Tp - (Ul - Ue - Ub) * (Tp - Ta) / (x2 + x1);$

return $newTc, Ul$

end proc

$CollEF :=$**proc**$(W, d, hfi, kab, \delta\_ab, k\_pv, \delta pv, Ul)$

local $m, F, Fprime;$

$$m := \sqrt{\text{abs}\left(\frac{Ul}{kab \cdot \delta\_ab + k\_pv \cdot \delta pv}\right)};$$

$$F := \frac{\tanh\left(\dfrac{m \cdot (W - d)}{2}\right)}{\dfrac{m \cdot (W - d)}{2}};$$

$$Fprime := \frac{\dfrac{1}{Ul}}{W \cdot \left(\dfrac{1}{Ul \cdot (d + (W - d) \cdot F)} + \dfrac{1}{\pi \cdot d \cdot hfi}\right)};$$

return $Fprime;$

end proc

proc$(W, d, hfi, kab, \delta\_ab, k\_pv, \delta pv, Ul)$ **(37)**

    local $m, F, Fprime;$

    $m := \text{sqrt}(\text{abs}(Ul / (kab * \delta\_ab + k\_pv * \delta pv)));$

    $F := 2 * \tanh(1 / 2 * m * (W - d)) / (m * (W - d));$

    $Fprime := 1 / (Ul * W * (1 / (Ul * (d + (W - d) * F)) + 1 / (\pi * d * hfi)));$

    return $Fprime$

end proc

$FlatPlateSim :=$**proc**$(Ta, v, Ts, L, o, Cpa, \epsilon c, \epsilon p, Ue, Ub, W, d, hfi, kab, \delta\_ab, k\_pv, \delta pv, mfr, Ac, S, Ti,$
    $cpf, \alpha p, \tau c)$

local $Tpinit, Tcinit, Ul, Tc, Tp, newTc, Fprime, Fr, Qu, \eta c, To, newTp, Pitt, Pitt2, Tfm, Qe, \eta e;$

$Tpinit := Ta + 50;$

$Tp := Tpinit;$

$newTp := Tp + 50;$

$Pitt := 0;$

while $\text{abs}(newTp - Tp) > 0.1$ **do**

    if $Pitt = 0$ **then** $Tcinit := \dfrac{Ta + Tpinit}{2}$ **else** $Tcinit := \dfrac{Ta + newTp}{2}$ **end if**;

    $Tc := Tcinit;$

if $Pitt > 0$ **then** $Tp := newTp$ **end if**;
$newTc, Ul := CoverTemp(Tp, Tc, v, Ts, L, o, Cpa, \epsilon c, \epsilon p, Ue, Ub)$;

while $\text{abs}(newTc - Tc) > 0.1$ **do**
$Tc := newTc$;
$newTc, Ul := CoverTemp(Tp, Tc, v, Ts, L, o, Cpa, \epsilon c, \epsilon p, Ue, Ub)$;
end do;
$Tc := newTc$;
$Fprime := CollEF(W, d, hfi, kab, \delta\_ab, k\_pv, \delta pv, Ul)$;
$\text{Fr} := \dfrac{mfr \cdot cpf}{Ac \cdot Ul} \cdot \left(1 - \exp\left(-\dfrac{Ac \cdot Ul \cdot Fprime}{mfr \cdot cpf}\right)\right)$;
$Qu := Ac \cdot Fr \cdot \left((S \cdot \alpha p \cdot \infty - S \cdot 0.12) - Ul \cdot (Ti - Ta)\right)$;
$newTp := Ti + \dfrac{\dfrac{Qu}{Ac}}{Fr \cdot Ul} \cdot (1 - Fr)$;
$Qu := Ac \cdot Fr \cdot \left((S \cdot \alpha p \cdot \infty - S \cdot (0.12 \cdot (1 - 0.0045 \cdot (newTp - 298)))) - Ul \cdot (Ti - Ta)\right)$;
$newTp := Ti + \dfrac{\dfrac{Qu}{Ac}}{Fr \cdot Ul} \cdot (1 - Fr)$;
$Pitt2 := Pitt + 1$;
$Pitt := Pitt2$;

if $Pitt > 4$ **then** $newTp := \dfrac{newTp + Tp}{2}$; **end if**;

end do;
$\eta c := \dfrac{Qu}{S \cdot Ac}$;
$To := Ti + \dfrac{Qu}{mfr \cdot cpf}$;
$Qe := S \cdot (0.12 \cdot (1 - 0.0045 \cdot (newTp - 298))) \cdot Ac$;
$\eta e := \dfrac{Qe}{S \cdot Ac}$;

return $Qu, \eta c, To, Tp, Qe, \eta e, Ul$;
end proc

proc$(Ta, v, Ts, L, o, Cpa, \epsilon c, \epsilon p, Ue, Ub, W, d, hfi, kab, \delta\_ab, k\_pv, \delta pv, mfr, Ac, S, Ti, cpf, \alpha p, \infty)$ **(38)**
local $Tpinit, Tcinit, Ul, Tc, Tp, newTc, Fprime, Fr, Qu, \eta c, To, newTp, Pitt, Pitt2, Tfm, Qe, \eta e$;
$Tpinit := Ta + 50$;
$Tp := Tpinit$;
$newTp := Tp + 50$;
$Pitt := 0$;
while $0.1 < \text{abs}(newTp - Tp)$ **do**
    if $Pitt = 0$ **then** $Tcinit := 1/2 * Ta + 1/2 * Tpinit$ **else**
        $Tcinit := 1/2 * Ta + 1/2 * newTp$
    end if;
    $Tc := Tcinit$;

```
        if 0 < Pitt then Tp := newTp end if;
        newTc, Ul := CoverTemp(Tp, Tc, v, Ts, L, o, Cpa, εc, εp, Ue, Ub);
        while 0.1 < abs(newTc − Tc) do
            Tc := newTc; newTc, Ul := CoverTemp(Tp, Tc, v, Ts, L, o, Cpa, εc, εp, Ub)
        end do;
        Tc := newTc;
        Fprime := CollEF(W, d, hfi, kab, δ_ab, k_pv, δpv, Ul);
        Fr := mfr * cpf * (1 − exp( − Ac * Ul * Fprime / (mfr * cpf) ) ) / (Ac * Ul);
        Qu := Ac * Fr * (S * αp * τc + ( − 1) * S * 0.12 − Ul * (Ti − Ta));
        newTp := Ti + Qu * (1 − Fr) / (Ac * Fr * Ul);
        Qu := Ac * Fr * (S * αp * τc + ( − 1) * S * 0.12 * (1 + ( − 1) * 0.0045
         * (newTp − 298)) − Ul * (Ti − Ta));
        newTp := Ti + Qu * (1 − Fr) / (Ac * Fr * Ul);
        Pitt2 := Pitt + 1;
        Pitt := Pitt2;
        if 4 < Pitt then newTp := 1 / 2 * newTp + 1 / 2 * Tp end if
    end do;
    ηc := Qu / (S * Ac);
    To := Ti + Qu / (mfr * cpf);
    Qe := S * 0.12 * (1 + ( − 1) * 0.0045 * (newTp − 298)) * Ac;
    ηe := Qe / (S * Ac);
    return Qu, ηc, To, Tp, Qe, ηe, Ul
end proc
```

$$with(ExcelTools) : inputs := Import(\ )$$

$$
\begin{bmatrix}
\textit{1..8760 x 1..4 Array} \\
\textit{Data Type: anything} \\
\textit{Storage: rectangular} \\
\textit{Order: Fortran\_order}
\end{bmatrix}
\tag{39}
$$

```
testrun := proc(cpf, mfr, inputs)
 local outputsTar1, Ta, v, To, S, Qu, ηc, Ts, i, Tp, Qe, ηe, mfr1, Ti1, Ti;

 outputsTar1 := Matrix(8760, 8);

 for i from 1 to 8760 do
 Ta := inputs(i, 1) + 273;
 Ts := Ta − 6;
 v := inputs(i, 2);
```

$S := inputs(i, 3);$
$Ti := inputs(i, 4);$

#Case 1;
if $S = 0$ **then**
$mfr1 := 0;$
$Qu := 0;$
$\eta c := 0;$
$To := Ta;$
$Tp := 0;$
$Qe := 0;$
$\eta e := 0;$
$Ti1 := 0;$

$outputsTar1(i, 1) := mfr1;$
$outputsTar1(i, 2) := Qu;$
$outputsTar1(i, 3) := \eta c;$
$outputsTar1(i, 4) := To;$
$outputsTar1(i, 5) := Tp;$
$outputsTar1(i, 6) := Qe;$
$outputsTar1(i, 7) := \eta e;$
$outputsTar1(i, 8) := Ti1;$

else
$Qu, \eta c, To, Tp, Qe, \eta e, Ul := FlatPlateSim(Ta, v, Ts, L, o, Cpa, \epsilon c, \epsilon p, Ue, Ub, W, d, hfi, kab, \delta\_ab,$
$\quad k\_pv, \delta pv, mfr, Ac, S, Ti, cpf, \alpha p, \tau c);$

$outputsTar1(i, 1) := mfr;$
$outputsTar1(i, 2) := Qu;$
$outputsTar1(i, 3) := \eta c;$
$outputsTar1(i, 4) := To;$
$outputsTar1(i, 5) := Tp;$
$outputsTar1(i, 6) := Qe;$
$outputsTar1(i, 7) := \eta e;$
$outputsTar1(i, 8) := Ti;$

end if;

end do;

end proc

Warning, `Ul` is implicitly declared local to procedure `testrun`

proc(*cpf, mfr, inputs*)   **(40)**
    local *outputsTar1, Ta, v, To, S, Qu, ηc, Ts, i, Tp, Qe, ηe, mfr1, Ti1, Ti, Ul*;
    outputsTar1 := Matrix(8760, 8);
    for *i* **to** 8760 **do**
        Ta := inputs(i, 1) + 273;

```
            Ts := Ta − 6;
            v := inputs(i, 2);
            S := inputs(i, 3);
            Ti := inputs(i, 4);
            if S = 0 then
                mfr1 := 0;
                Qu := 0;
                ηc := 0;
                To := Ta;
                Tp := 0;
                Qe := 0;
                ηe := 0;
                Ti1 := 0;
                outputsTar1(i, 1) := mfr1;
                outputsTar1(i, 2) := Qu;
                outputsTar1(i, 3) := ηc;
                outputsTar1(i, 4) := To;
                outputsTar1(i, 5) := Tp;
                outputsTar1(i, 6) := Qe;
                outputsTar1(i, 7) := ηe;
                outputsTar1(i, 8) := Ti1
            else
                Qu, ηc, To, Tp, Qe, ηe, Ul := FlatPlateSim(Ta, v, Ts, L, o, Cpa, ϵc, ϵp, Ue, Ub, W, d,
                hfi, kab, δ_ab, k_pv, δpv, mfr, Ac, S, Ti, cpf, αp, τc);
                outputsTar1(i, 1) := mfr;
                outputsTar1(i, 2) := Qu;
                outputsTar1(i, 3) := ηc;
                outputsTar1(i, 4) := To;
                outputsTar1(i, 5) := Tp;
                outputsTar1(i, 6) := Qe;
                outputsTar1(i, 7) := ηe;
                outputsTar1(i, 8) := Ti
            end if
        end do
    end proc
outputsTar1 := testrun(cpf, mfr, inputs)
```

$$\begin{bmatrix} \textit{8760 x 8 Matrix} \\ \textit{Data Type: anything} \\ \textit{Storage: rectangular} \\ \textit{Order: Fortran\_order} \end{bmatrix}$$

(41)

$with(ExcelTools) : Export(outputsTar1)$

>
>

HANNAH VARIABLES:
Collector:
Area of one Collector (m^2) STANDARD
$Ac\_ET := 1$

$$1 \qquad\qquad (1)$$

Cylindrical Reciever/Absorber
Reciever Emissivity APRICUS
$\varepsilon r\_ET := 0.93$

$$0.93 \qquad\qquad (2)$$

Outside Diameter (m) APRICUS
$Droutside\_ET := 0.047$

$$0.047 \qquad\qquad (3)$$

Thickness (m) APRICUS?
$t\_ET := 0.0018$

$$0.0018 \qquad\qquad (4)$$

Inside Diameter (m) APRICUS
$Drinside\_ET := Droutside\_ET - 2 \cdot t\_ET$

$$0.0434 \qquad\qquad (5)$$

Unit Length of Reciever (m)
$Lunit\_ET := 1$

$$1 \qquad\qquad (6)$$

Length of Reciever (m) APRICUS
$Lr\_ET := 1$

$$1 \qquad\qquad (7)$$

Thermal Conductivity (W/mK) FOR COPPER
$kr\_ET := 401$

$$401 \qquad\qquad (8)$$

Aperture Area (m^2) APRICUS
$Aa\_ET := 0.727273$

$$0.727273 \qquad\qquad (9)$$

Cover
Outer Glass Diameter (m) APRICUS
$Dco\_ET := 0.058$

$$0.058 \qquad\qquad (10)$$

Glass Thickness (m) APRICUS
$tg\_ET := 0.0018$

$$0.0018 \qquad\qquad (11)$$

Inner Glass Diameter (m) APRICUS
$Dci\_ET := Dco\_ET - 2 \cdot tg\_ET$

$$0.0544 \qquad\qquad (12)$$

Emissivity of glass
$\varepsilon g\_ET := 0.8$

$$0.8 \qquad\qquad (13)$$

Thermal Conductivity (W/mK) APRICUS
$kg\_ET := 1.2$

$$1.2 \qquad\qquad (14)$$

Working Fluid
Fluid Flow Rate (kg/s) APRICUS
$mfr\_ET := 0.0078$

$$0.0078 \qquad\qquad (15)$$

Heat Transfer Coefficient inside Tubes (W/m²K)
$hf\_ET := 300$

$$300 \qquad\qquad (16)$$

Specific Heat (J/kgK)
$Cp\_ET := 3600$

$$3600 \qquad\qquad (17)$$

Surroundings
Defining pi
$pi := 3.14159$

$$3.14159 \qquad\qquad (18)$$

Area of Receiver (m²)
$Ar\_ET := 0.638242$

$$0.638242 \qquad\qquad (19)$$

PREVIOUS VARIABLES:
Stefan-Boltzmann Constant (Wm⁻²K⁻⁴)
$\sigma := 5.67 \cdot 10^{-8}$

$$5.670000000 \; 10^{-8} \qquad\qquad (20)$$

$ETSim := \textbf{proc}\,(\,Ta\_ET, Dco\_ET, Lunit\_ET, \varepsilon g\_ET, Ts\_ET, Ac\_ET, S\_ET, Aa\_ET, mfr\_ET, Cp\_ET,$
    $Tinlet\_ET, Ar\_ET)$
$\textbf{local}\ Trinit\_ET, Tr\_ET, newTr\_ET, Pitt\_ET, Pitt2\_ET, Qloss\_ET, newQloss\_ET, Ul\_ET, Qu\_ET,$
    $FR\_ET, dT\_ET, To\_ET, \eta c\_ET, hw\_ET, Tcinside\_ET, PittQ\_ET, PittQ2\_ET, AvgTempDrop\_ET,$
    $\rho a\_ET, kair\_ET, \mu\_ET, Reynolds\_ET, Nu\_ET, Fprime\_ET, F2prime\_ET;$

$Tr\_ET := Ta\_ET + 50;$
$newTr\_ET := Tr\_ET + 50;$
$Pitt\_ET := 0;$

$\textbf{while}\ \text{abs}(newTr\_ET - Tr\_ET) > 0.1\ \textbf{do}$
    $\textbf{if}\ Pitt\_ET = 0\ \textbf{then}\ Qloss\_ET := \varepsilon g\_ET \cdot pi \cdot Dco\_ET \cdot \sigma \cdot (Ta\_ET^4 - Ts\_ET^4);$
    $\textbf{end if};$

    $\textbf{if}\ Pitt\_ET > 0\ \textbf{then}\ Tr\_ET := newTr\_ET;$
    $\textbf{end if};$

$$Tcinside\_ET := Ta\_ET + \frac{Qloss\_ET \cdot \ln\left(\dfrac{Dco\_ET}{Dci\_ET}\right)}{2 \cdot pi \cdot kg\_ET \cdot 1};$$

$$newQloss\_ET := \frac{\text{pi} \cdot Droutside\_ET \cdot \sigma \cdot \left(Tr\_ET^4 - Tcinside\_ET^4 \right)}{\left(\dfrac{1}{\epsilon r\_ET} \right) + \left(\dfrac{1 - \epsilon g\_ET}{\epsilon g\_ET} \right) \cdot \dfrac{Droutside\_ET}{(Dci\_ET)}};$$

$PittQ\_ET := 0;$

while abs($newQloss\_ET - Qloss\_ET$) > 0.1 **do**

$Qloss\_ET := newQloss\_ET;$

$$Tcinside\_ET := Ta\_ET + \frac{Qloss\_ET \cdot \ln\left(\dfrac{Dco\_ET}{Dci\_ET} \right)}{2 \cdot \text{pi} \cdot kg\_ET \cdot 1};$$

$$newQloss\_ET := \frac{\text{pi} \cdot Droutside\_ET \cdot \sigma \cdot \left(Tr\_ET^4 - Tcinside\_ET^4 \right)}{\left(\dfrac{1}{\epsilon r\_ET} \right) + \left(\dfrac{1 - \epsilon g\_ET}{\epsilon g\_ET} \right) \cdot \dfrac{Droutside\_ET}{(Dco\_ET - tg\_ET)}};$$

$PittQ2\_ET := PittQ\_ET + 1;$
$PittQ\_ET := PittQ2\_ET;$
if $PittQ\_ET > 3$ **then** $newQloss\_ET := \dfrac{newQloss\_ET + Qloss\_ET}{2};$
end if;

end do;
$Qloss\_ET := newQloss\_ET;$

$$Ul\_ET := \frac{Qloss\_ET}{Ar\_ET \cdot (Tr\_ET - Ta\_ET)};$$

$$Fprime\_ET := \frac{\dfrac{1}{Ul\_ET}}{\dfrac{1}{Ul\_ET} + \dfrac{Droutside\_ET}{hf\_ET \cdot Drinside\_ET} + \left(\dfrac{Droutside\_ET}{2 \cdot kr\_ET} \cdot \ln\left(\dfrac{Droutside\_ET}{Drinside\_ET} \right) \right)};$$

$$F2prime\_ET := \frac{mfr\_ET \cdot Cp\_ET}{Ar\_ET \cdot Ul\_ET \cdot Fprime\_ET} \cdot \left(1 - \exp\left(-\frac{Ar\_ET \cdot Ul\_ET \cdot Fprime\_ET}{mfr\_ET \cdot Cp\_ET} \right) \right);$$

$FR\_ET := Fprime\_ET \cdot F2prime\_ET;$

$$Qu\_ET := Aa\_ET \cdot FR\_ET \cdot \left(S\_ET - \left(\frac{Ar\_ET}{Aa\_ET} \right) \cdot Ul\_ET \cdot (Tr\_ET - Ta\_ET) \right);$$

$$dT\_ET := \frac{Qu\_ET}{mfr\_ET \cdot Cp\_ET};$$

$$To\_ET := Tinlet\_ET + dT\_ET;$$

$$AvgTempDrop\_ET := Qu\_ET \cdot \left(\frac{1}{\mathrm{pi} \cdot Drinside\_ET \cdot Lr\_ET \cdot hf\_ET} + \frac{\ln\left(\dfrac{Droutside\_ET}{Drinside\_ET}\right)}{2 \cdot \mathrm{pi} \cdot kr\_ET \cdot Lr\_ET} \right);$$

$$newTr\_ET := \frac{(Tinlet\_ET + To\_ET)}{2} + AvgTempDrop\_ET;$$

$$Pitt2\_ET := Pitt\_ET + 1;$$
$$Pitt\_ET := Pitt2\_ET;$$
if $Pitt\_ET > 3$ **then** $newTr\_ET := \dfrac{newTr\_ET + Tr\_ET}{2};$

end if;

end do;

$$\eta c\_ET := \frac{Qu\_ET}{S\_ET \cdot Ac\_ET};$$

return $Qu\_ET, \eta c\_ET, To\_ET, Tr\_ET, Qloss\_ET, Ul\_ET, FR\_ET, Tcinside\_ET, Fprime\_ET;$
end proc

proc$\big(Ta\_ET, Dco\_ET, Lunit\_ET, \varepsilon g\_ET, Ts\_ET, Ac\_ET, S\_ET, Aa\_ET, mfr\_ET, Cp\_ET,$ **(21)**
  $Tinlet\_ET, Ar\_ET \big)$
  local $Trinit\_ET, Tr\_ET, newTr\_ET, Pitt\_ET, Pitt2\_ET, Qloss\_ET, newQloss\_ET, Ul\_ET,$
  $Qu\_ET, FR\_ET, dT\_ET, To\_ET, \eta c\_ET, hw\_ET, Tcinside\_ET, PittQ\_ET, PittQ2\_ET,$
  $AvgTempDrop\_ET, \rho a\_ET, kair\_ET, \mu\_ET, Reynolds\_ET, Nu\_ET, Fprime\_ET, F2prime\_ET;$
  $Tr\_ET := Ta\_ET + 50;$
  $newTr\_ET := Tr\_ET + 50;$
  $Pitt\_ET := 0;$
  while $0.1 < \mathrm{abs}(newTr\_ET - Tr\_ET)$ **do**
    if $Pitt\_ET = 0$ **then** $Qloss\_ET := \varepsilon g\_ET * \pi * Dco\_ET * \sigma * (Ta\_ET^{\wedge}4 - Ts\_ET^{\wedge}4)$
    end if;
    if $0 < Pitt\_ET$ **then** $Tr\_ET := newTr\_ET$ **end if**;
    $Tcinside\_ET := Ta\_ET + 1/2 * Qloss\_ET * \ln(Dco\_ET / Dci\_ET) / (\pi * kg\_ET);$
    $newQloss\_ET := \pi * Droutside\_ET * \sigma * (Tr\_ET^{\wedge}4 - Tcinside\_ET^{\wedge}4) / (1 / \varepsilon r\_ET$
    $+ (1 - \varepsilon g\_ET) * Droutside\_ET / (\varepsilon g\_ET * Dci\_ET));$
    $PittQ\_ET := 0;$
    while $0.1 < \mathrm{abs}(newQloss\_ET - Qloss\_ET)$ **do**
      $Qloss\_ET := newQloss\_ET;$
      $Tcinside\_ET := Ta\_ET + 1/2 * Qloss\_ET * \ln(Dco\_ET / Dci\_ET) / (\pi * kg\_ET);$
      $newQloss\_ET := \pi * Droutside\_ET * \sigma * (Tr\_ET^{\wedge}4 - Tcinside\_ET^{\wedge}4) / (1 / \varepsilon r\_ET$
      $+ (1 - \varepsilon g\_ET) * Droutside\_ET / (\varepsilon g\_ET * (Dco\_ET - tg\_ET)));$

$$PittQ2\_ET := PittQ\_ET + 1;$$

$$PittQ\_ET := PittQ2\_ET;$$

if $3 < PittQ\_ET$ **then** $newQloss\_ET := 1/2 * newQloss\_ET + 1/2 * Qloss\_ET$

end if

end do;

$$Qloss\_ET := newQloss\_ET;$$

$$Ul\_ET := Qloss\_ET / (Ar\_ET * (Tr\_ET - Ta\_ET));$$

$$Fprime\_ET := 1 / (Ul\_ET * (1 / Ul\_ET + Droutside\_ET / (hf\_ET * Drinside\_ET) + 1/2 * Droutside\_ET * \ln(Droutside\_ET / Drinside\_ET) / kr\_ET));$$

$$F2prime\_ET := mfr\_ET * Cp\_ET * (1 - \exp(-Ar\_ET * Ul\_ET * Fprime\_ET / (mfr\_ET * Cp\_ET))) / (Ar\_ET * Ul\_ET * Fprime\_ET);$$

$$FR\_ET := Fprime\_ET * F2prime\_ET;$$

$$Qu\_ET := Aa\_ET * FR\_ET * (S\_ET - Ar\_ET * Ul\_ET * (Tr\_ET - Ta\_ET) / Aa\_ET);$$

$$dT\_ET := Qu\_ET / (mfr\_ET * Cp\_ET);$$

$$To\_ET := Tinlet\_ET + dT\_ET;$$

$$AvgTempDrop\_ET := Qu\_ET * (1 / (\pi * Drinside\_ET * Lr\_ET * hf\_ET) + 1/2 * \ln(Droutside\_ET / Drinside\_ET) / (\pi * kr\_ET * Lr\_ET));$$

$$newTr\_ET := 1/2 * Tinlet\_ET + 1/2 * To\_ET + AvgTempDrop\_ET;$$

$$Pitt2\_ET := Pitt\_ET + 1;$$

$$Pitt\_ET := Pitt2\_ET;$$

if $3 < Pitt\_ET$ **then** $newTr\_ET := 1/2 * newTr\_ET + 1/2 * Tr\_ET$ **end if**

end do;

$$\eta c\_ET := Qu\_ET / (S\_ET * Ac\_ET);$$

return $Qu\_ET, \eta c\_ET, To\_ET, Tr\_ET, Qloss\_ET, Ul\_ET, FR\_ET, Tcinside\_ET, Fprime\_ET$

end proc

$with(ExcelTools) : inputs\_ET := Import()$

$$\begin{bmatrix} 1..8760 \ x \ 1..4 \ Array \\ Data \ Type: \ anything \\ Storage: \ rectangular \\ Order: \ Fortran\_order \end{bmatrix} \tag{22}$$

$testrun\_ET :=$**proc**$(Cp\_ET, mfr\_ET, inputs\_ET)$

local $outputs\_ET, Ta\_ET, v\_ET, To\_ET, S\_ET, Qu\_ET, \eta c\_ET, Ts\_ET, i\_ET, Tr\_ET, mfr1\_ET, Ti1\_ET, Tinlet\_ET, Qloss\_ET, Ul\_ET, FR\_ET;$

$outputs\_ET := Matrix(8760, 6);$

for i_ET **from** 1 **to** 8760 **do**

$Ta\_ET := inputs\_ET(i\_ET, 1) + 273;$

$Ts\_ET := Ta\_ET - 6;$

$v\_ET := inputs\_ET(i\_ET, 2);$
$S\_ET := inputs\_ET(i\_ET, 3);$
$Tinlet\_ET := inputs\_ET(i\_ET, 4);$

if $S\_ET = 0$ **then**
$mfr1\_ET := 0;$
$Qu\_ET := 0;$
$\eta c\_ET := 0;$
$To\_ET := Ta\_ET;$
$Tr\_ET := 0;$
$Ti1\_ET := 0;$

$outputs\_ET(i\_ET, 1) := mfr1\_ET;$
$outputs\_ET(i\_ET, 2) := Qu\_ET;$
$outputs\_ET(i\_ET, 3) := \eta c\_ET;$
$outputs\_ET(i\_ET, 4) := To\_ET;$
$outputs\_ET(i\_ET, 5) := Tr\_ET;$
$outputs\_ET(i\_ET, 6) := Ti1\_ET;$

else

$Qu\_ET, \eta c\_ET, To\_ET, Tr\_ET, Qloss\_ET, Ul\_ET, FR\_ET, Tcinside\_ET, Fprime\_ET := ETSim(Ta\_ET,$
$\quad Dco\_ET, Lunit\_ET, \varepsilon g\_ET, Ts\_ET, Ac\_ET, S\_ET, Aa\_ET, mfr\_ET, Cp\_ET, Tinlet\_ET, Ar\_ET);$

$outputs\_ET(i\_ET, 1) := mfr\_ET;$
$outputs\_ET(i\_ET, 2) := Qu\_ET;$
$outputs\_ET(i\_ET, 3) := \eta c\_ET;$
$outputs\_ET(i\_ET, 4) := To\_ET;$
$outputs\_ET(i\_ET, 5) := Tr\_ET;$
$outputs\_ET(i\_ET, 6) := Tinlet\_ET;$

end if;

end do;

end proc
Warning, `Tcinside_ET` is implicitly declared local to procedure `testrun_ET`
Warning, `Fprime_ET` is implicitly declared local to procedure `testrun_ET`

proc$(Cp\_ET, mfr\_ET, inputs\_ET)$ **(23)**
    local $outputs\_ET, Ta\_ET, v\_ET, To\_ET, S\_ET, Qu\_ET, \eta c\_ET, Ts\_ET, i\_ET, Tr\_ET,$
    $mfr1\_ET, Ti1\_ET, Tinlet\_ET, Qloss\_ET, Ul\_ET, FR\_ET, Tcinside\_ET, Fprime\_ET;$
    $outputs\_ET := Matrix(8760, 6);$
    for i_ET **to** 8760 **do**
        $Ta\_ET := inputs\_ET(i\_ET, 1) + 273;$
        $Ts\_ET := Ta\_ET - 6;$
        $v\_ET := inputs\_ET(i\_ET, 2);$
        $S\_ET := inputs\_ET(i\_ET, 3);$

```
        Tinlet_ET := inputs_ET(i_ET, 4);
        if S_ET = 0 then
            mfr1_ET := 0;
            Qu_ET := 0;
            ηc_ET := 0;
            To_ET := Ta_ET;
            Tr_ET := 0;
            Ti1_ET := 0;
            outputs_ET(i_ET, 1) := mfr1_ET;
            outputs_ET(i_ET, 2) := Qu_ET;
            outputs_ET(i_ET, 3) := ηc_ET;
            outputs_ET(i_ET, 4) := To_ET;
            outputs_ET(i_ET, 5) := Tr_ET;
            outputs_ET(i_ET, 6) := Ti1_ET
        else
            Qu_ET, ηc_ET, To_ET, Tr_ET, Qloss_ET, Ul_ET, FR_ET, Tcinside_ET,
            Fprime_ET := ETSim(Ta_ET, Dco_ET, Lunit_ET, εg_ET, Ts_ET, Ac_ET, S_ET,
            Aa_ET, mfr_ET, Cp_ET, Tinlet_ET, Ar_ET);
            outputs_ET(i_ET, 1) := mfr_ET;
            outputs_ET(i_ET, 2) := Qu_ET;
            outputs_ET(i_ET, 3) := ηc_ET;
            outputs_ET(i_ET, 4) := To_ET;
            outputs_ET(i_ET, 5) := Tr_ET;
            outputs_ET(i_ET, 6) := Tinlet_ET
        end if
    end do
end proc
outputs_ET := testrun_ET(Cp_ET, mfr_ET, inputs_ET)
```

$$\begin{bmatrix} \textit{8760 x 6 Matrix} \\ \textit{Data Type: anything} \\ \textit{Storage: rectangular} \\ \textit{Order: Fortran\_order} \end{bmatrix} \qquad (24)$$

```
with(ExcelTools) : Export(outputs_ET)
```

>

Appendix B: Sample Excel Worksheet for Building Feasibility Study– Parallel Layout

This appendix contains the Excel sheet for the parallel layout for a typical case study building, included in the supplemental data file as Parallel_Layout_Worksheet_for_Single_Building.xlsx.

Appendix C: Sample Excel Worksheet for Building Feasibility Study– Series Layout

This appendix contains the Excel sheet for the series layout for a typical case study building, included in the supplemental data file as Series_Layout_Worksheet_for_Single_Building.xlsx.

Appendix C: Sample Excel Worksheet for District Heating Feasibility

This appendix contains the Excel sheet to calculate district heating impacts for a known building cluster, included in the supplemental data file as District_Heating_Worksheet.xlsx.

Appendix D: Sample Excel Worksheet for District GHG Reduction Feasibility

This appendix contains the Excel sheet to calculate district-scale impacts, included in the supplemental data file as District_GHG_Reduction_Spreadsheet.xlsx.